QEF-1-21

[redacted]

CENTRAL RESEARCH LIBRARY
DOCUMENT COLLECTION

MARTIN MARIETTA ENERGY SYSTEMS LIBRARIES
3 4456 0360677 4

AEC RESEARCH AN[illegible]ORT

ORNL-1606
Progress

DECLASSIFIED
CLASSIFICATION CHANGED TO:
BY AUTHORITY OF: AEC - 2-19-59
BY: Susan Bowman 4-15-59

LABORATORY RECORDS
1954

SOLID STATE DIVISION

SEMIANNUAL PROGRESS REPORT

FOR PERIOD ENDING AUGUST 31, 1953

CENTRAL RESEARCH LIBRARY
DOCUMENT COLLECTION

LIBRARY LOAN COPY

DO NOT TRANSFER TO ANOTHER PERSON

If you wish someone else to see this document, send in name with document and the library will arrange a loan.

OAK RIDGE NATIONAL LABORATORY
U.S. ATOMIC ENERGY COMMISSION

OAK RIDGE NATIONAL LABORATORY
OPERATED BY
CARBIDE AND CARBON CHEMICALS COMPANY
A DIVISION OF UNION CARBIDE AND CARBON CORPORATION

UCC

POST OFFICE BOX P
OAK RIDGE, TENNESSEE

[redacted]

[redacted]

[redacted]

ORNL-1606

This document consists of 116 pages.

Copy 4 of 155 copies. Series A.

Contract No. W-7405-eng-26

SOLID STATE DIVISION

SEMIANNUAL PROGRESS REPORT

For Period Ending August 31, 1953

D. S. Billington, Director

Edited by

J. T. Howe

DATE ISSUED

NOV 20 1953

OAK RIDGE NATIONAL LABORATORY

Operated by

CARBIDE AND CARBON CHEMICALS COMPANY

A Division of Union Carbide and Carbon Corporation

Post Office Box P

Oak Ridge, Tennessee

[redacted]

MARTIN MARIETTA ENERGY SYSTEMS LIBRARIES

3 4456 0360677 4

[redacted]

INTERNAL DISTRIBUTION

1. C. E. Center
2. Biology Library
3. Health Physics Library
4-5. Central Research Library
6. Reactor Experimental Engineering Library
7-11. Laboratory Records Department
12. Laboratory Records, ORNL R.C.
13. C. E. Larson
14. W. B. Humes (K-25)
15. L. B. Emlet (Y-12)
16. A. M. Weinberg
17. E. H. Taylor
18. E. J. Murphy
19. E. D. Shipley
20. D. S. Billington
21. F. C. VonderLage
22. R. C. Briant
23. J. A. Swartout
24. S. C. Lind
25. F. L. Culler
26. A. H. Snell
27. A. Hollaender
28. M. T. Kelley
29. G. H. Clewett
30. K. Z. Morgan
31. T. A. Lincoln
32. A. S. Householder
33. C. S. Harrill
34. C. E. Winters
35. D. W. Cardwell
36. E. M. King
37. C. P. Keim
38. L. K. Jetter
39. E. J. Boyle
40. W. D. Manly
41. C. D. Susano
42. B. S. Borie
43. R. J. Gray
44. J. H. Frye, Jr.
45. E. E. Stansbury
46. G. P. Smith
47. J. E. Cunningham
48. E. C. Miller
49. A. M. Cohen
50. J. O. Betterton, Jr.
51. R. B. Oliver
52. T. H. Blewitt
53. J. H. Crawford, Jr.
54. W. E. Brundage
55. O. Sisman
56. G. W. Keilholtz
57. J. T. Howe
58. R. H. Kernohan
59. S. E. Dismuke
60. J. C. Wilson
61. W. J. Sturm
62. M. T. Robinson
63. J. W. Cleland
64. K. Lark-Horovitz (consultant)
65. M. C. Wittels
66. R. A. Weeks
67. W. W. Parkinson
68. C. D. Bopp
69. C. E. Baumann
70. J. B. Trice
71. J. G. Morgan
72. G. E. Klein
73. R. G. Berggren
74. D. K. Holmes
75. D. K. Stevens
76. A. J. Miller
77. R. S. Livingston
78. R. J. Jones
79. D. D. Cowen
80. P. M. Reyling

[redacted]

[redacted]

81. G. C. Williams
82. D. Binder
83. M. J. Feldman
84. C. C. Webster
85. J. M. Warde
86. W. O. Harms
87. W. R. Willis
88. F. Seitz (consultant)
89. E. P. Wigner (consultant)
90. R. L. Sproull (consultant)
91. R. W. Johnson

EXTERNAL DISTRIBUTION

92-99. Argonne National Laboratory
100-102. Atomic Energy Commission, Washington
103-106. Brookhaven National Laboratory
107-110. Carbide and Carbon Chemicals Company (Y-12 Plant)
111-113. Knolls Atomic Power Laboratory
114-115. General Electric Company, Richland
116. Hanford Operations Office
117-120. Los Alamos Scientific Laboratory
121-122. New York Operations Office
123. Patent Branch, Washington
124-138. Technical Information Service, Oak Ridge
139-140. University of California Radiation Laboratory, Berkeley
141-142. University of California Radiation Laboratory, Livermore
143. Massachusetts Institute of Technology (Kaufmann)
144. Battelle Memorial Institute
145-147. North American Aviation, Inc.
148. Westinghouse Electric Corporation
149. Savannah River Operations Office, Augusta
150-153. Phillips Petroleum Company
154. Materials Laboratory (WADC) 1 copy – Helen Akerd
155. Directorate of Research (WADC) 1 copy – Helen Akerd

[redacted]

[redacted]

Reports previously issued in this series are:

ORNL-1025	Period Ending January 31, 1951
ORNL-1095	Period Ending April 30, 1951
ORNL-1128	Period Ending July 31, 1951
ORNL-1214	Period Ending October 31, 1951
ORNL-1261	Period Ending January 31, 1952
ORNL-1301	Period Ending May 10, 1952
ORNL-1359	Period Ending August 10, 1952
ORNL-1429	Period Ending November 10, 1952
ORNL-1506	Period Ending February 10, 1953

[redacted]

[redacted]

CONTENTS

PART I

SUMMARY 3

RADIATION METALLURGY 8
- Creep Under Irradiation 8
- Thermocouples 9
- Extensometers 10
- MTR Creep Test 10
- Impact Tests 10
- Fatigue Tests 12
- High-Temperature Strain Gages 12
- Remote Electropolisher 13
- Procedure of Remote Electropolishing and Etching 13
- Special Mounting Techniques 14
- Indium Replica Technique 16
- Work Performed and Status of Hot Metallography Projects 18
- Service Work 19

NUCLEAR MEASUREMENTS 22
- Neutron-Spectrum Measurements in the BSF 22
- MTR Neutron Flux-Radiation Damage Measurement Project 23
- Nuclear Heating in the LITR 25

ENGINEERING PROPERTIES 29
- LITR Fluoride-Fuel Loop 29
- LITR Sodium Stress-Corrosion Loop 31
- ORNL Graphite Reactor Sodium-Inconel Loop 33
- Sodium–Beryllium Oxide Radiation-Corrosion Test 34
- Radiation-Induced Changes in the Engineering Properties of Metals 36

FUSED SALTS 39
- Fused-Salt Capsule Tests in the LITR 39
- Fused-Salt Capsule Tests in the MTR 40
- MTR Capsule Calculations 42
- Thermal Flux in Facility A-38 of the MTR 43
- Analysis of Fluoride Fuels for Cs^{137} 43
- Shielded Petrographic Microscope for Irradiated Samples 43
- Electrical Conductivity of Fluorides 44
- High-Temperature Properties of Potassium Monofluorophosphate 44

SPECIAL PROJECTS 47
- Annealing of Irradiated Graphite-UO_2 Materials 47
- Physical-Property Tests on Thorium 50

[redacted]

[redacted]

Transformation of Cd-Au Single Crystals
Abnormal Aftereffects in Aluminum
Curie Temperature of Ni-Be Alloy
Effect of Reactor Irradiation on the Thermal Conductivity and Other Properties of Structural Materials
Thermal Conductivity of Dielectrics at Low Temperatures

PART II

SUMMARY

SOLID STATE REACTIONS
Low-Temperature Irradiation of *p*-Type Germanium
Behavior of *n*-Type Germanium Bombarded at Low Temperatures
Acceptor States in Bombarded Germanium
Gold-doped Germanium
Magnetic Susceptibility of Germanium
Neutron Irradiation of Indium Antimonide
Low-Temperature Irradiation of Cu-Be Alloy
Rectifier Bombardment
Radiation Effects in Ionic Crystals
A-C Resistance Comparator

ENGINEERING PROPERTIES
Radiation Stability of Plastics and Elastomers
Dynamic Properties of Irradiated Elastomers
X-Ray Diffraction Patterns of Plastics

SPECIAL PROJECTS
Irradiation of Quartz
Irradiation of Miscellaneous Materials
Use of K_β Radiation for the X-Ray Analysis of Reflections Unresolved in the K_α Region
Neutron Irradiation of LiF Crystals

[redacted]

[redacted]

PUBLICATIONS

Publications of the Solid State Division during the past six months were:

C. D. Bopp, *Gamma Radiation Induced in Engineering Materials*, ORNL-1371 (May 6, 1953).

R. M. Carroll, *A Simple Electromagnetic Flowmeter for Liquid Metals*, ORNL-1461 (March 4, 1953).

W. J. Sturm, R. J. Jones, and M. J. Feldman, *The Stability of Several Inconel-UF_4 Fused Salt Fuel Systems Under Proton Bombardment*, ORNL-1530 (July 21, 1953).

Publications that were in press at the close of the period were:

D. K. Stevens, *The Magnetic Susceptibility of Annealed and Fast Neutron Bombarded Germanium*, ORNL-1599.

The Laboratory was host to the classified Radiation Damage Conference of the American Physical Society March 23-24, 1953. The talks given are being collected and will appear as ORNL CF-53-3-276.

[redacted]

Part I

SECRET PROJECTS

SOLID STATE DIVISION SEMIANNUAL PROGRESS REPORT

SUMMARY

RADIATION METALLURGY

Creep Under Irradiation. A cantilever creep specimen run in the ORNL graphite reactor at ARE pressure-shell conditions showed no enhanced creep caused by irradiation when compared with International Nickel Company data for hot-rolled plate under about the same conditions of stress and temperature.

Tests have shown that the creep behavior of Inconel plate from which all in-pile creep specimens have been made is not affected by orientation of specimen surface with respect to original surface of the plate, although tests performed by the Metallurgy Division have shown that there are marked surface effects on creep of a decarburized surface on thin, tensile creep specimens.

Between 1500 and 1600°F, the temperature dependence of the creep rate of Inconel does not appear to be markedly affected by LITR irradiation, inert atmospheres, or both.

Bench and LITR creep tests were also made on type 347 stainless steel at 8000 psi over a temperature range of 1200 to 1400°F and at 1500 psi over a range of 1400 to 1550°F. The high-stress data curves for irradiated and unirradiated specimens converge at higher temperatures, and the low-stress data curves converge at lower temperatures; whether this is an indication of a very strong creep-rate dependence of the irradiation effects is not yet known.

Thermocouples. A platinum melting-point capsule containing sodium chloride has been operated in the LITR for checking changes in thermocouple output caused by irradiation; the change is less than 10°F for a three-week exposure in the HB-3 facility of the LITR. Unsteady temperature on the LITR creep apparatus has been traced to the glass-metal seals used to bring the thermocouple leads into the inert atmosphere. A solderless connection made with ceramic insulators and Sauereisen cement appears to alleviate the difficulty.

Extensometers. Calibration of a set of four Bourdon tubes for extensometer elements has shown that it is possible to manufacture tubes in quantity with calibration factors differing by only a few per cent. Temperature coefficients of only 0.03%/°F for a full-scale range of only 0.020 in. have been achieved from room temperature to 600°F.

MTR Creep Test. Minor design changes have been made in the MTR creep apparatus, and tests requested by Phillips Petroleum Company have been performed. Approval for its insertion has been obtained pending a leak test of the experimental can after its arrival at Arco. Assembly of the apparatus has begun and it will be shipped to the MTR within a few weeks.

Impact Tests. The modified, remotely controlled impact testing machine has been checked out with a number of various metal specimens.

Impact tests made on irradiated and unirradiated specimens of high-purity iron, low-carbon steel, types 304, 304L, and 347 stainless steel, iodide titanium, and commercial-purity titanium indicate that irradiation has a marked effect on the notched-bar impact properties of the carbon steels but apparently has little, if any, effect on the impact properties of the other metals. However, the irradiations were of rather short duration.

A new specimen geometry has been developed and further refinements to the impact machine are in progress.

Fatigue Tests. Subsize specimens are being developed for rotating-beam and sheet-bending types of fatigue machines.

High-Temperature Strain Gages. Since high-temperature strain-gage wires show large resistance changes caused by irradiation, tests are being run to determine whether it will be possible to compensate for the changes by the use of an unstrained "dummy" gage. The gages will be usable if the "dummy" gage is satisfactory and if the gage factor does not vary greatly with irradiation. The Cornell Aeronautical Laboratory has furnished pairs of gages bonded to metal strips for the compensation experiments and a number of gage wires for irradiation to saturation, if possible, of resistance changes. After irradiation, CAL will fabricate the wires into gages on test strips for gage-factor determination.

Remote Electropolisher. A remotely controlled electropolisher has been designed and built for electropolishing radioactive metallographic specimens. Provisions were made for both heating and cooling the electrolytes, depending on the requirements of the polishing job under consideration. The

anode utilizes a permanent magnet to hold the mounted sample and to provide electrical contact.

Procedure of Remote Electropolishing and Etching. The cell constants of the remote electropolishing machine have been determined for polishing and etching type 347 stainless steel, for polishing uranium, and for etching Inconel. Details of baths used, electrode distances, current densities, time of operation, etc. are given for each of the metals studied to date.

Special Mounting Techniques. Special mounting techniques are necessary to provide suitable electrical contacts for electropolishing samples. The specimens are mounted in a pressure compact of uncured bakelite powder that is then center-drilled from the rear to the specimen. A small compression spring is inserted, the magnetic holding and identifying disk is placed over the top, and the specimen is cured in the standard way except for additional cooling time under pressure to prevent the spring from breaking out. About 80% of the specimens produced by this method were usable.

A second method follows the same procedure except that a low-melting alloy rod is substituted for the spring. A rod with a melting point of 130°C can be used even though the mounting temperature, measured on the external surface of the mount, reaches 145 to 150°C. Satisfactory specimen mounts can be obtained by this method and there will be no rejects.

Indium Replica Technique. Much of the tedious hot-cell work can be eliminated by use of replicas of radioactive specimens. The replicas can be handled in the normal manner, and studies of the metallurgical structures can be made with standard metallurgical equipment. Indium replicas of polished and etched Inconel have been successfully produced.

Work Performed and Status of Hot Metallography Projects. Metallurgical studies, photographs, and interpretations were made for the Fused Salts and Engineering Properties Sections of the Solid State Division and for the Metallurgy Division. Several samples were also processed for the G-E Group.

Service Work. Density, dimensional stability, and hardness measurements were made for Phillips Petroleum Company on irradiated and control specimens of aluminum, beryllium, and type 347 stainless steel. The hardness of all the materials was increased by irradiation; densities and dimensions changed very little, if at all.

The Templin tensile-tester grips are being modified to provide satisfactory holding of the smooth shanks of the MTR specimens. A remotely attached extensometer has been developed and has been tested at strain magnifications of 6000.

Assistance was given G-E personnel in the plans for adaptation of a remotely operated Instron tensile tester for elevated-temperature tests of the bond strength of irradiated sandwich-type fuel elements.

NUCLEAR MEASUREMENTS

Neutron-Spectrum Measurements in the BSF. Nuclear-threshold detectors were used to obtain flux traverse patterns along the vertical axis of a special element in the BSF, lattice loading No. 16-B. The points obtained for the radioactivants aluminum, magnesium, sulfur, gold, and cobalt are in agreement with the fission-spectrum curve normalized at 2.8 Mev to the present value for the neutron flux above the sulfur(n,p) threshold.

These measurements will be used by another group to determine the number of fast neutrons above the respective threshold energies for activation of $O^{17}(n,p)N^{17}$ and $O^{16}(n,p)N^{16}$ reactions.

MTR Neutron Flux-Radiation Damage Measurement Project. The experiments to be run in the MTR are radioactivation tests with threshold detectors, probe-type fission-chamber measurements with fission threshold detectors, and measurements of neutron damage in copper single crystals and diamond, as indicated by electrical conductivity changes and lattice parameter changes, respectively. These experiments are of immediate interest in the correlation of damage in liquid-metal loops and are also of considerable importance to general reactor studies.

A plug has been designed to automatically handle the loading and unloading of the radioactivants. Measurements will be made with threshold detectors whose characteristics are known; several new threshold reactions will also be measured for the first time in fission-type spectra.

Threshold-type fission chambers will increase the reliability of results. Preliminary tests of the first of these chambers have been made in the LITR, and operation with U^{235}, U^{238}, and Np^{237} has been satisfactory.

Nuclear Heating in the LITR. A calorimeter was fabricated for use in determining the nuclear heating of various materials in the LITR. Materials tested

were nylon, aluminum, copper, type 347 stainless steel, and lead. Nuclear heating was found to be almost independent of specific material for MTR-type lattice configurations; the average value adjacent to the lattice is 0.19 watt per gram of material for a reactor power of 1.5 megawatts. This corresponds to 3.8 watts/g for the maximum heating rate in the MTR at 30 megawatts. There is a reduction in the heating rate by a factor of 10 at approximately 16 in. from the lattice when no shielding is used. Elastic scattering of neutrons produces very little heat.

ENGINEERING PROPERTIES

LITR Fluoride-Fuel Loop. The MTR fluoride-fuel loop has been revised for operation in the LITR. In addition to the changes that have been made in physical dimensions, it will be necessary to operate the loop with a pump outside the reactor, since development of an in-pile pump has been unsuccessful. This creates problems of handling longer radioactive sections and of shielding the portion outside the reactor; however, it permits a greater temperature differential than that possible with the in-pile design.

The design of the apparatus is about 70% complete, and fabrication is about 25% complete.

LITR Sodium Stress-Corrosion Loop. An Inconel loop containing sodium was operated in the LITR for 95 hr at about 1070°F and for 66 hr at about 1270°F. A stress of 1500 psi was maintained on the tubular corrosion specimen. Sample specimens were cut from various positions in the corrosion specimen and examined metallographically.

Radiation exposures as a function of distance from the end of the hole were estimated from the activity of sections of the stainless steel jacket cut at regularly spaced intervals. These estimates are in agreement with the thermal-neutron distribution for hole HB-2 if self-shielding is taken into consideration.

Activity measurements were made on both the sodium and the Inconel specimen to determine the amount of metal transfer. The sodium has apparently picked up some palladium from the nickel-palladium braze. Further measurements of the long-lived activities are being made for identification of other elements as a supplement to the chemical analysis.

No corrosion or penetration of sodium into the Inconel can be found, although erosion of the Inconel occurred at the surface opposite the entrance tube.

ORNL Graphite Reactor Sodium-Inconel Loop. After a heater failure, the sodium-Inconel loop was removed from the reactor, the heaters were replaced, and the loop was reinserted. The controls have been made automatic, but operation has been temporarily deferred.

Sodium–Beryllium Oxide Radiation-Corrosion Test. The ARE will have a beryllium oxide moderator cooled by liquid sodium. Beryllium oxide blocks immersed in sodium and contained in stainless steel capsules were irradiated in hole HB-2 of the LITR. The temperature at the beginning of the test was 1500°F, but after 17 hr it gradually dropped to about 1000°F. During this time, the thermocouples shorted completely, but operation continued with heater input based on the power requirements to obtain 1500°F on the mockup and on measurements of power input by the reactor. The irradiation was carried out for 328 hr at 1500°F, 45 hr at 1300°F, and 110 hr at 750°F; total exposure was 2×10^{19} nvt (thermal). Control samples were subjected to the same heat treatment.

The BeO blocks were protected from the atmosphere with oil during and after removal from the capsules, and the oil and the sodium were removed by heating the blocks to 800 to 825°C for about 1 hr under vacuum. The specimens were then soaked in water for seven to ten days and heated in vacuum again. The average weight loss was 0.0005 g on both irradiated and control samples, and chemical analyses confirmed the absence of corrosion. The surfaces of all specimens remained smooth, the corners remained sharp, and there were no cracks or pits.

Radiation-induced Changes in the Engineering Properties of Metals. A request to irradiate tensile, impact, and metallographic metal specimens in the MTR has been approved.

The specimens will be cooled with reactor cooling water but must be clad to prevent corrosion. Thin sheets of lead and aluminum (pressed on), aluminum tubing (spun on), and aluminum metal spray were tested for cladding and heat transmission characteristics. Only the last two methods of cladding appear to be suitable for heat-treatable iron alloys, but in both these methods, the problem of removing specimens from the hot cell remains to be solved.

FUSED SALTS

Fused-Salt Capsule Tests in the LITR. A study of the effect of radiation on the corrosion of Inconel capsules by ARE fuel No. 30 at 815°C indicates that radiation causes an intergranular corrosion, whereas control samples show only subsurface voids or globular corrosion. The irradiated capsules displayed a time-corrosion dependence of approximately 0.5 mil/100 hr. The corrosion attack in similar capsules tested without irradiation is reported to reach a saturation between 60 and 120 hr; the irradiated specimens have, thus far, indicated no saturation up to 685 hours. Maximum corrosion occurred in the salt section of the capsule, with decreasing attack in the intermediate and vapor sections.

Fused-Salt Capsule Tests in the MTR. To avoid the vaporization of ZrF_4 from the salt and the variation in uranium concentration, the MTR corrosion capsules were designed with as small a vapor space as possible. The salt will be sampled by core-drilling progressively larger sections of the salt column so that the composition of definite sections may be examined; this eliminates the possibility of composition changes inherent in sampling molten salt. Five samples, of which four were irradiated in the MTR and one was a control, have been cored by the solid-salt sampling method. Analyses were made by mass spectrometry, and chemical analyses were performed by potentiometric and polarographic techniques. Only one series of corings showed uranium concentrations in which the concentration differed appreciably from the center to the outer edge. Further tests with large-diameter capsules will be run in the LITR and the MTR.

MTR Capsule Calculations. It was feared that, during startup of the MTR with a succession of power increases, there might be overheating in the capsules caused by momentary increases above normal in the fission heating. Calculations indicate that the reactor power may be increased on as short a period as desired without waiting for steady-state conditions and that no overheating will occur in the capsules.

Calculations for a 100-mil-dia Inconel capsule indicate that the flux at the center of the capsule is about 10% below the value as measured by unencased cobalt. The flux perturbation at the Inconel-moderator interface is about 8%.

The temperature distribution in a typical MTR salt capsule was computed with the use of several simplifying assumptions. The error introduced by the simplifications is 3%. The power generation across the capsule changes by 11%. The variation of the average power from the power generation near the outside of the fuel is 5%.

Thermal Flux in Facility A-38 of the MTR. The thermal-neutron flux in the A-38 facility of the MTR was remeasured as a check on earlier work by exposure of cobalt foil. The flux was determined to be $(2.36 \pm 0.16) \times 10^{14}$ neutrons/cm^2·sec; this value is about 15% lower than that obtained previously. About half the discrepancy results from the use of a lower value for the half life of Co^{60}; the remaining difference is attributed to differences in calibration of the ORNL and the MTR ion chambers.

Analysis of Fluoride Fuels for Cs^{137}. An attempt has been made to use the fission product Cs^{137} as an internal dosimeter for MTR irradiations of fluoride fuels. A known quantity of Cs^+ was added to a solution of the irradiated salt, and the $CsClO_4$ was then precipitated out. Recovery of Cs^{137} is not complete, probably because some Xe^{137} is lost from the liquid fuel before decay to Cs^{137} occurs. Analysis of the fuels for Cs^{137} has not yet been satisfactory as an internal monitor, but further checks will be made.

Shielded Petrographic Microscope for Irradiated Samples. A petrographic microscope has been adapted for remote operation for studying the phases present in irradiated fluoride fuels.

Electrical Conductivity of Fluorides. A circuit has been designed so that in-pile measurements of the conductivity of fused salts can be made. Power is supplied by an audio-frequency signal generator, and detection is accomplished by a balanced high-gain amplifier feeding directly into the vertical plates of an oscilloscope. Measurements can be made to ±0.0005 ohm on the 0- to 1.1-ohm scale and to ±0.002 ohm on the 0- to 11.1-ohm scale. The equipment is most satisfactory at 1 kc, but good results can be obtained from 500 cps to 5 kc.

High-Temperature Properties of Potassium Monofluorophosphate. Because of the low viscosity of the monofluorophosphates, tests were made of the high-temperature stability of K_2PO_3F and of its compatability with container materials. No decomposition of the salt occurred in graphite at 800°C and under vacuum after 2 hours. The use of Inconel or

stainless steels with K_2PO_3F appears to be undesirable.

SPECIAL PROJECTS

Annealing of Irradiated Graphite-UO_2 Materials. It has been found that about three-fourths of the neutron damage induced in graphite-UO_2 bars can be annealed out at 425°C and that the annealing is temperature dependent rather than time dependent. Analysis of electrical conductivity changes in graphite-UO_2 bars indicates that good correlation can be established between the fraction of fission damage, as indicated by conductivity changes, and the probability of escape of fission fragments from the UO_2 matrix into the graphite.

Physical-Property Tests on Thorium. The density, dynamic modulus of elasticity, electrical resistivity, and relative thermal conductivity of six thorium-metal rods were measured in the controlled apparatus in order to establish their degree of homogeneity and the degree of reproducibility of results. The rods will be irradiated in the MTR and returned to ORNL for postirradiation measurements.

Transformations of Cd-Au Single Crystals. An alloy of 49 at. % cadmium and 51 at. % gold goes through an apparent diffusionless transformation in the region just above room temperature. A single crystal of Cd-Au was irradiated in the low-temperature phase for one week in the ORNL graphite reactor. The transformation was studied by following the resistance-temperature characteristics of the material. There was no difference between the preirradiation and the postirradiation behavior.

Abnormal Aftereffects in Aluminum. A preliminary investigation was made of the untwisting of wires which have been deformed by torsion beyond their elastic limit. In order to determine whether the effects found by other investigators could be reproduced, 2S aluminum wire was twisted and measured in a device constructed at ORNL. As the wires were untwisting after being plastically deformed, an etchant was introduced, and a twisting or abnormal aftereffect was observed. The effect has been observed by other investigators and is reproducible. It is hoped that a knowledge of this phenomenon may be useful in corrosion studies of stainless steel in future experiments.

Curie Temperature of Ni-Be Alloy. Methods were investigated for the accurate determination of the Curie temperature. Changes in the inductance of a coil with a ferromagnetic core measured as a function of temperature by means of an Anderson bridge seem to give the best results.

A Ni-Be alloy containing 2.3 wt % beryllium has been fabricated, and preliminary tests have been made.

Effect of Reactor Irradiation on Thermal Conductivity and Other Properties of Structural Materials. Irradiations made on types 316 and 310 stainless steel, Inconel, and high-purity nickel at temperatures of 250 to 830°C caused no changes in the electrical or thermal conductivity beyond those attributed to experimental error. Periods of exposure were for several months in the ORNL graphite reactor or for several hundred hours in the LITR; one Inconel sample was irradiated for 406 hr in the MTR.

Thermal Conductivity of Dielectrics at Low Temperatures. A cryostat for use at temperatures of 2 to 90°K has been built and has been tested at 80°K. Experimental techniques are being developed.

RADIATION METALLURGY

CREEP UNDER IRRADIATION

W. W. Davis J. C. Wilson
J. C. Zukas

A cantilever creep test of Inconel was run at 1300°F at a stress of 6000 psi in the ORNL graphite reactor for 600 hr to simulate the conditions of the ARE pressure shell. The corresponding bench test has not yet been run, but the creep strain was less than 0.08% at 600 hr, and the secondary creep rate was about 0.05%/1000 hr. For comparison, International Nickel Company data for hot-rolled plate give 6200 psi as the stress required to give a creep rate of 0.1%/1000 hr at 1300°F.

The effect of creep strength of the decarburized layer normally existing on Inconel sheet is being investigated by the Metallurgy Division because the surface condition is thought to influence the creep behavior. The cantilever test, used for in-pile work in the Solid State Division, would be peculiarly sensitive to any changes in strength of surface layers relative to the bulk of the metal because the surface fibers that are most highly stressed might lie in the decarburized zone. A series of cantilever beams was machined from the Inconel plate from which all in-pile test specimens have been made. In one pair of test bars, the surface of the plate constituted the tension and compression faces of the beam, and another pair was oriented with the plate surface at the sides of the beam; the in-pile test specimens were made in the latter manner. In a bench test at 3000 psi and 1500°F, no difference (±10%) was found in the creep behavior of the specimens. Metallographic determination of the degree of decarburization in this plate has not yet been made, but the tests proved that the creep behavior is not being influenced by orientation of the specimen surface with respect to the mill-finished surface.

The results[1] of a pair of creep tests of Inconel in argon at 2000 psi carried out in the Metallurgy Division showed that the creep rate was extremely temperature sensitive; changing the test temperature from 1500 to 1511°F resulted in an increase in the creep rate by a factor of almost 6. The effect of temperature on the creep rate (determined in the first few hundred hours of operation) of Inconel at 3000 psi is shown in Fig. 1. The upper band represents the range of values for tests conducted in the LITR in helium; the lower band shows a summary for the bench tests in air. Two points are also shown for both a helium bench test and a LITR test in air. Although there is a fair amount of scatter in the results, it is apparent that the temperature dependence of the creep rate is not seriously affected by this wide variety of test conditions. The reference slope shown was taken from International Nickel Company data for hot-rolled Inconel.

A number of other creep-rate determinations on the bench and in the ORNL graphite reactor, both in air, and in the LITR, in air and in helium, show that the temperature dependence of the creep rate

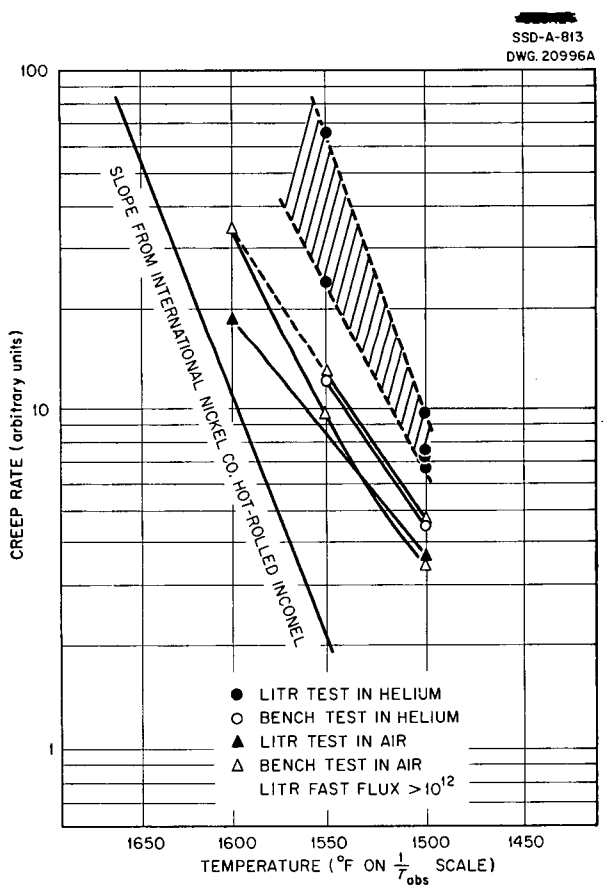

Fig. 1. Temperature Dependence of the Creep Rate of Inconel at 3000 psi.

[1] R. B. Oliver *et al.*, *ANP Quar. Prog. Rep. Sept. 10, 1952*, ORNL-1375, p. 132.

is not sensitive to test conditions over the range of variables tested.

Some pre- and postirradiation tests of constant-strength, cantilever-beam Inconel creep specimens irradiated at room temperature in the LITR have been run. The purpose of the work was to determine whether there was a real creep-reducing effect of irradiation, the kinetics of annealing of the effect, and to determine whether annealing during testing would result in temporary increases in creep rate, such as those observed when annealing (after cold-working) takes place during a creep test.[2] Data obtained at 1500°F and 3000 psi were presented previously,[3] and it was noted that the irradiated specimens had a lower creep rate during the early part of the extension than they did later. Another test at 1800 psi and at the same temperature gave the same results. Tests at temperatures down to 1300°F and at stresses that would keep the creep rate approximately constant at each temperature are being run. The metal used for this work has a decarburized surface layer as a result of the mill-annealing practice; for future specimens, the decarburized layer can be machined off before testing because of the sufficient thickness of the material furnished by R. B. Oliver of the Metallurgy Division.

Figure 2 shows the creep rate vs. temperature relationship for type 347 stainless steel. At 8000 psi in the LITR at temperatures from 1200 to 1400°F, the creep rates under irradiation are lower than those of bench tests by about 30% at 1200°F and by about 20% at 1400°F. Data obtained under similar conditions are repeated from earlier work in the ORNL graphite reactor,[4] but the disparity in the bench-test results at lower temperatures appears to be too great to be explained by any other reason than a difference in the metals tested. Chemical analyses of the bench-test specimens will be made to check this supposition.

Also shown in Fig. 2 are the results for LITR and bench tests of type 347 stainless steel over the same range of creep rates at higher temperatures (with a stress of 1500 psi). The tendency for the high-stress curve to converge at higher temperatures and the low-stress curve to do the opposite is not understood, unless there is a very strong creep-rate dependence of the irradiation effects. For corresponding temperatures, the creep rate at the higher stress is roughly 50 times that at the lower stress.

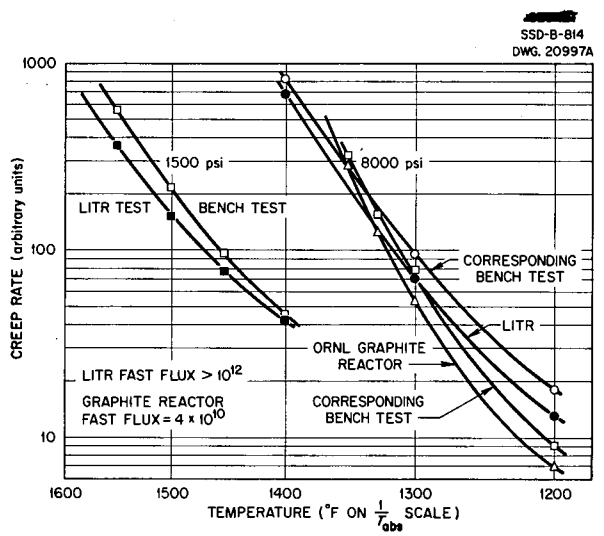

Fig. 2. Temperature Dependence of the Creep Rate of Type 347 Stainless Steel.

THERMOCOUPLES

W. W. Davis J. C. Wilson
J. C. Zukas

A platinum melting-point capsule containing sodium chloride was incorporated in a LITR creep rig after several months of bench testing. The data have not been thoroughly analyzed, but the apparent change in thermocouple output during irradiation is certainly less than 10°F for a three-week exposure in the HB-3 facility of the LITR. Postirradiation melting-point curves were determined for the capsule and couple, and after the activity decays, the same capsule will be used for further tests.

In the LITR creep apparatus, a large number of pressure-tight lead-through seals for thermocouple wires are required when tests are performed in inert atmospheres. Unsteady temperature indications were encountered when the thermocouples were brought out through inexpensive, commercial glass-metal seals similar to those used on metal vacuum

(2) J. N. Greenwood and H. K. Worner, *J. Inst. Metals* 64, 135 (1939).

(3) J. C. Wilson, J. C. Zukas, and W. W. Davis, *ANP Quar. Prog. Rep. June 10, 1953*, ORNL-1556, p. 95.

(4) J. C. Wilson, J. C. Zukas, and W. W. Davis, *Solid State Quar. Prog. Rep. May 10, 1952*, ORNL-1301, Fig. 2, p. 6.

tubes. The trouble is believed to have been caused by stray air currents that changed the temperature gradient over the short length of the metal tube to which the thermocouple wire is soldered; errors of as much as 35°F can arise from this source. A solderless connection made with ceramic insulators and Sauereisen cement appears to alleviate the difficulty. Rough measurements have been made on the effect of large temperature gradients along thermocouple lead wires away from the hot junction, and it has been found that errors of as much as 10°F can be introduced. The need for a cement with good heat conductivity and good electrical isolation to bond thermocouples to metallic surfaces has led to in-pile testing of a dental cement.

Because a large number of people are interested in the vagaries of thermocouples, an informal symposium on the subject is being planned for the fall, and a number of contributors have volunteered to present data.

EXTENSOMETERS

R. A. Weeks J. C. Wilson

Four figure-eight Bourdon tubes for use as extensometers in the MTR creep test have been fabricated and have been calibrated from room temperature to above 600°F; the calibration constants (defined as the movement of the tube tip per unit of applied pressure) of all the tubes were within ±3% of the mean. With a range of motion of about 0.020 in., the calibration constant increases about 0.03%/°F. For the contact edges, hardened type 410 stainless steel edges have proved to be satisfactory and, in conjunction with an electrometer circuit, give a consistent make-break sensitivity of better than 10×10^{-6} inch. Effects of irradiation on the calibration constant have not been conclusive, but postirradiation measurements will be possible in the MTR installation.

MTR CREEP TEST

N. E. Hinkle J. C. Wilson

A number of design modifications in the MTR creep apparatus have been made that improve the cooling of some of the more critical metal parts. Several tests requested by Phillips Petroleum Company have been performed, and insertion approval has been granted subject to a leak test of the experimental can upon its arrival at the site.

In an experimental mockup, the bursting strength of the experimental can was checked by subjecting the apparatus to an internal pressure of 400 psi; the normal operating pressure will be about 80 psi. The operability of a siphon tube designed to scavenge gases from pockets above the level of the outlet water connection on the reactor end of the apparatus was tested and was found to be satisfactory. Pressure-drop measurements during fluid flow tests showed that sufficient cooling could be obtained from the MTR water supply, which has a rather low pressure head at high flows. For heat-transfer tests, gamma heating of the experimental can was simulated by building in 3 kw of heaters. A transparent end fitted to the end of the water jacket allowed observation of the cooling-water stream at the point of direction reversal, and no cavitation was observed. The shop has started assembly of the apparatus, and shipment to the MTR site is expected within a few weeks.

IMPACT TESTS

R. G. Berggren N. E. Hinkle
J. C. Wilson

Modification of the remotely controlled impact testing machine has been completed, and the machine was operated in a hot cell to conduct impact tests on irradiated high-purity iron, a low-carbon steel, types 304, 304L, and 347 stainless steel, iodide titanium, and commercial-purity titanium. Operating experience indicates that further refinements to the impact testing machine are desirable.

The high-purity iron tested was of the vacuum-melted type manufactured by the National Research Corporation. Analysis of this iron was: 0.00032% N_2, 0.02% O_2, 0.0015% C. Impact specimens[5] were machined from stock that was swaged to $\frac{1}{4}$ in. in diameter. The metal was vacuum annealed $\frac{1}{2}$ hr at 1570°F and irradiated in the HB-4 facility of the LITR to a dosage ranging from 0.5×10^{17} nvt (>0.5 Mev) at one end to 2.5×10^{17} nvt (>0.5 Mev) at the other end of the specimens. There was considerable scatter in the impact-test data for both the ten control notches and the ten irradiated notches tested. No difference in impact strength or in transition temperature between the control

[5] R. G. Berggren and R. H. Kernohan, *Solid State Quar. Prog. Rep. Jan. 31, 1952*, ORNL-1261, p. 20.

and irradiated specimens was apparent at this dosage. The results should be considered as preliminary, and further tests will be run.

A low-carbon steel (analysis: 0.17% C, 0.20% S, 0.12% P, 0.70% Mn), vacuum annealed ½ hr at 1630°F (grain size ASTM-6, DPH 119 to 125), was irradiated in a vertical beryllium piece of the LITR to a calculated dosage of 2×10^{18} nvt (fast, as measured by cadmium ratio). The results, shown in Fig. 3, indicate a rise in impact transition temperature of about 50°C and a drop in "ductile" energy absorption of about 70%. These results are in fair agreement with previous results on carbon steels[5,6] which show substantial reduction in "ductile" impact energy and a rise of the impact transition temperature.

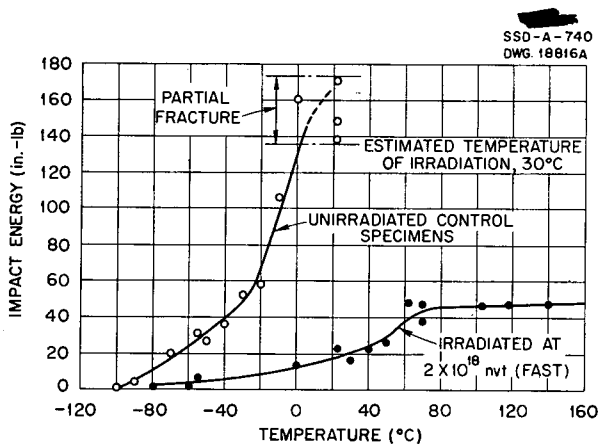

Fig. 3. Impact Strength of an Irradiated Carbon Steel.

Type 304L stainless steel specimens, annealed 1 hr, air quenched, and irradiated in a vertical beryllium piece of the LITR to a dosage of 1.7×10^{19} nvt (fast, as measured by cadmium ratio), did not fracture upon impact testing of both the control and the irradiated specimens at temperatures down to –196°C.

Type 304 stainless steel, annealed, and type 347 stainless steel, both in the annealed and as-received conditions, that had been irradiated in the HB-4 facility of the LITR to a dosage of 1.5×10^{17} nvt (>0.5 Mev) to 7.5×10^{17} nvt (>0.5 Mev) did not fracture upon impact testing of both the control and irradiated specimens at temperatures down to –196°C.

In the stainless steel specimens, tested with this notch geometry,[7] it was apparent that insufficient triaxiality of stress was induced in the notch and that the energy of the hammer was dissipated in the bending of the specimen.

Both commercial-purity and iodide titanium have been irradiated and impact tested. The commercial-purity titanium was Titanium Metals Corporation Ti 75A stock prepared by swaging, vacuum annealing 1 hr at 500°C, and furnace cooling. Analysis showed 0.008 to 0.012% H_2. The iodide titanium was arc melted, swaged, vacuum annealed 1 hr at 500°C, and furnace cooled. Analysis of the two melts tested showed 0.014 and 0.008% H_2. Impact specimens of these alloys were irradiated in the HB-4 facility of the LITR to a dosage of 1.5×10^{17} to 7.5×10^{17} nvt (>0.5 Mev). There was considerable scatter in the impact-test data for the control specimens,[8,9] but the impact values for the irradiated specimens were well within the scatter band for the corresponding control specimens. There was no observable effect of radiation on impact strength at this dosage.

The above tests indicate that several changes in the specimen design are necessary or desirable.

A new specimen geometry (Fig. 4) that has been developed induces greater triaxiality of stresses at the root of the notch. The major features are the square specimen shape (0.2 in. on a side) and the straight notch (0.060 in. deep, 0.005-in. root radius, 45-deg flank angle). Specimens of an austenitic stainless steel (type 347) in this geometry have been impact tested, and fibrous fractures, accompanied by little or no plastic deformation of the specimen outside the fracture zone, were obtained at test temperatures of –40°C and below. Specimens of other metals will be tested to determine the suitability of this geometry.

Occasionally, specimens only partially fractured remain in the vise of the machine and are struck by the pendulum on its return swing, and this results

(6) R. G. Berggren and N. E. Hinkle, *Solid State Quar. Prog. Rep. Nov. 10, 1952*, ORNL-1429, p. 9.

(7) Subsize cylindrical Izod bars, 0.204 in. in diameter, notched at 1-in. intervals with circumferential notches 0.020 in. deep, 45-deg flank angle, and 0.005-in. root radius.

(8) W. J. Fretague, *HRP Quar. Prog. Rep. Oct. 1, 1952*, ORNL-1424, Fig. 54, p. 124.

(9) W. J. Fretague, *HRP Quar. Prog. Rep. Jan. 1, 1953*, ORNL-1478, Fig. 30, p. 89.

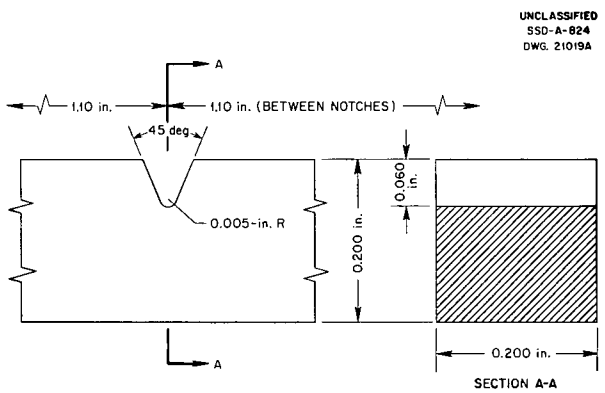

Fig. 4. Subsize Izod Impact Specimen.

in damage to the machine and to the specimen. A device to prevent such occurrences is being developed.

Because of the time involved in conducting impact tests in the hot cell, a second impact machine (the property of the Metallurgy Division) will be modified to simulate as closely as possible the characteristics of the machine now used for testing in the hot cell. If tests show that results from the two machines are comparable, the control specimens will be tested in the second machine.

Considerable time and effort have been spent in obtaining metal stock for testing. As a result, there is now on hand or on order, high-purity iron, a series of carbon steels with carbon contents up to about 1% (which will be studied with carbon content and heat treatment as variables), carbon steels of the types normally used for unfired pressure-vessel construction, stainless steels (types 304, 304L, and 347) that are typical reactor structural materials, and steels such as types 301, 302, and 305 for determining whether radiation effects are a function of "balance" compositions. In addition, a number of special steels are on hand.

Considerable effort has also been expended in developing shop procedures for machining economically the large number of specimens required.

Service work has been performed for personnel from the Metallurgy Division on the impact testing of titanium, thorium, and zirconium alloys.

FATIGUE TESTS

R. G. Berggren

Tests are planned for studying the influence of irradiation on the fatigue properties of metals.

The conclusion from the little amount of work reported is that irradiation has no appreciable effect on the fatigue in metals. However, replotting of the data of Leeser and Kemme[10] for type 304 stainless steel on log-log paper resulted in some rectification of the S-N curves, and it appears that the fatigue life (cycles to failure for a given test condition) of the irradiated specimens is 20 to 30% lower than that of the controls.

Subsize specimens are being developed for use in both sheet-bending and rotating-beam type machines so that a maximum number of specimens may be irradiated in a given facility without encountering difficulty from gamma heating. Control specimens are being run on the sheet-bending machine, and fittings and inspection jigs have been designed for the rotating-beam machine.

HIGH-TEMPERATURE STRAIN GAGES

R. G. Berggren J. C. Wilson

Previously reported results[11,12] on irradiation of high-temperature strain-gage wires showed that large resistance changes are caused by radiation.

The gages may be usable if the radiation-induced changes in resistance may be compensated for by an unstrained "dummy" gage (as in applying temperature compensation in conventional strain-gage circuits) and if the gage factor does not vary greatly with irradiation. To determine whether resistance compensation is possible, the Cornell Aeronautical Laboratory (CAL) has furnished pairs of gages bonded to metal strips for irradiation and concurrent measurement of individual gage resistances, as well as for studying the behavior of the two gages in adjacent arms of a bridge circuit. To check the effect of irradiation on gage factor, a number of gage wires have been furnished for irradiation to saturation, if possible, of resistance changes. The wires will then be sent to CAL for fabrication into gages on test strips for gage-factor calibration.

---

(10) D. O. Leeser and J. E. Kemme, *Fatigue Tests on Irradiated and Control Specimens of Stainless Steel Type 304, Zirconium, and a Tin-Zirconium Alloy*, ANL-JM-7 (presented at ORNL Radiation Damage Conference, March 23-24, 1953).

(11) R. G. Berggren and J. C. Wilson, *Solid State Quar. Prog. Rep. Nov. 10, 1952*, ORNL-1429, p. 10.

(12) R. G. Berggren and J. C. Wilson, *Solid State Quar. Prog. Rep. Feb. 10, 1953*, ORNL-1506, p. 9.

REMOTE ELECTROPOLISHER

M. J. Feldman

The advantages of electrolytically polishing and etching irradiated samples had not been overlooked when the mechanical polishing equipment was being designed for remote work. It was felt, however, that the mechanical process would provide a much greater latitude in the immediate handling of specimens. An electropolisher (Fig. 5) has now been designed to fit into the already established remote metallographic process. The sample will be remotely cut, mounted (by using one of two special techniques, cf. "Special Mounting Techniques," this report), and lapped, after which it will be transferred to the electropolisher for finishing.

The tank on the right in Fig. 5 holds a removable glass container in which the electrolyte is placed. The double-walled container provides means for continuous cooling of the solution. A glass container that can be heated has also been designed for use without the water flow when the higher temperature electrolytes are used. The double-walled tank shown at the left in Fig. 5 is the washing tank; anode, cathode, and sample are lowered into a continuously flowing water bath. The cathode is a hollow pancake type with a continuous air stream vented through small holes in the periphery for agitation of the bath. The anode utilizes a permanent magnet for holding the mounted sample and for making electrical contact and has about 1 in. of manual adjustment with reference to the cathode. The anode-cathode separation is also electrically adjustable over a distance of 2.5 inches. The sample is raised and lowered hydraulically and is transferred from one tank to the other by an electrically powered cam motion. All motions are accomplished by raising, lowering, or rotating the central shaft.

Fig. 5. Remotely Controlled Elecropolishing and Etching Machine.

PROCEDURE OF REMOTE ELECTROPOLISHING AND ETCHING

R. U. Acton

Electrolytic polishing and etching is somewhat more difficult with the remote machine than with the glass-beaker technique because the variables of temperature, electrode distance, cathode size, and agitation have a limiting range. At present, the cell constants of the machine for polishing and etching type 347 stainless steel, polishing and etching uranium, and etching Inconel have been determined.

For polishing type 347 stainless steel (Fig. 6), the electrolyte consisted of 10 parts of glacial acetic acid to 7 parts of perchloric acid.[13] This particular concentration of acids does not have the explosion hazard that other perchloric acid solutions have, and a bakelite mount can be safely used. An electrode distance of $2\frac{1}{16}$ in. was found to be quite satisfactory with a current density of 1.5 to 2 amp/in.^{2}; the time of polishing was 5 minutes. A stainless steel cathode was used with a violent stream of air bubbles for agitation. The etching was done in a 10% oxalic acid solution at 6 volts for 30 sec at room temperature.

Uranium (Fig. 7) was polished very satisfactorily with 5 parts of orthophosphoric acid, 5 parts of ethylene glycol, and 8 parts of ethyl alcohol as the electrolyte.[14] The other cell constants were

[13] G. L. Kehl, *The Principles of Metallographic Laboratory Practice*, 2d ed., p. 369, McGraw-Hill, New York, 1943.

[14] R. F. Dickerson, *Notes from the Conference on Uranium Metallography at Battelle Memorial Institute on July 10, 1949*, TID-5076, p. 8 (Feb. 7, 1952).

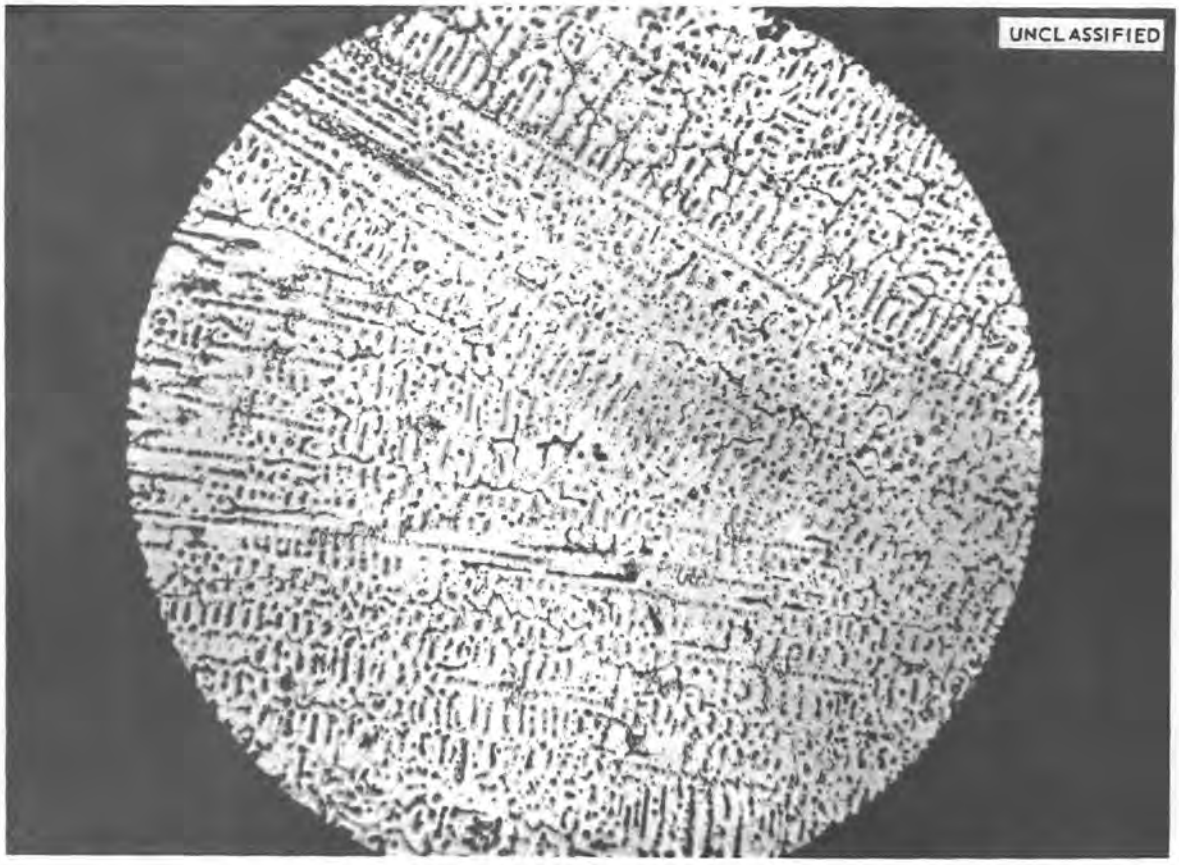

Fig. 6. Specimen of Cast Type 347 Stainless Steel Prepared on Remotely Controlled Electropolishing and Etching Machine.

30 ma/cm^2, 10-min polishing time, ½- to 1-in. electrode distance, and violent air agitation at room temperature.

All the work of this group with Inconel has been on corrosion studies, and, because the destruction of the edge of any sample is inherent in electropolishing as a result of high current concentrations at the edges, no time has been given to the development of a polishing procedure for this metal. However, with electrolytic etching, edge destruction is not inherent because very low current densities and very short exposure times are used. The electrolyte used for the etching of Inconel was a 10% solution of oxalic acid.[15] The cell constants were 6 volts for 15 sec at room temperature with mild agitation; a mechanically polished, electroetched sample is shown in Fig. 8.

[15] *Fusion Welding of Nickel and High Nickel Alloys*, technical bulletin T-2, revised May 1951, p. 34, Development and Research Division, The International Nickel Company, Inc., New York.

SPECIAL MOUNTING TECHNIQUES

M. J. Feldman A. E. Richt

The problem of preparing a bakelite-mounted sample suitable for remotely controlled electrolytic polishing has been given serious consideration. The usual methods of drilling or tapping the mounted sample and inserting a suitable electric contact are obviously not applicable to hot-cell manipulation. Since the inclusion of the soft steel identifying and magnetic gripping washer is necessary to this process, the problem became simply that of providing a means of electrical contact between two metallic sections (the washer and the sample) in a bakelite mount. Two methods have been devised for accomplishing this purpose.

Figure 9 shows the first method. A bakelite premold (pressure compact of uncured bakelite powder) is center drilled, and a small compression spring is inserted in the hole (E). The hole and the spring are so matched as to provide a snug

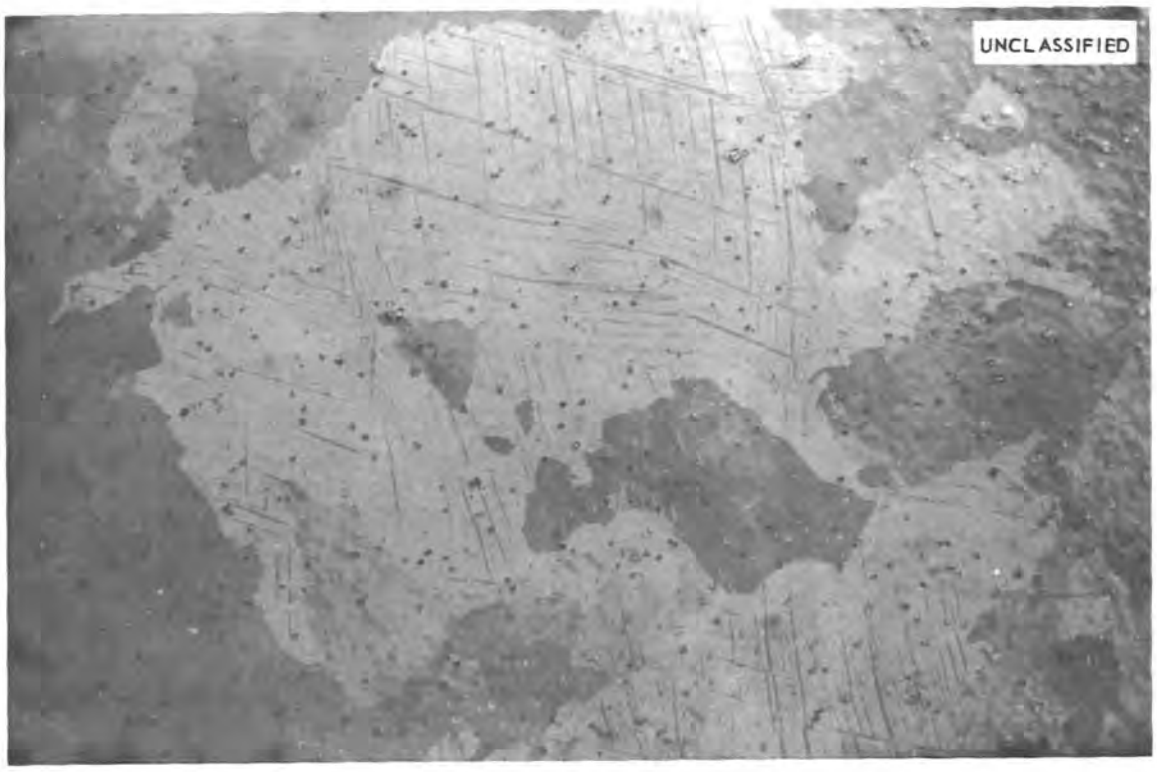

Fig. 7. Specimen of Uranium Prepared on Remotely Controlled Electropolishing and Etching Machine. Polarized light.

Fig. 8. Specimen of Inconel Mechanically Polished and Electroetched on Remotely Controlled Machine.

fit (F). The ends of the spring are bent parallel to the axis of the spring and are clipped to provide a sharp point. If the hole in the premold has been correctly sized, the spring and the premold are an integral unit and are easily handled in the hot cell. The sample is placed in the mounting press, the premold is placed on top of the sample, and the identifying disk is placed on the magnetized, upper mounting cylinder. Mounting techniques do not differ from standard procedure, with the exception of a longer time of cooling under pressure to allow the mount to hold the compressive force of the spring. A sectioned sample is shown at G. While this method was successful, it did not measure up to the standards which must be used in the metallography of hot samples. The spring method was successful eight out of ten times, but rather than chance the possible 20% failure, an even more dependable method was developed.

In the second method (Fig. 10), the premold is also used, but the spring used in the first method is replaced by a rod of low-melting alloy (B). The hole in the premold is drilled to provide a snug fit for the alloy rod, and this makes a single unit (C). The sample, premold, and washer are placed in the mounting press as in the first method, and standard techniques are followed. Some reasonable care should be exercised in the selection of the length

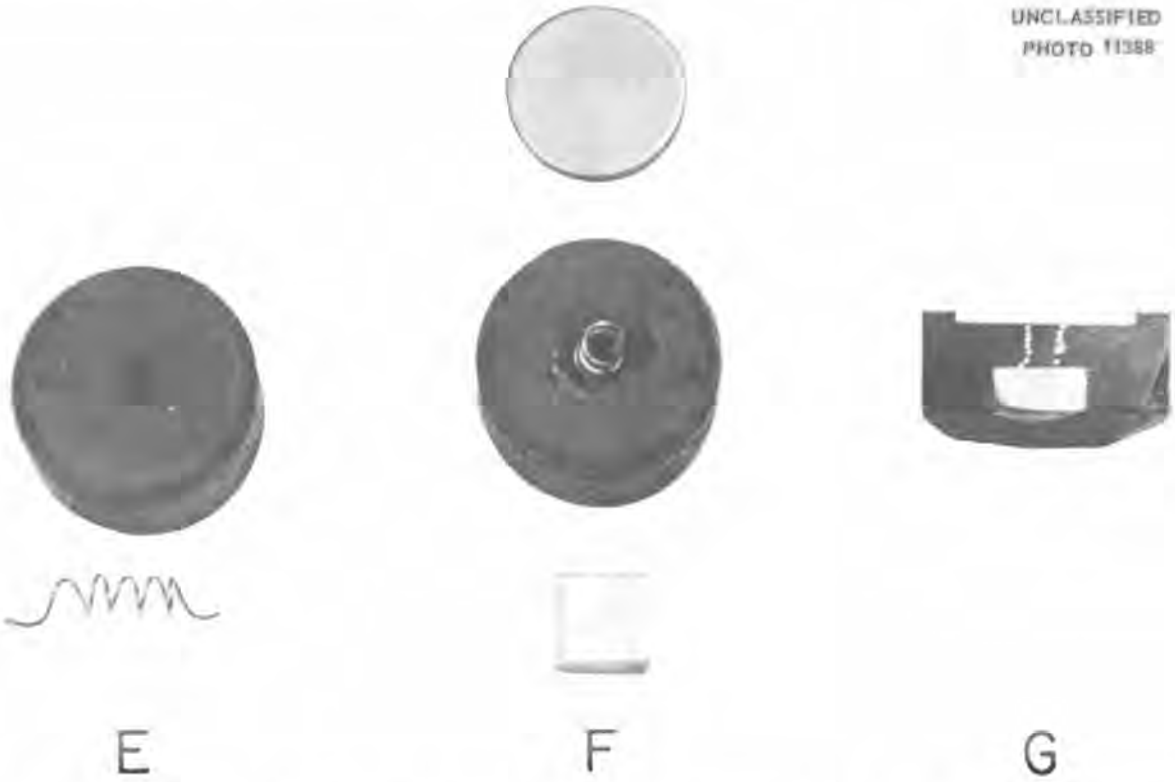

Fig. 9. Component Parts and Section of Specimen Mounted with Wire Spring for Electrical Contact.

of alloy rod relative to the thickness of the sample. Also, on samples that contain a hole, the hole in the premold can be placed eccentric to the centered sample. The selection of the alloy rod is somewhat dependent upon the usual mounting temperatures employed. The best results are obtained with an alloy whose composition is 56% Bi, 40% Sn, and 4% Zn (wt %) and whose melting point is 130°C; the mounting temperature is 145 to 150°C, but this is read on the external surfaces of the mount, and no melting of the alloy rod during mounting has been noted. The high temperature (relative to the melting point of the rod) allows for a very plastic deformation of the rod as seen at D, which shows the cross section of two samples mounted in this manner. In general, it is felt that the electrical connection is mechanical in nature, as shown in Fig. 11. In some instances, there appeared to be a wetting of the sample surface by the alloy rod, as shown in Fig. 12. The alloy rod method of mounting for electropolishing has been very successful, and, with care in the selection of rod length, mounts can be produced without rejects.

An added merit of these two methods is their ease of application to regular laboratory mounting techniques in which a mounted sample is to be electropolished or etched. The premolds are commercially available, the springs are simple to wind, and the alloy rod is easily cast in a section of pyrex tubing which has been drawn down to a very small hole at the lower end and spread to form a small funnel at the upper end.

INDIUM REPLICA TECHNIQUE

M. J. Feldman

The study of the use of indium for replication of polished and etched specimens is of interest for two reasons: the properties of indium are unique for this purpose, and the application of replica techniques to the metallography of irradiated metals opens a very valuable field. The use of replicas eliminates the necessity of micro- or macroviewing and photographing facilities in the cell and also permits the use of the electron microscope in this work.

UNCLASSIFIED
PHOTO 11389

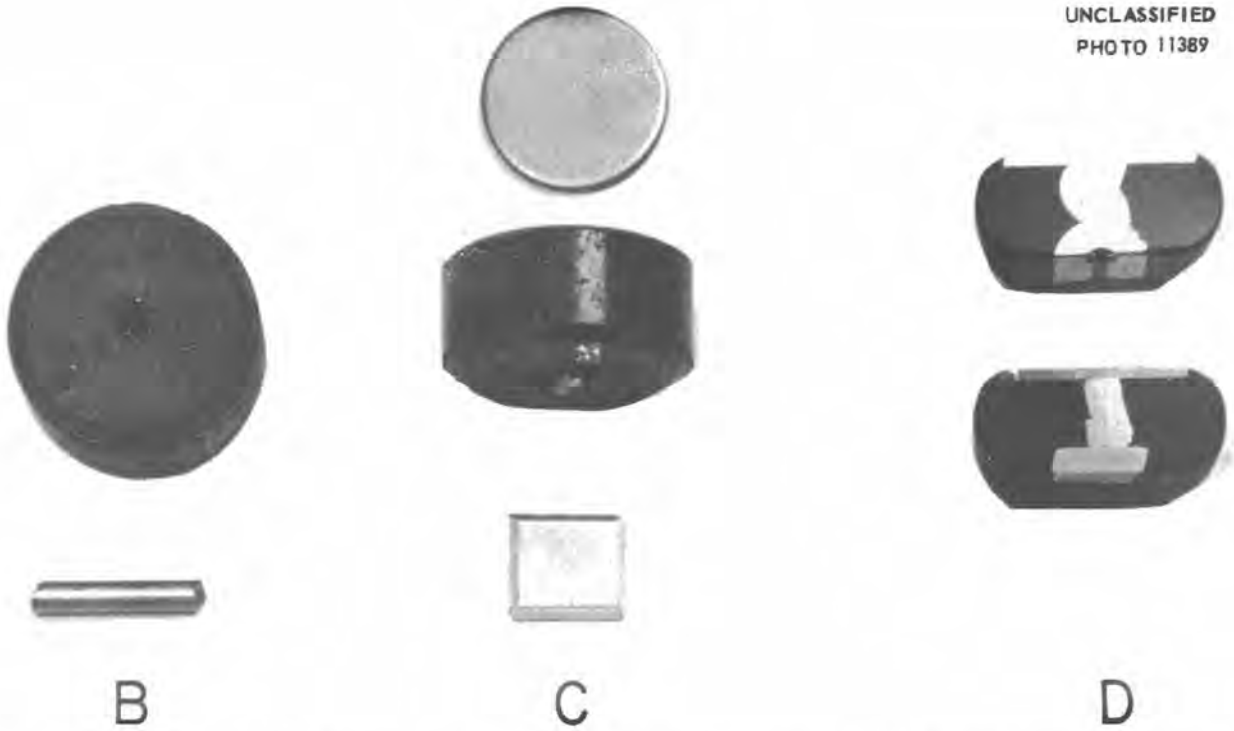

Fig. 10. Component Parts and Section of Specimen Mounted with Alloy Rod for Electrical Contact.

Fig. 11. Mechanical Bond Between Alloy Rod and Specimen for Electropolishing and Etching. 100X. Reduced 32%.

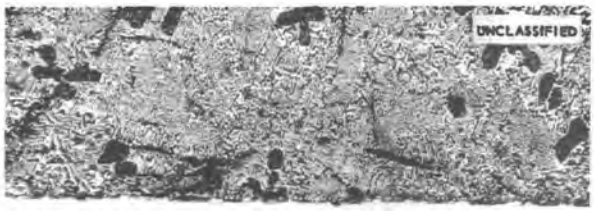

Fig. 12. Juncture of Alloy Rod and Specimen Showing Surface Wetting. 100X. Reduced 32%.

The indium sheet ($\frac{1}{16}$ in.) is mounted to a section of polystyrene rod by placing a $\frac{1}{2}$-in.-square section of the sheet on the benzene-softened end of the rod and by applying enough pressure to flow the indium over the end of the rod. When the softened polystyrene face has hardened, the excess indium is trimmed off. The indium surface is next carefully scraped to remove as much of the oxide as possible. The indium and the polished and etched sample (I and H, respectively, Fig. 13) are then placed together, and a pressure of 100 to 200 psi is exerted for a short time. Exact times, pressures, and surface conditions for various metals will be ascertained in the later stages of this work. There are many factors yet to be determined, as shown by

present work on the replication of Inconel. Indium replicas of a freshly etched (glycerol regia) surface of Inconel caused adherence of the indium to the Inconel. When the etched Inconel was allowed to remain in air for a few hours prior to replication, there was no problem of sticking. Figure 14 shows the results of indium replication of Inconel.

WORK PERFORMED AND STATUS OF HOT METALLOGRAPHY PROJECTS

M. J. Feldman R. U. Acton
A. E. Richt

During the past six months, metallographic photographs and interpretations were made for the following groups.

Fig. 13. Polished and Etched Specimen and Indium Replica.

Fused Salts Section of the Solid State Division. Nine irradiated fluoride-fuel capsules were metallographically examined for the Fused Salts Section of the Solid State Division. Three capsules were irradiated in the MTR, while the other six were irradiated in the LITR. To correlate this work, seven control samples have been processed. Figures 15 and 16 are photographs of the MTR and LITR irradiated capsules.

Engineering Properties Section of the Solid State Division. Sections of a sodium loop were metallographically examined for the Engineering Properties Section. The loop, exposed in the LITR, contained a creep-test specimen which was also run. Figure 17 is a photograph of the flow tube through which liquid sodium was flowing.

General Electric Company, Lockland. Four sets of samples were processed for the G-E Group at Lockland, Ohio. Three were irradiated fuel sandwiches, and the fourth was for an evaluation of two types of protective coatings on stainless steel under ORNL graphite reactor and LITR irradiations. Figure 18 shows a section of a UO_2–stainless steel fuel sandwich that had been irradiated in the LITR.

Metallurgy Division. Two samples have been examined for the Metallurgy Division. The first was a series of sections from an ORNL graphite reactor slug jacket. The sections were checked to evaluate the evenness and soundness of the aluminum and Al-Si bond. The second sample was an

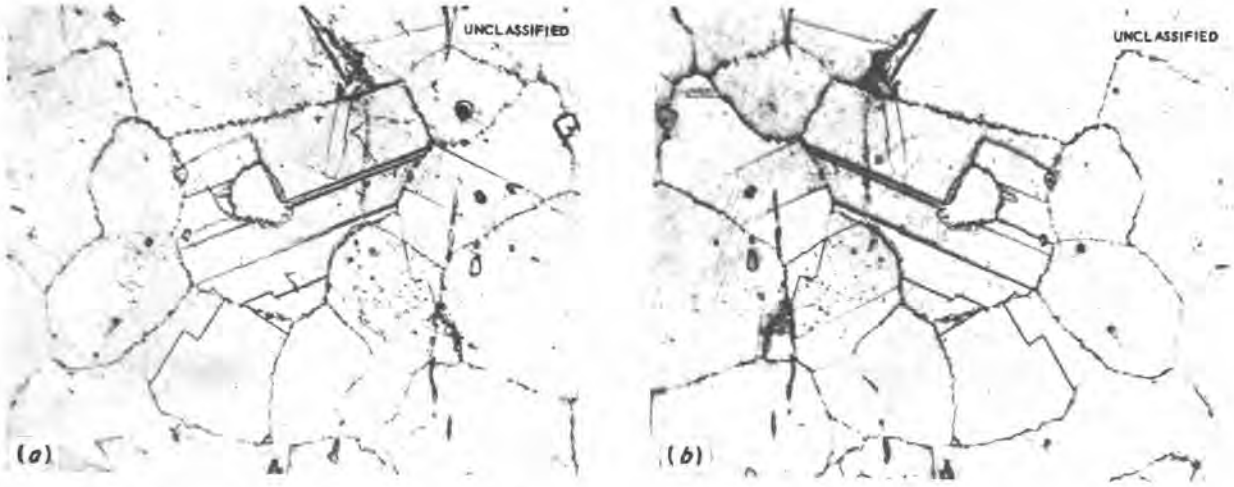

Fig. 14. Comparative Photomicrographs of Inconel Specimen and Indium Replica. (*a*) Indium replica, (*b*) Inconel specimen. 500X. Reduced 29%.

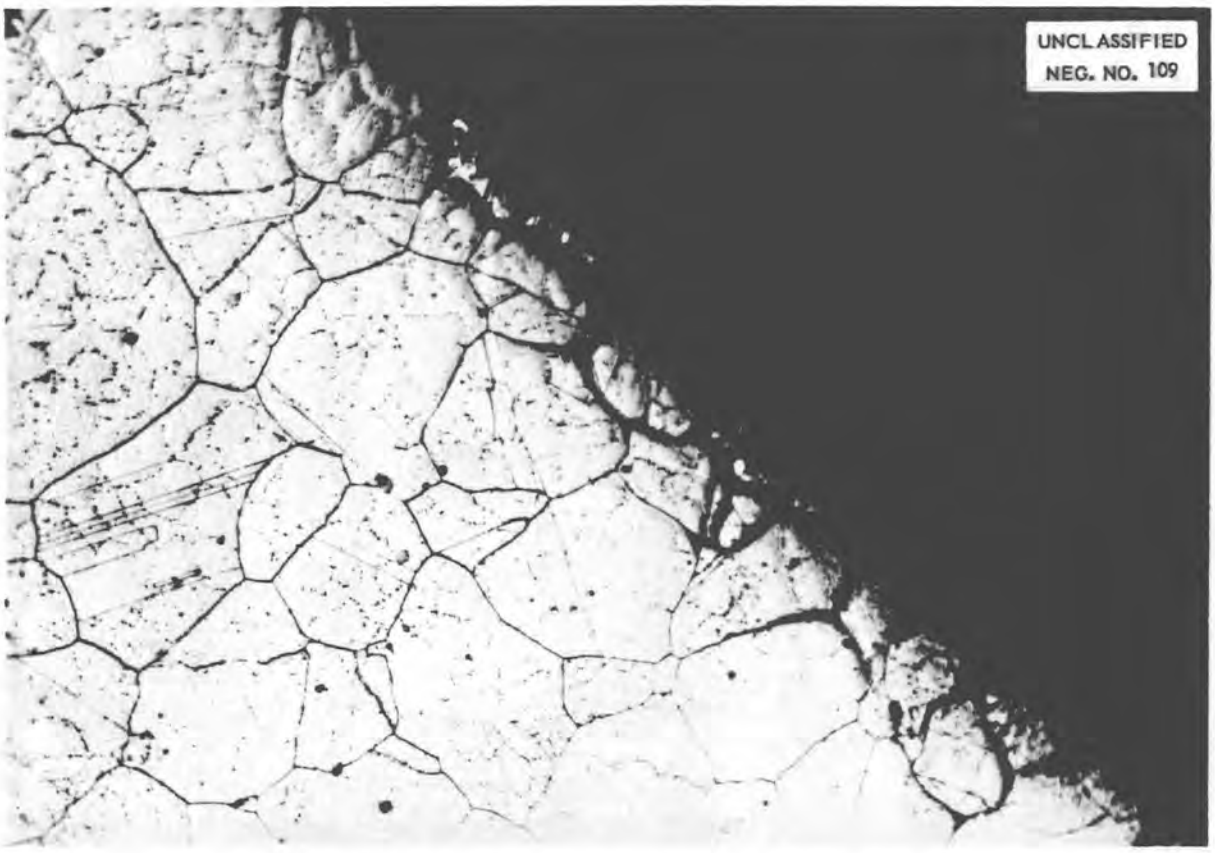

Fig. 15. Fuel Capsule Irradiated in LITR. 250X.

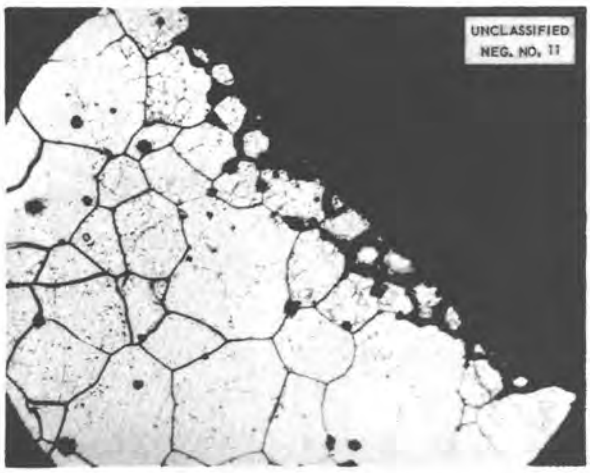

Fig. 16. Fuel Capsule Irradiated in MTR. 250X. Reduced 33%.

experimental fuel tube made by the Powder Metallurgy Group and had been irradiated in the sodium loop. Figure 19 shows one portion of a section of the slug jacket.

SERVICE WORK

R. W. Hall[16] J. C. Wilson

At the request of the Phillips Petroleum Company, density, dimensional stability, and hardness measurements were made on the first of a series of irradiated and control specimens of aluminum, beryllium, and type 347 stainless steel. The specimens were cylindrical tensile bars $3\frac{1}{2}$ in. long with $\frac{1}{4}$-in.-dia test sections and $\frac{11}{32}$-in.-dia shoulders. The irradiated specimens, in contact with the reactor cooling water, had been exposed in the MTR in an L piece to 3×10^{20} nvt (fast). Before the measurements were made, the irradiated specimens were chemically cleaned to remove the scale which had formed on them during the irradiation.

Rockwell hardness measurements were made on the shoulders of the tensile specimens, and, as indicated in Table 1, the hardness of all the materials was increased by irradiation. The hardness

[16] On loan from NACA, Cleveland.

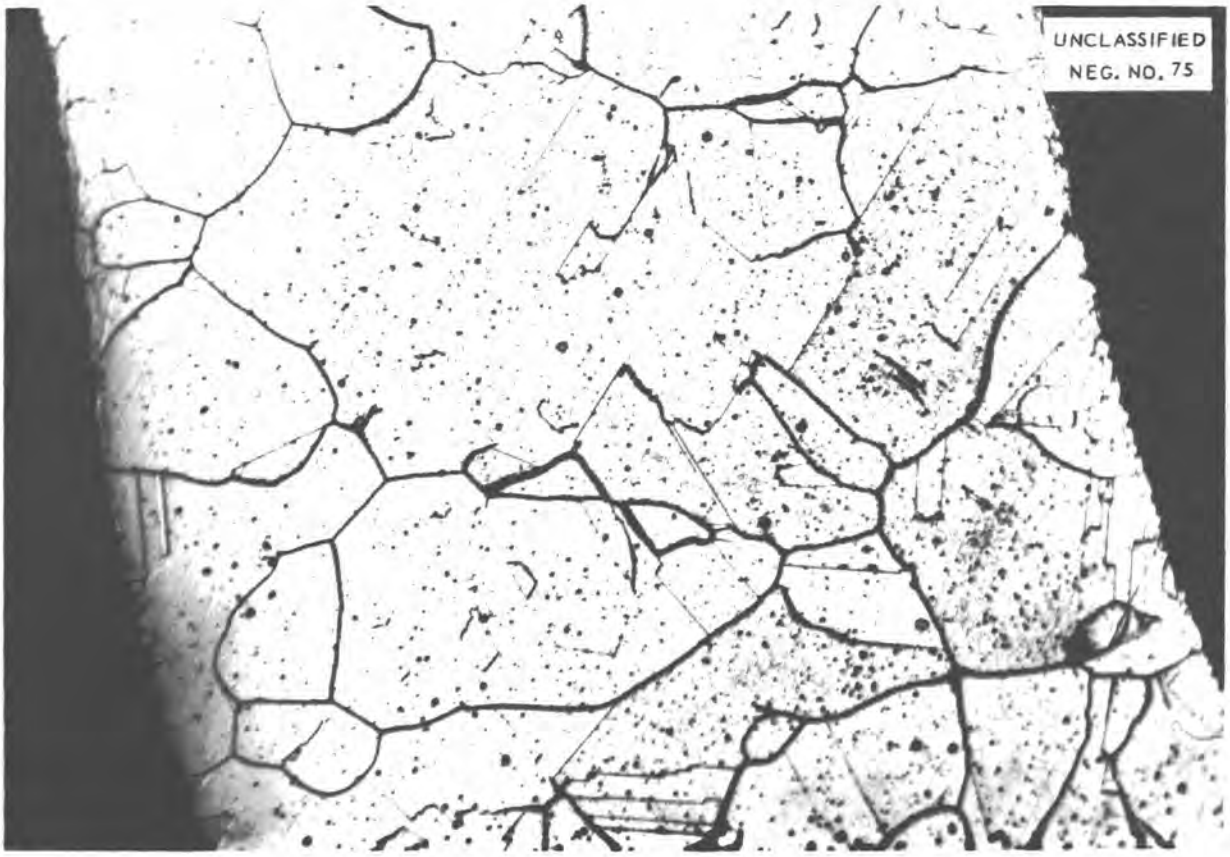

Fig. 17. Section of Irradiated Sodium Loop. 200X.

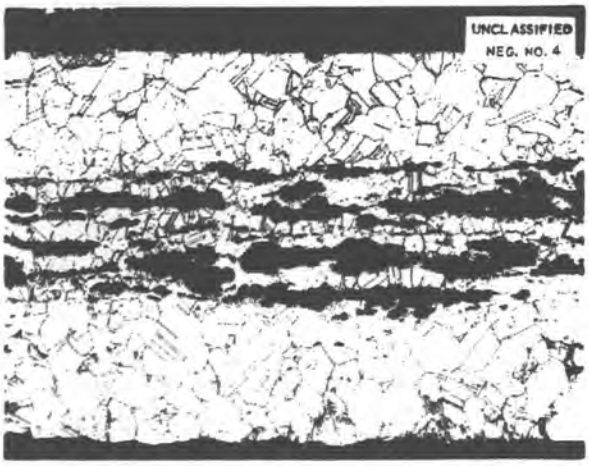

Fig. 18. G-E Fuel Sandwich Irradiated in ORNL Graphite Reactor. 250X.

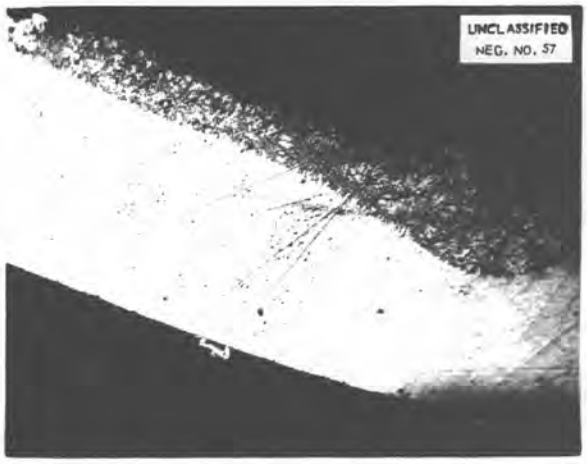

Fig. 19. ORNL Graphite Reactor Slug Jacket. 55X. Reduced 32%.

TABLE 1. HARDNESS AND DENSITY OF METALS IRRADIATED TO 3×10^{20} nvt (FAST)

METAL	SPECIMEN NUMBER AND CONDITION	ROCKWELL HARDNESS		DENSITY AT 25°C (g/cc)
		Average	Range	
2S aluminum	1, irradiated	42 F	37 to 46 F	2.712
	17, control	2½ F	−9½ to +10 F	2.713
	18, control	1½ F	−16½ to +11 F	2.713
356S aluminum	5, irradiated	61½ B	57½ to 68 B	2.660
	19, control	25½ B	23 to 29 B	2.663
	20, control	26 B	21½ to 29 B	2.667
QMV beryllium	9, irradiated	87½ B	86½ to 88½ B	1.847
	21, control	68 B	67½ to 69 B	1.847
	22, control	70½ B	68½ to 72 B	1.847
347 stainless steel	13, irradiated	20 C	17½ to 22 C	7.896
	23, control	14 C	13½ to 15 C	7.890
	24, control	13 C	12 to 14 C	7.907

scales were chosen so that any anticipated hardness increases would be encompassed and so that the specimen hardness numbers would fall on a part of the range of the testing machine that would permit small changes in hardness to be resolved. If required, more precise hardness measurements can be made with the remotely operated Tukon hardness tester on the unstrained portions of the specimen shanks after the tensile test.

Density measurements were made by hydrostatic weighing in carbon tetrachloride on a remotely operated balance with a precision of approximately 0.05%. Because of the difference in density of the two control specimens in the case of type 356S aluminum and type 347 stainless steel, there is considerable uncertainty as to the extent of any radiation-induced changes. However, density measurements made by Phillips Petroleum Company personnel on control coupons cut from the same stock as the specimens measured here gave the following density values in grams per cubic centimeter: type 347 stainless steel, 7.908; type 356S aluminum, 2.670; type 2S aluminum, 2.714; and type QMV beryllium, 1.846. It may be seen that these values agree fairly well with the higher figures in Table 1. The cause of the difference in the stainless steel controls is not known; but since the type 356S aluminum is a cast alloy, density changes from specimen to specimen are not unexpected.

Length and diameter measurements made on the irradiated and chemically cleaned specimens and compared with preirradiation values determined by Phillips personnel showed no dimensional change greater than 0.001 in. (the precision of the preirradiation measurements).

Qualitative magnetic measurements with an Aminco-Brenner Magne-Gage showed that irradiated stainless steel specimen No. 13 and unirradiated specimen No. 24 were similar, but that No. 23 was considerably less magnetic than either of the above. It should be noted that No. 23 differed in density (Table 1) from the two companion specimens.

Two 10,000-lb-capacity Templin grips have been fitted with double-acting air cylinders for remotely controlling the motion of the jaws so that MTR tensile samples may be pulled. The smooth cylindrical shanks of the specimens have been difficult to grip tightly, and special jaw modifications to overcome the difficulty are under way.

An extensometer that has been under development for some time was tested for use on the MTR specimens; it may be attached to the specimen remotely. The output can be plotted against stress on an x-y recorder, and the amplification (in terms of inches of chart movement per inch of specimen extension) can be continuously varied from 0 to 6000. This is about six times the sensitivity of commercial recording extensometers that are generally not adaptable to remote operation.

Assistance was given to personnel of the GE-ANP Division (Lockland) on the adaptation of the remotely operated Instron tensile testing machine for elevated-temperature tests of the bond strength of irradiated sandwich-type fuel elements.

NUCLEAR MEASUREMENTS

NEUTRON-SPECTRUM MEASUREMENTS IN THE BSF[1]

J. B. Trice F. W. Smith[2]

A series of fast-neutron flux measurements was made by using nuclear threshold detectors to obtain flux traverse patterns along the vertical axis of a special element in the BSF, lattice loading No. 16-B (see Fig. 20). This method was used because it is more uniquely adaptable than other methods for measuring neutrons in locations which are not readily accessible. The purpose of the measurements was to find the number of fast neutrons above the respective threshold energies for activation of the $O^{17}(n,p)N^{17}$ and $O^{16}(n,p)N^{16}$ reactions being studied by the Shielding Group. Both these reactions are of interest to the Submarine Reactor Shielding Program or, for that matter, to any reactor program in which water must circulate through a high neutron flux field and through a region in which personnel may be biologically endangered by the radioactivity induced in the water. The reaction $O^{17}(n,p)N^{17}$ is of unique interest because N^{17}, with its 4-sec decay period, emits a neutron with an energy of about 1 Mev. Details of the experiments in which the reaction cross sections were measured have been reported by Cochran *et al.*[3]

Aluminum, magnesium, sulfur, and cobalt were the radioactivants used for making the vertical neutron traverses which extended from about 6 in. below the reactor center line to about 9 in. above the top of the lattice (about 25 in. above the center line), as shown in Fig. 21. Neutron fluxes above 8.1, 6.2, 4.6, and 2.8 Mev were obtained respectively by the reactions $Al^{27}(n,\alpha)Na^{24}$, $Mg^{24}(n,p)Na^{24}$, $Al^{27}(n,p)Mg^{27}$, and $S^{31}(n,p)P^{31}$. Thermal-flux traverses were obtained from gold and cobalt measurements. Figure 22 shows the flux traverses obtained by these radioactivants; Fig. 23 shows how closely these measurements correspond to a fission spectrum at the reactor center line. The heavy line shown is the fission spectrum curve as measured by Watt[4] and normalized at 2.8 Mev to the present value for the neutron flux above the sulfur(n,p) threshold.

[1] Solid State and Physics Divisions joint project.

[2] Consolidated Vultee Aircraft Corp.

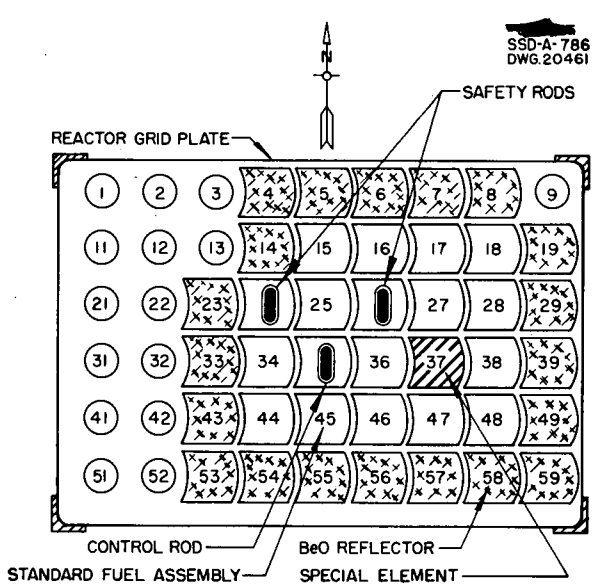

Fig. 20. BSF Fuel Assembly, Loading No. 16-B.

[3] R. G. Cochran, F. C. Maienschein, J. B. Trice, K. M. Henry, and T. A. Love, "Cross Sections for Neutron-induced Activities in O^{16} and O^{17}" (to be published).

[4] B. E. Watt, *Energy Spectrum of Neutrons from Fissions Induced by Thermal Neutrons*, LA-718 (Dec. 17, 1948).

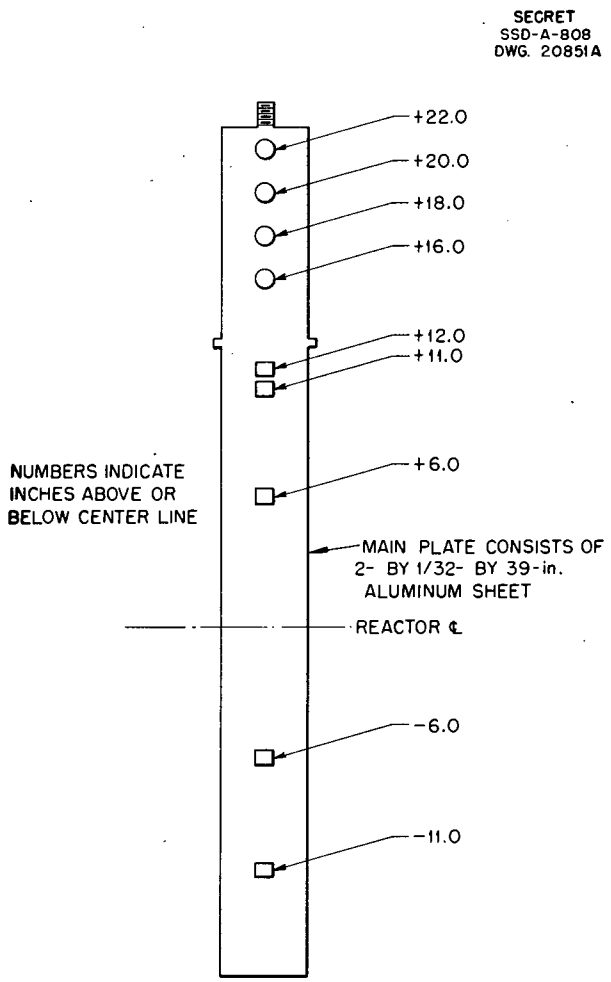

Fig. 21. Sample Holder for Test in BSF.

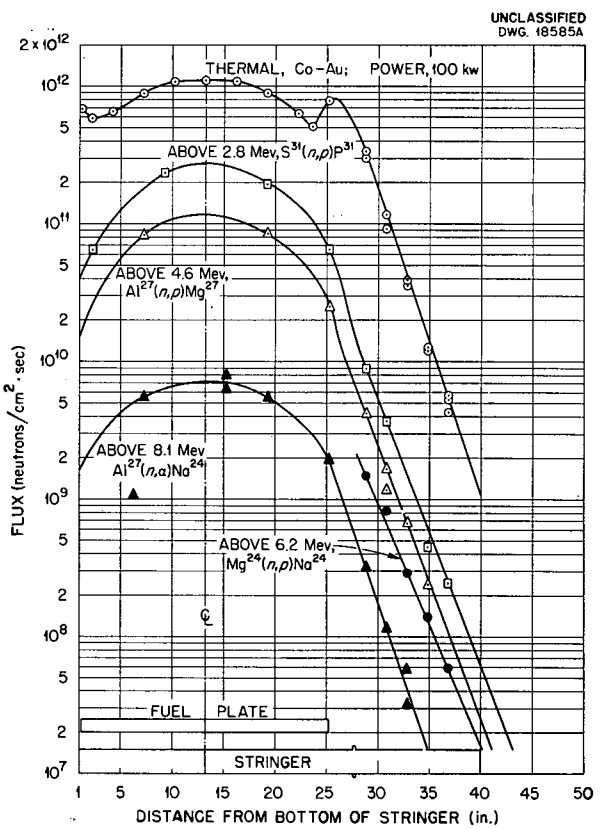

Fig. 22. Flux Traverses in Special Element of BSF.

MTR NEUTRON FLUX-RADIATION DAMAGE MEASUREMENT PROJECT

J. B. Trice P. M. Uthe[5]

The project for the measurement of MTR neutron flux-radiation damage evolved from an experiment in which the neutron-flux spectra along the axis of the HB-3 facility in the MTR were to be measured. The results were to have been used for correlation studies between the fast-neutron-flux energy distribution and the radiation-induced corrosion in an Inconel loop filled with a high-temperature liquid fuel of the type being studied in the present ANP series. Since the beginning of the experiment, however, it has been evident that the flux measurements alone could yield information of interest to reactor studies in general, as well as to a specific liquid-fuel corrosion problem. For this reason, the flux-measurement project has become somewhat larger in scope than it was at its inception. The three phases of the experiment now include a series of radioactivation tests in which various so-called threshold detectors are used, measurements with three probe-type fission chambers in which fission threshold detectors are used, and measurements of neutron damage in copper single crystals and in diamond, as indicated by changes of electrical conductivity and lattice parameter, respectively.

Design drawings for a plug to handle the radioactivant tests have been completed. This special plug includes the following features:

1. All samples are automatically loaded and unloaded by means of compressed air.
2. The transfer of radioactive materials from hot irradiation containers to nonradioactive capsules is done by means of a remotely controlled mechanism inside the shielded external part of the plug facility.

[5] USAF.

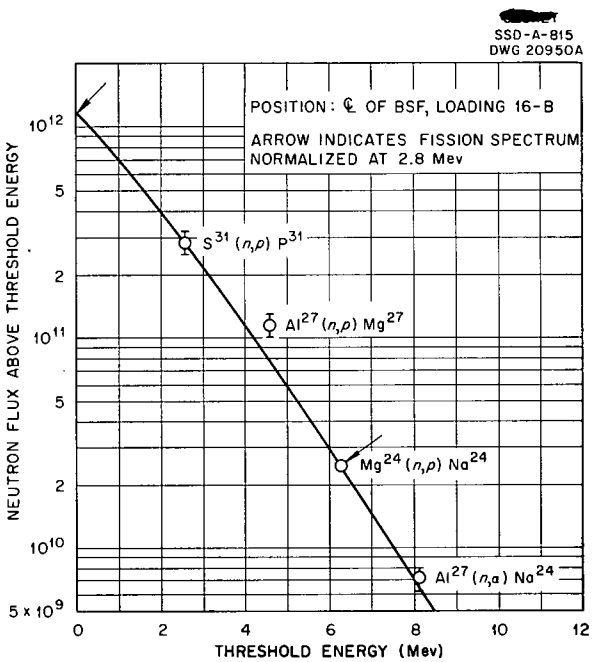

Fig. 23. Neutron Flux Above Threshold Energy as a Function of Threshold Energy.

3. Samples are contained in capsules that are fixed in long rectangular rabbits and injected into the high-flux region where, at rest position, they are exposed to neutrons along a 36-in. section of the plug adjacent to the reactor lattice. This permits an unusually long traverse measurement to be made.

4. The internal regions are water cooled to dissipate heat resulting from gammas.

It will be possible to make complete measurements with threshold detectors whose characteristics are already well known. This will supply a considerable amount of information concerning the flux-energy distribution along the hole axis. However, it will also be possible to measure several threshold reactions for the first time in fission-type spectra.

It is thought that the threshold type of fission chambers will provide a great increase in the reliability of results which are initially obtained with ordinary radioactivants, principally because the fission cross sections as functions of neutron energy are more reliably known. The first of a series of three such chambers was operated satisfactorily with 96 μg of U^{238} in a fast-neutron flux of approximately 10^{11} nv in hole HB-2 of the LITR. This chamber, designed and constructed by R. E. Zedler of the Instrumentation and Controls Division, is shown schematically with its associated electronic equipment in Figs. 24 and 25. Operation in fast-neutron-field intensities of 10^{11} nv for 50 hr continuously, and with no appreciable variation in counting rate, indicated a good resistance to radiation damage. The response, however, was nonlinear because of the high gamma ionization which caused coincidence losses. Less fissionable material on the counter electrode will not correct this condition.

The flexibility of the chamber is indicated by its successful operation with U^{235}, U^{238}, and Np^{237}. For the MTR tests, Th^{232} and, if possible, U^{236} will be added to this list of fissionable threshold detectors.

Preliminary calibration tests indicate that the chamber detection efficiency is greater than 99%.

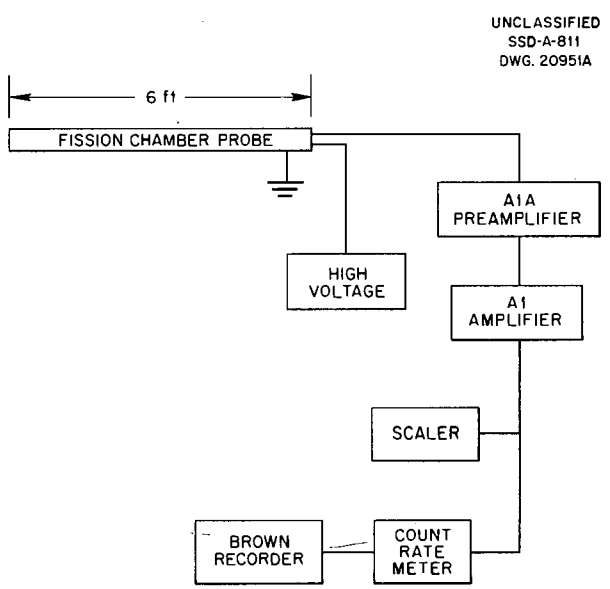

Fig. 24. Schematic Diagram of Fission Chamber and Associated Electronic Equipment.

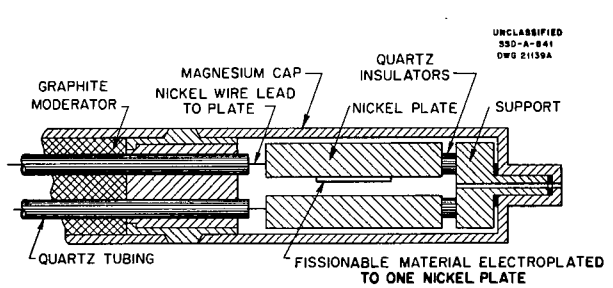

Fig. 25. Fission Chamber.

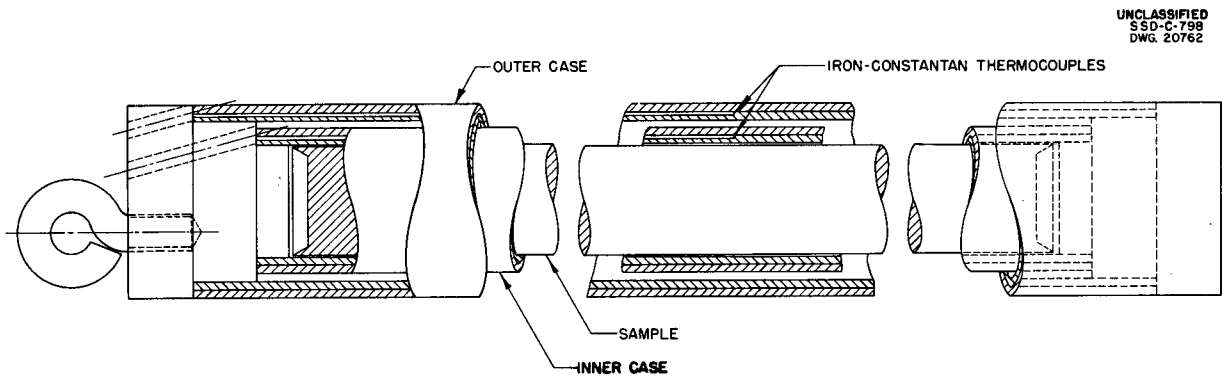

Fig. 26. Schematic Diagram of Nuclear-Heat Calorimeter.

NUCLEAR HEATING IN THE LITR

J. B. Trice F. W. Smith
F. J. Muckenthaler[6]

A nuclear-heat calorimeter used to measure the radiation-induced heating in various materials is shown in Fig. 26; a schematic diagram of the electrical calibration circuit is shown in Fig. 27. Materials for the recent tests in the LITR, hole HB-2, were chosen partly because of their sensitivity to neutrons and to gamma rays. Thus, a cylindrical specimen of nylon was chosen to represent hydrogenous materials. Aluminum, copper, type 347 stainless steel, and lead (solid and hollow) were chosen for investigation of the gamma absorption as a function of atomic number for structural materials with Z numbers ranging from 23 to 80. It was thought that these metals would be a representative group of reactor materials.

Calorimeter calibration curves shown in Fig. 28 indicate the nuclear heating rate expected as a function of the calorimeter-wall thermocouple voltages. These curves give the outward heat flux as a function of temperature drop across the walls and of the temperature of the outer calorimeter wall – whose rate of heat loss is determined uniquely from its interaction with the external environment – and were obtained by simulating electrically the calorimeter specimen.

For these measurements, the lattice loading shown in Fig. 29 is representative. Measurements taken along hole HB-2 from the ¼-in. aluminum plate (which separates HB-2 from the fissioning material) outward along the hole axis for almost 2 ft are given in Figs. 30 through 35. Examination

[6] Shielding Group, Physics Division.

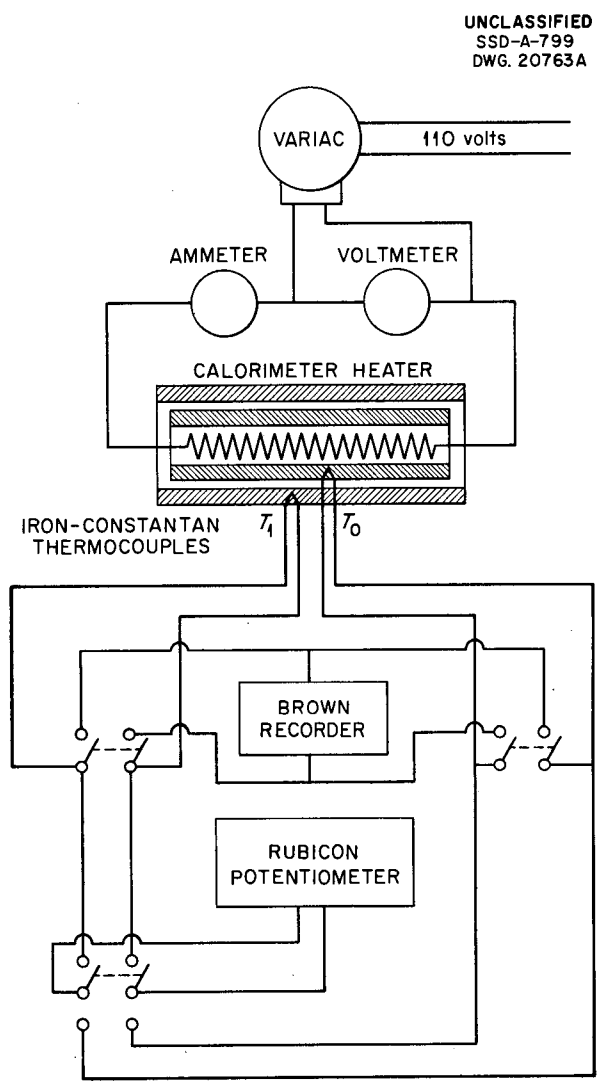

Fig. 27. Electrical Calibration Circuit for Nuclear-Heat Calorimeter.

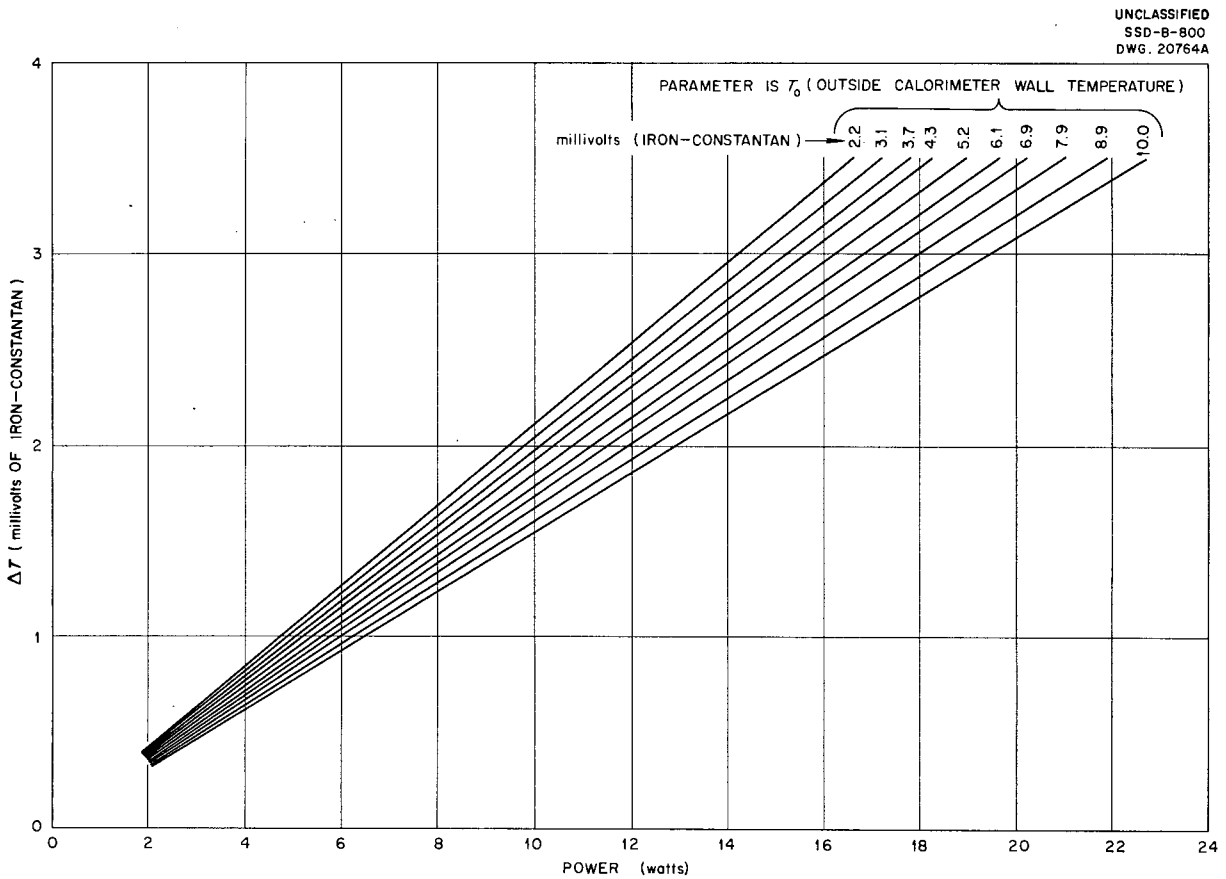

Fig. 28. Calibration Curves for Nuclear-Heat Calorimeter.

of these curves shows that nuclear heating is almost independent of specific material for MTR-type lattice configurations. Adjacent to the lattice the average value for aluminum, copper, stainless steel, lead, and nylon is 0.19 watt per gram of material at a reactor power of 1.5 megawatts. This corresponds to 3.8 watts/g for the maximum heating rate in the MTR at 30 megawatts. It should be emphasized that this is the maximum heating rate and hence would not be a very representative number to use for designing an experimental apparatus to occupy a large region in the HB hole. A reduction by a factor of 10 in the nuclear heating rate occurs at approximately 16 in. from the lattice when no shielding is used in the HB hole. Heat-production estimates for the apparatus in this region would be maximum since the material inside the hole would serve as a radiation shield and would therefore intercept many heat-producing gamma rays.

It is evident from Fig. 35 that elastic scattering of neutrons produces very little heat even in hydrogenous materials, since the heating rate for nylon (high hydrogen content) is about the same as (in fact, slightly less than) that for aluminum and the other materials tested.

The experimental values were reproducible to within ±5%, and it is estimated that the over-all errors add up to a total value no greater than ±10%.

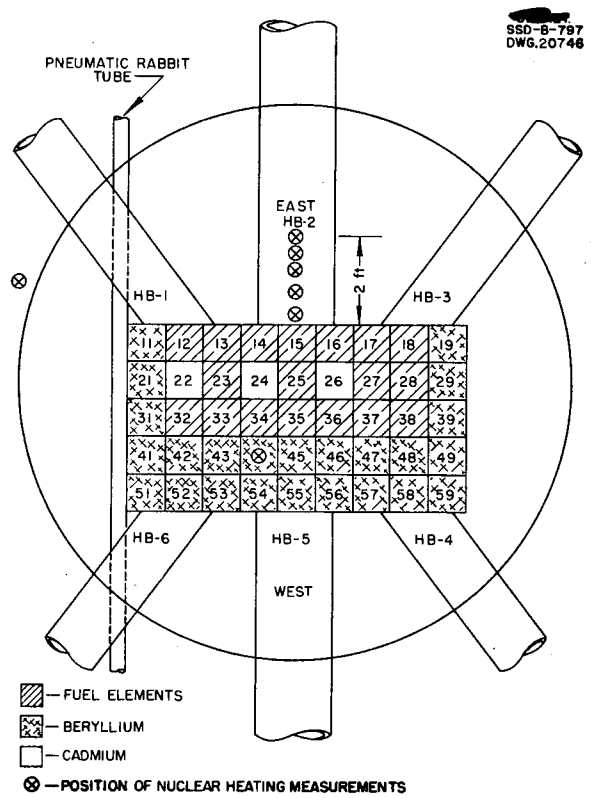

Fig. 29. Lattice Loading of LITR During HB-2 Nuclear Measurements.

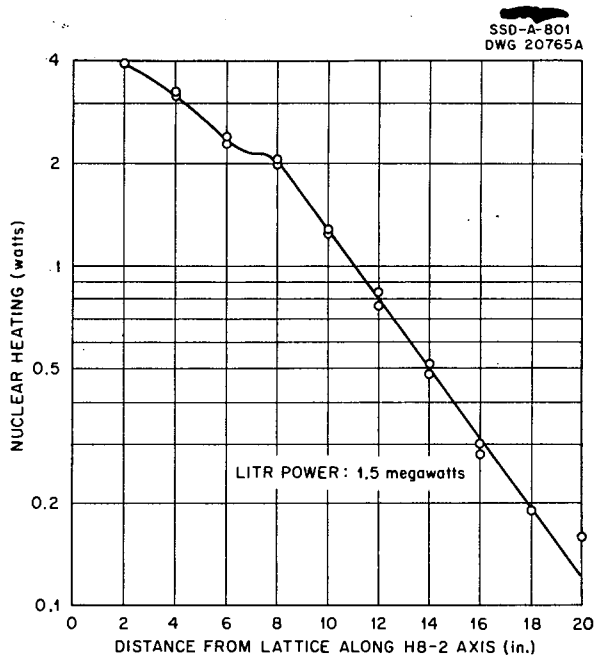

Fig. 30. Rate of Nuclear Heating of Empty Calorimeter in HB-2.

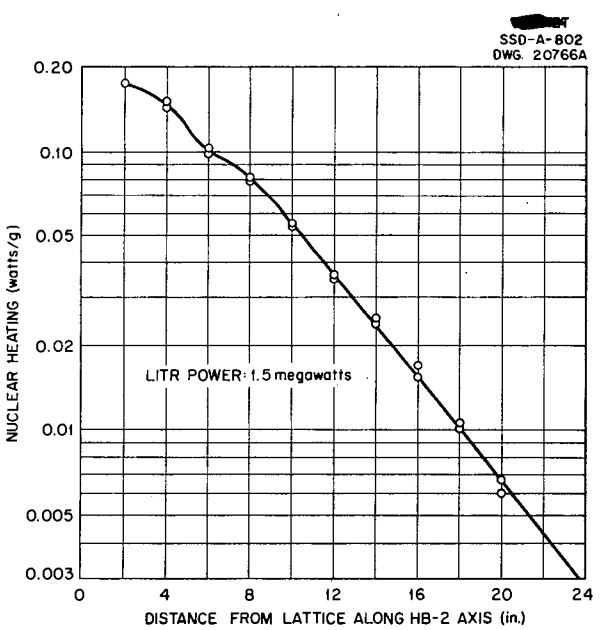

Fig. 31. Nuclear Heating of Aluminum in HB-2.

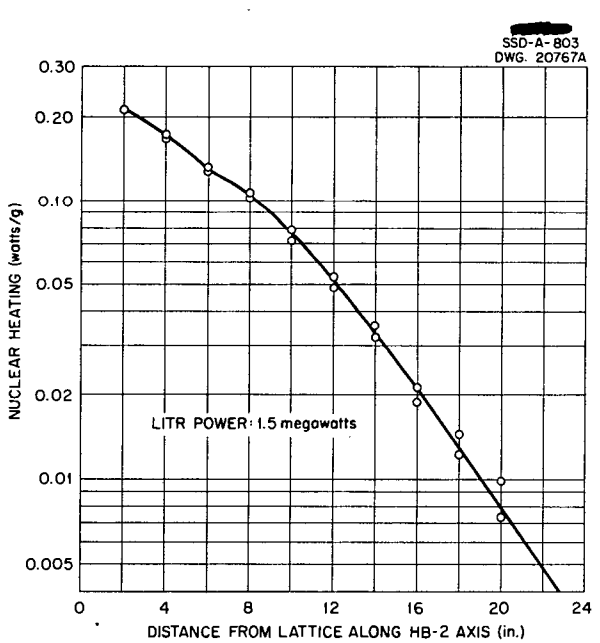

Fig. 32. Nuclear Heating of Copper in HB-2.

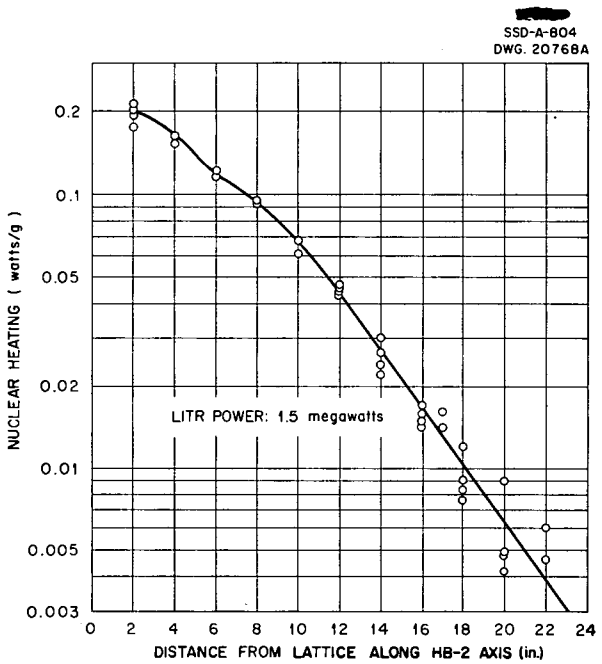

Fig. 33. Nuclear Heating of Type 347 Stainless Steel in HB-2.

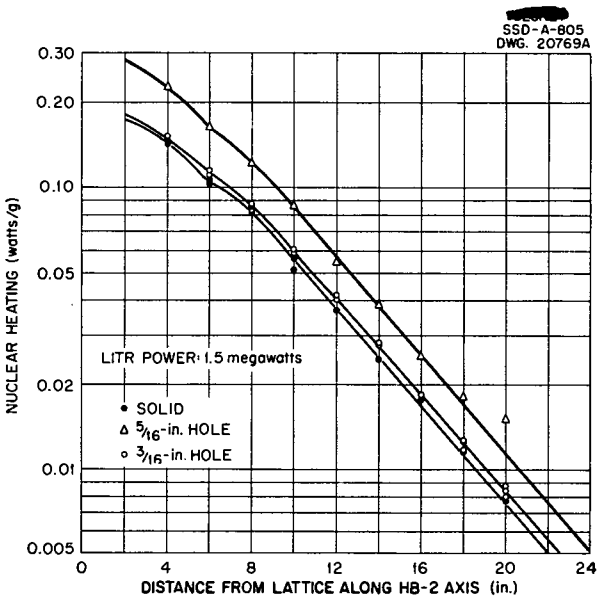

Fig. 34. Nuclear Heating of Lead in HB-2.

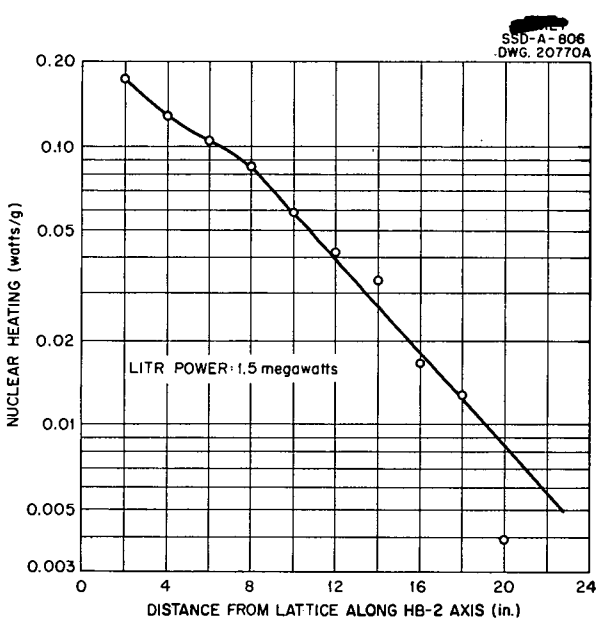

Fig. 35. Nuclear Heating of Nylon in HB-2.

ENGINEERING PROPERTIES

LITR FLUORIDE-FUEL LOOP

W. E. Brundage
M. T. Morgan
A. S. Olson
O. Sisman

The experiment devised for studying the fuel stability and the dynamic corrosion of Inconel by fluoride fuels under irradiation in the MTR[1] has been revised for operation in the LITR.

A first revision consisted largely of dimensional changes for adapting the design to the HB-2 hole of the LITR. A second revision was necessary when no satisfactory packing could be found for the small centrifugal in-pile pump (driven by an air motor) intended for the experiment. The only suitable pump now available is a modified version of a gas-sealed centrifugal sump pump designed by the ANP Experimental Engineering Department.[2]

The use of the sump pump will require that the pump be placed outside the reactor shield, and this will complicate the experiment because the addition of a large amount of external shielding will be necessary. A difficult handling problem will also be created because the length of the radioactive section will be 15 ft instead of the 4 ft specified in the original design.

The modification will permit additional heat to be added electrically to the loop and will thus permit operation at a larger temperature differential between the pump and the reactor end of the loop than was possible with the first design. A disadvantage of the revised design is the high dilution factor of about 50 to 1 caused by the large volume outside the reactor in the type of pump which must be used. The dilution factor for the first design was 10 to 1.

The revised system is shown schematically in Fig. 36. The drive mechanism for the pump will be placed outside the shield so as to reduce the amount of shielding necessary. Ferroboron and cadmium shielding will be mounted as shown to reduce the fission taking place past the reactor end of the loop. Additional metal to provide a heat sink and fins to increase the radiation to the water-cooled jacket have been brazed to the irradiated section. These precautions are necessary to prevent a rapid temperature rise in case of a flow stoppage while the reactor is operating. The heat exchanger and the venturi assembly will be placed just inside the face of the reactor to simplify construction and assembly.

The pressure transmitters used in conjunction with the venturi were originally developed to fit the small space available in the first design. Although more space is now available, these transmitters are still preferred because of the small holdup of fuel. The transmitter consists of two chambers separated by a thin flexible diaphragm, as shown in Fig. 37. Closing of the electrical contacts operates the relay; the relay reverses the motor; and the motor rotates the pressure-regulator control valve so as to increase the pressure in the gas chamber when the contacts close and to decrease the pressure when the contacts open. The pressure required to maintain the balance is recorded by means of a Baldwin SR-4 pressure cell and a Brown millivolt recorder.

The pressure transmitter is now in operation at 1500°F, and gas pressure has been substituted for the fuel in the chamber. It did not seem necessary to make this test in the presence of the fluoride fuel because similar tests on the diaphragm have been carried out by the ANP Experimental Engineering Department and have indicated that a life of over 500 hr may be expected. No difficulties have been experienced in the three weeks that the test has been in progress. The inherent accuracy of the transmitter is better than 0.05 psi, provided that the pressure change is not more than 1.1 psi/sec. Pressure changes at a higher rate will cause a differential pressure between the chambers which will deform the diaphragm and cause a shift in the zero point of the cell. The diaphragm will recover slowly from this deformation. The zero shift may be determined by stopping the flow through the venturi and applying a known pressure to the system and observing the required balancing pressure.

At present, the design of the experiment is about 70% complete, and fabrication is about 25% complete.

---

[1] W. W. Parkinson and O. Sisman, *Solid State Quar. Prog. Rep. Nov. 10, 1952*, ORNL-1429, p. 13.

[2] R. C. Briant, *Objective and Status of ORNL-ANP Reactor Program. Presentation, USAF Advisory Committee, Washington, January 12, 1953*, ORNL CF-53-2-126, p. 13.

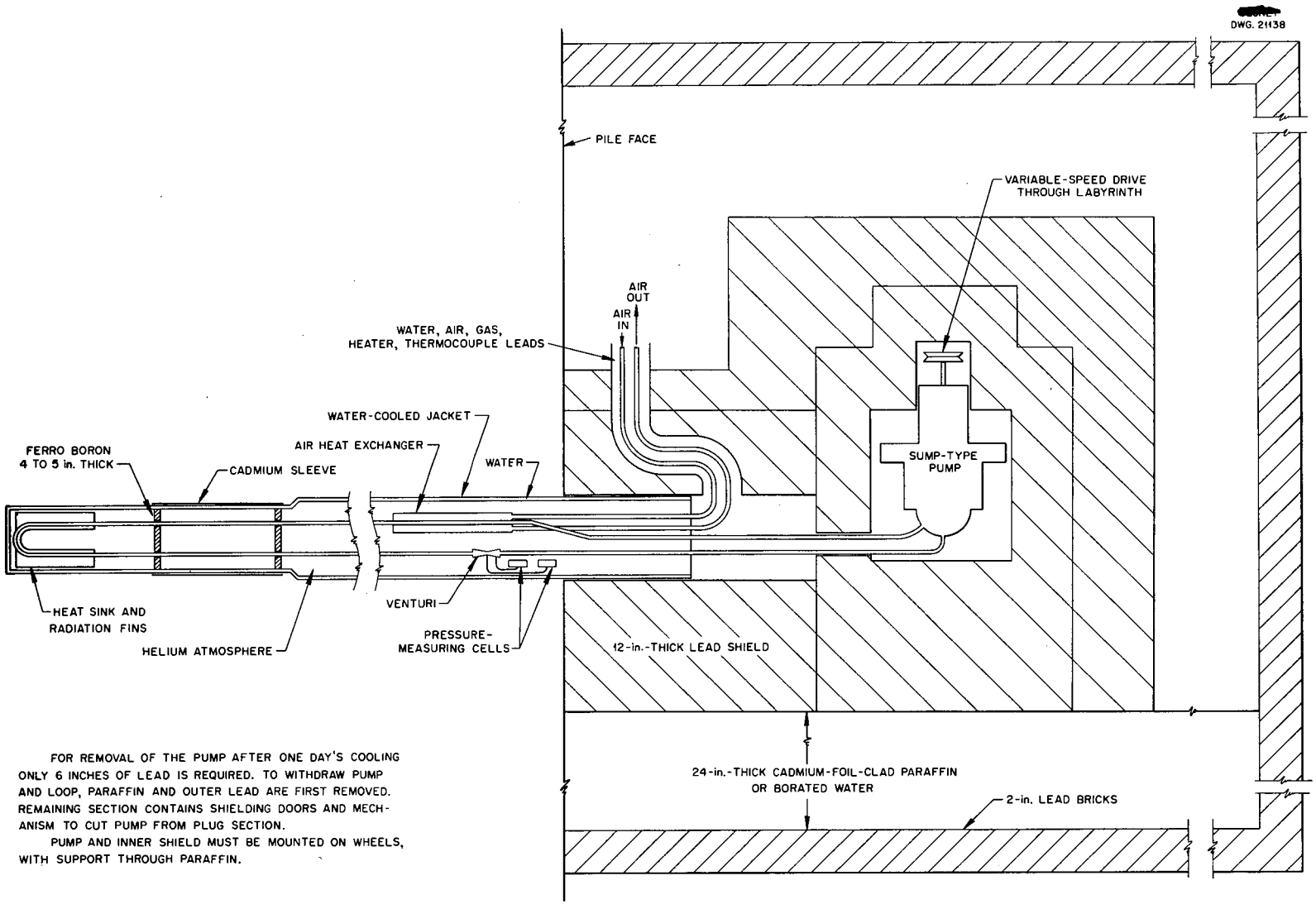

FOR REMOVAL OF THE PUMP AFTER ONE DAY'S COOLING ONLY 6 INCHES OF LEAD IS REQUIRED. TO WITHDRAW PUMP AND LOOP, PARAFFIN AND OUTER LEAD ARE FIRST REMOVED. REMAINING SECTION CONTAINS SHIELDING DOORS AND MECHANISM TO CUT PUMP FROM PLUG SECTION.

PUMP AND INNER SHIELD MUST BE MOUNTED ON WHEELS, WITH SUPPORT THROUGH PARAFFIN.

Fig. 36. LITR Fluoride-Fuel Loop.

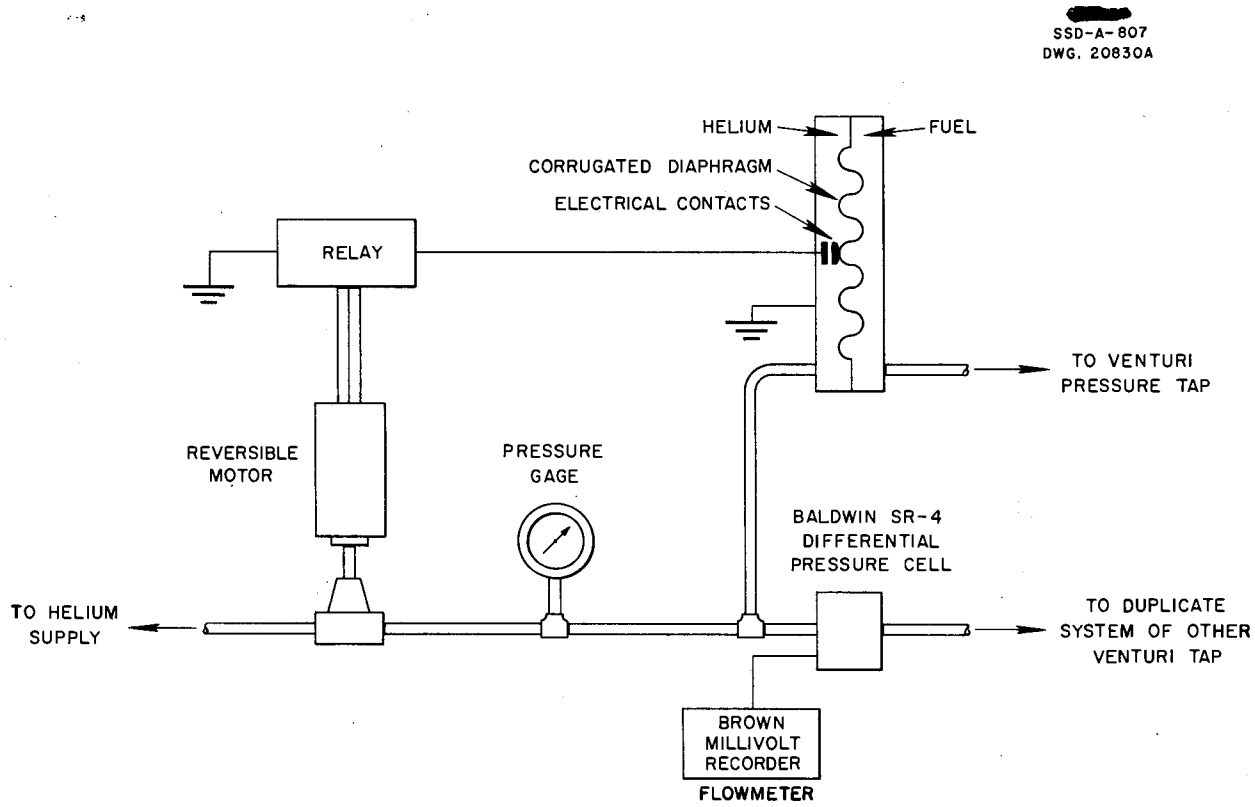

Fig. 37. Pressure Transmitter and System for Flow Measurement in Fuel Loop.

LITR SODIUM STRESS-CORROSION LOOP

W. W. Parkinson R. M. Carroll
F. M. Blacksher O. Sisman

Because of increased effort on the fused-salt systems, no new work is planned for liquid metals, and the work on current in-pile loops is gradually being terminated. The following data practically complete the work on the LITR sodium stress-corrosion loop which was discussed in detail in the last progress report.[3] This loop, of Inconel tubing containing sodium, was operated in the LITR for a period of 95 hr at about 1070°F and for 66 hr at about 1270°F. During this operation, a load was applied to the tubular corrosion specimen to maintain a stress of 1500 psi. At the termination of the experiment, the loop was disassembled and cut up in the hot cells, as described previously.

It had been planned to measure the integrated neutron flux by the activity of a cobalt foil attached to the end of the jacket, but the foil had oxidized and disintegrated to such an extent that it was useless as a monitor. Saw cuttings taken from the stainless steel jacket at regularly spaced intervals provided a measure of the relative exposure as a function of distance from the end of the hole. The variation in thermal-neutron flux as determined by these measurements is shown in Fig. 38. This curve differs from the thermal distribution for the experimental hole (HB-2) measured by Trice,[4] in that the apparent rate of decline in flux is greater than that of Trice's measurements. The greater rate is undoubtedly caused by the large amount of absorber present in the hole, which was empty when Trice made his measurements. The activity at zero distance, however, should be nearly the same as that measured in the empty hole, and it is assumed that this is the case. The curve was therefore normalized to the flux at zero distance obtained by Trice.

[3] W. E. Brundage *et al.*, *Solid State Quar. Prog. Rep. Feb. 10, 1953*, ORNL-1506, p. 15.

[4] J. B. Trice, *Solid State Quar. Prog. Rep. Aug. 10, 1952*, ORNL-1359, p. 10.

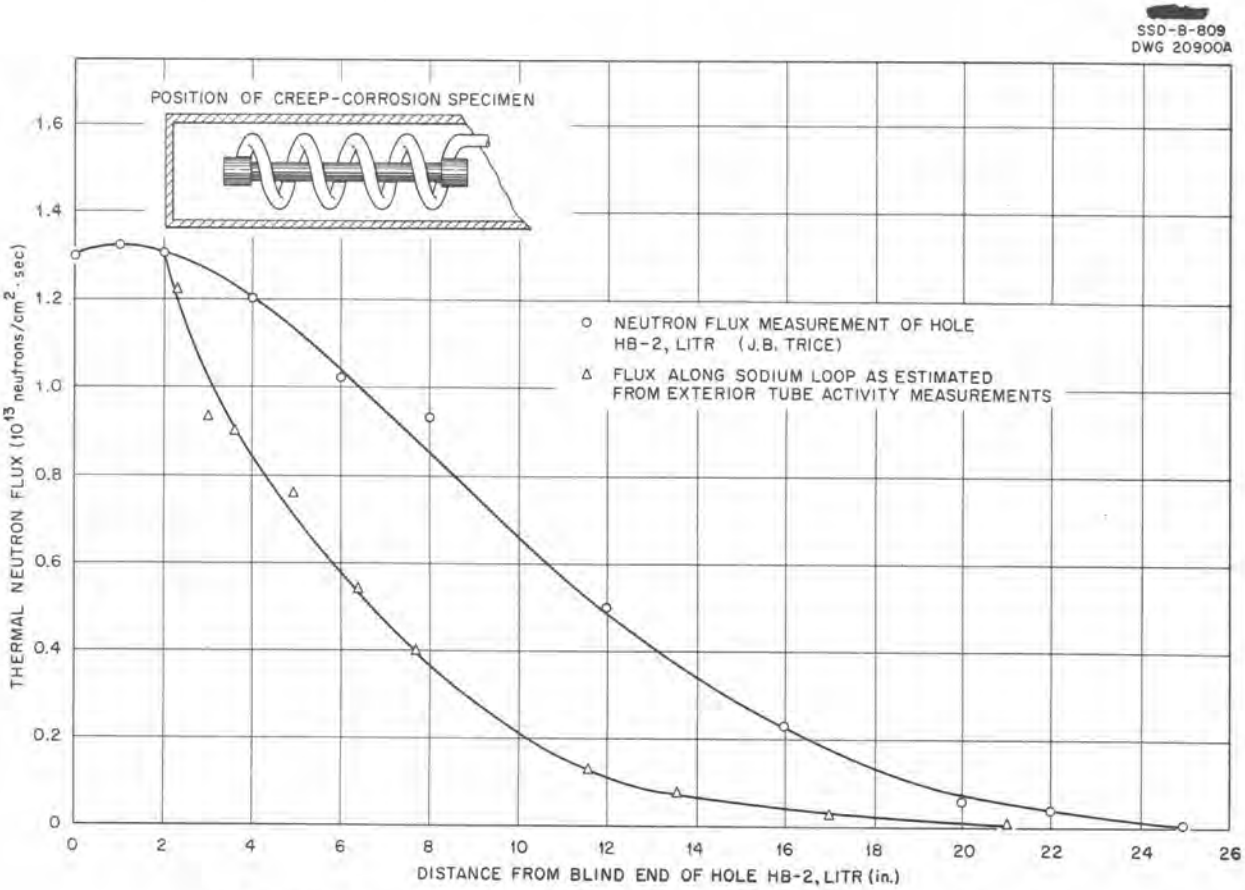

Fig. 38. Thermal-Neutron Distribution for LITR Sodium Loop.

Activity measurements have been made on the sodium from the loop and on the Inconel from the specimen to estimate the quantity of irradiated Inconel present as corrosion products in the sodium stream. The short-lived activity (10- to 13-hr half life) previously reported as making up the major part of the activity in the sodium has been tentatively identified as Pd^{103} by the absorption of the emitted gammas in aluminum,[5] although the half life is in only fair agreement. The palladium could have entered the sodium as a result of corrosion of the Ni-Pd brazed tube connection at one end of the specimen. Measurements on the long-lived components in the sodium are being continued in an attempt to identify other elements in addition to those identified by chemical analysis.

[5] J. D. Gile, H. R. Haymond, W. M. Garrison, and J. G. Hamilton, *Carrier-Free Radioisotopes from Cyclotron Targets; XVI. Preparation and Isolation of Pd^{103} from Rhodium*, UCRL-1144 (Feb. 19, 1951).

Metallographic examination of sections of the specimen located as shown in Fig. 39 show no intergranular corrosion or penetration, although erosion of the Inconel surface opposite the entrance

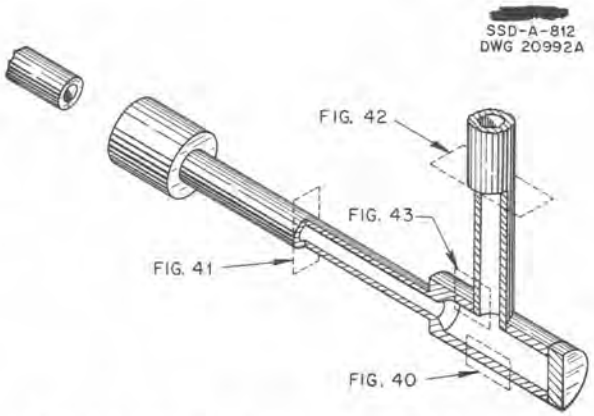

Fig. 39. LITR Stress-Corrosion Specimen.

Page 32 Column 1 Line 5 for (10- to 13-hr half read (10- to 13-day half

of the flow tube did occur, as shown in Fig. 40. Figure 41 is a photomicrograph of a transverse section of the stressed specimen which shows a structure apparently of the Widmannstaetten type. The origin of this structure is ambiguous because of the high temperature (2200°F for 10 min) to which the specimen was subjected during the brazing operation. The structure does not appear in the attached tubing (Fig. 42) which was subjected to the same brazing operation. The attached section was of drawn tubing, while the stressed specimen was machined from bar stock. Heat treatments are being conducted by the Radiation Metallurgy Section of the Solid State Division to establish the conditions giving rise to the Widmannstaetten-type structure.

The brazed joint exposed to the sodium is shown unetched in Fig. 43, and the porosity, which must have accounted for the sodium leak during operation of the loop, is clearly visible.

ORNL GRAPHITE REACTOR SODIUM-INCONEL LOOP

W. E. Brundage M. T. Morgan

The sodium-Inconel loop which was operated in the ORNL graphite reactor until a heater failure caused operation to be stopped[6] was successfully removed from the reactor, the heaters were replaced, and the loop was then reinserted in the reactor. In order that the loop could be operated without someone being in constant attendance, the control panel was modified to operate automatically. Although the loop will now function without constant attention, it seems desirable that an operator be in attendance for the first few days of a run to check the revised instrumentation. Lack of manpower has delayed startup of the experiment.

[6] C. D. Baumann *et al.*, *Solid State Quar. Prog. Rep. Feb. 10, 1953*, ORNL-1506, p. 13.

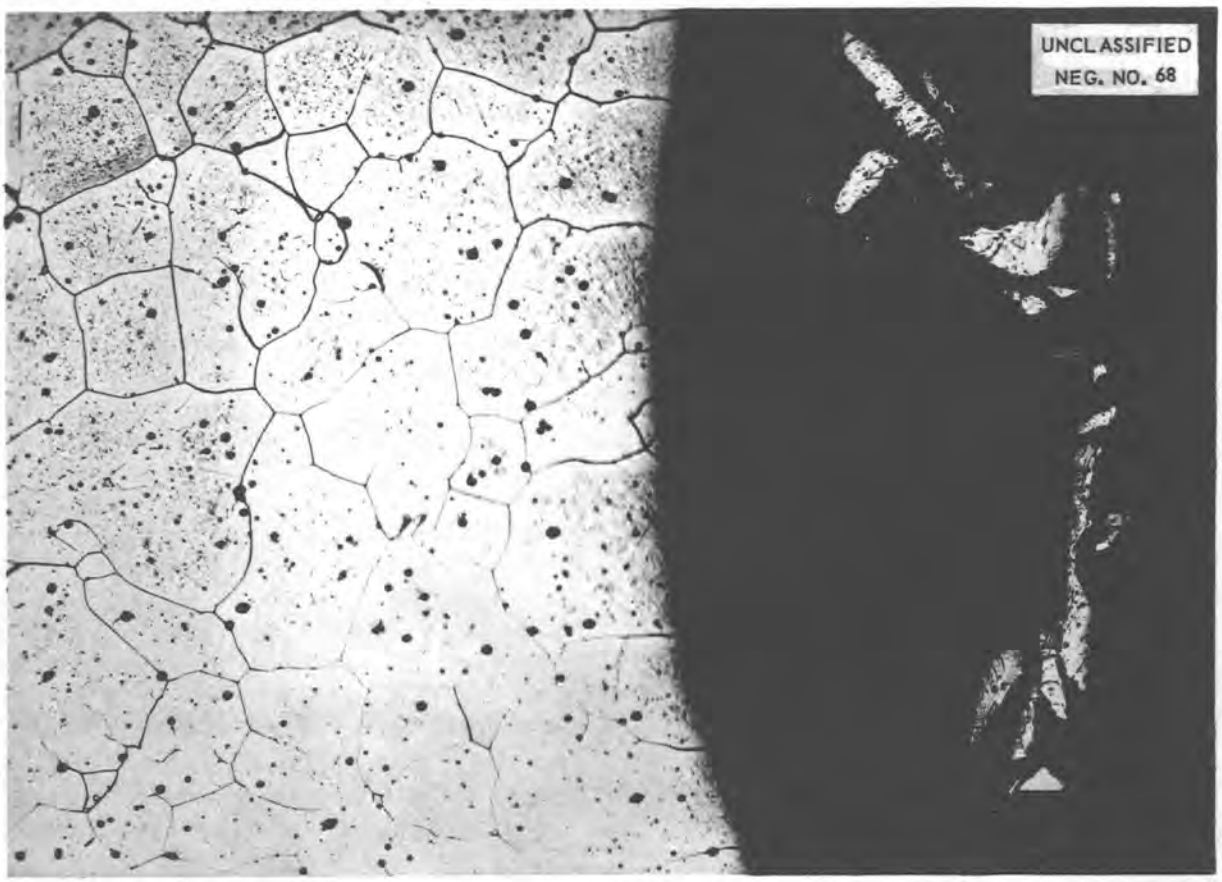

Fig. 40. Erosion of Inconel by Sodium. 75X.

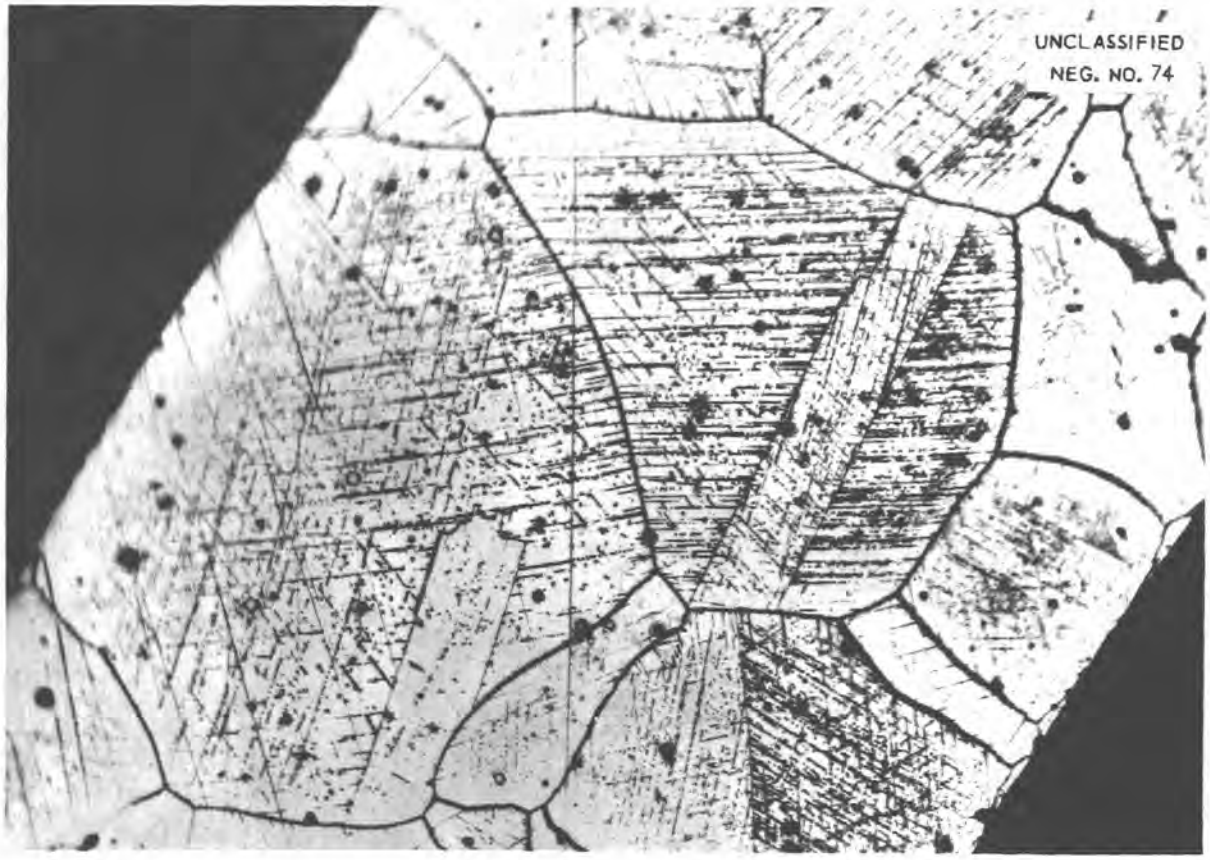

Fig. 41. Transverse Section of Inconel Specimen After Irradiation Under Tension. 200X.

SODIUM–BERYLLIUM OXIDE RADIATION-CORROSION TEST

W. E. Brundage
F. M. Blacksher
R. M. Carroll
C. Ellis
M. T. Morgan
W. W. Parkinson
O. Sisman

It is planned to use beryllium oxide as the moderator for the Aircraft Reactor Experiment, and the moderator blocks will be cooled by immersion in confined or slowly flowing sodium. To determine the extent of corrosion of the BeO by the coolant in the radiation field of the reactor, an experiment under static conditions has been carried out in the LITR.

Specimen blocks of BeO $\frac{1}{4}$ by $\frac{3}{16}$ by 1 in. were cut from various regions of the moderator blocks for the ARE to give samples of representative densities. The specimens were heated to 825°C in a vacuum furnace until the weights were constant. Each specimen was then placed in a stainless steel capsule, $2\frac{1}{4}$ by $\frac{9}{16}$ in., and a retaining spring was welded to the capsule to hold the BeO beneath the surface of the sodium. About 2 cc of sodium was charged into the capsule in a helium-filled dry-box, and the capsule was closed by being welded. Eight filled capsules were sealed in a can fitted with heaters, thermocouple leads, and inert-gas tubes, as shown in Fig. 44. The capsule assembly was attached to the universal plug described earlier,[7] and the assembly and the plug were inserted in the water-cooled reactor-hole liner and placed in hole HB-2 of the LITR. Operation was started at 1500°F, but after about 17 hr the indicated temperatures gradually dropped to around 1000°F with normal heater operation. Also, the gas-outlet line plugged during this time and it was assumed that sodium leaked out of one of the capsules and condensed in the cooler regions of the apparatus to short-circuit the thermo-

[7] W. E. Brundage, A. S. Olson, and O. Sisman, *Solid State Quar. Prog. Rep. Feb. 10, 1953*, ORNL-1506, p. 17.

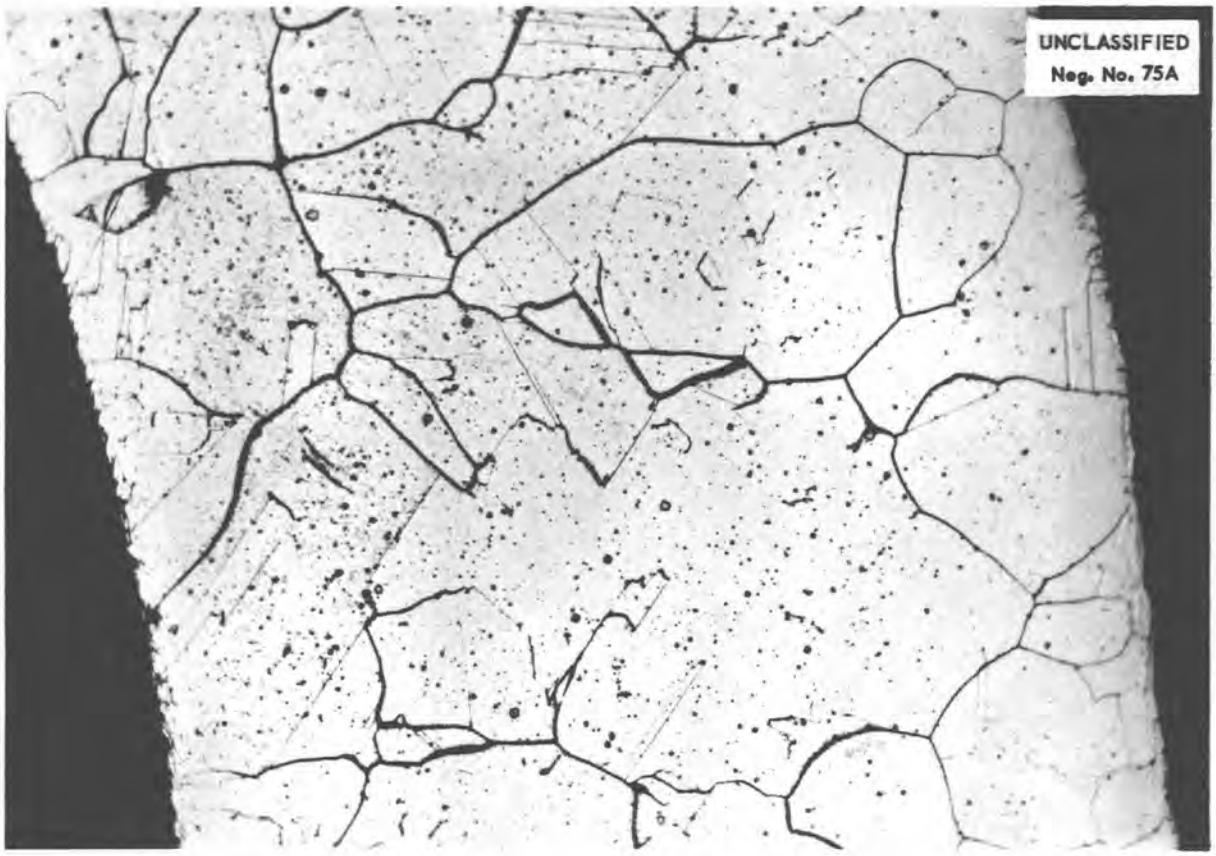

Fig. 42. Inconel Flow Tube. 200X.

couple leads – probably in the region of the hermetic seal. Operation was continued without temperature recording or automatic control of the heater power by utilizing previous estimates that were obtained from a mockup of the power requirements to maintain 1500°F and that were supplemented by measurements of the power input by the reactor. The irradiation was carried out for 328 hr at 1500°F, 45 hr at 1300°F, and 110 hr at 750°F. The same heat-treating schedule was used on eight unirradiated capsules prepared in the same manner as those irradiated.

When the capsules were opened (the irradiated ones in a hot cell), the BeO blocks were removed, and the sodium charges were dissolved in ethanol or ethanol-water mixtures. The empty capsules were leached in 15% NaOH for 48 to 72 hr to dissolve the BeO on the walls. The sodium and the leach solutions for each capsule were analyzed for beryllium by the Analytical Chemistry Division.

The BeO blocks, during and after removal from the capsules, were protected from the atmosphere by immersion under oil. The sodium and the oil were removed from the blocks by heating them to 800 to 825°C for about 1 hr under vacuum – a cleaning treatment similar to that used prior to insertion of the blocks in the capsules.

The BeO specimens were weighed and were found to have gained slightly (0.2%) rather than to have lost weight. The exceptions were one irradiated specimen from a capsule that contained very little sodium and an unirradiated control specimen from a capsule containing no sodium. So as to remove any possible sodium or Na_2O which might not have been removed by the vacuum heating, the specimens were soaked in water for seven to ten days. They were heated in vacuum again and reweighed. Both the irradiated and the unirradiated specimens averaged a weight loss of 0.0005 g, and all were within ±0.002 g (0.1%) of the original weight.

The results of the chemical analyses confirm the absence of corrosion. In all the solutions, both those of the sodium and of the capsule leachings,

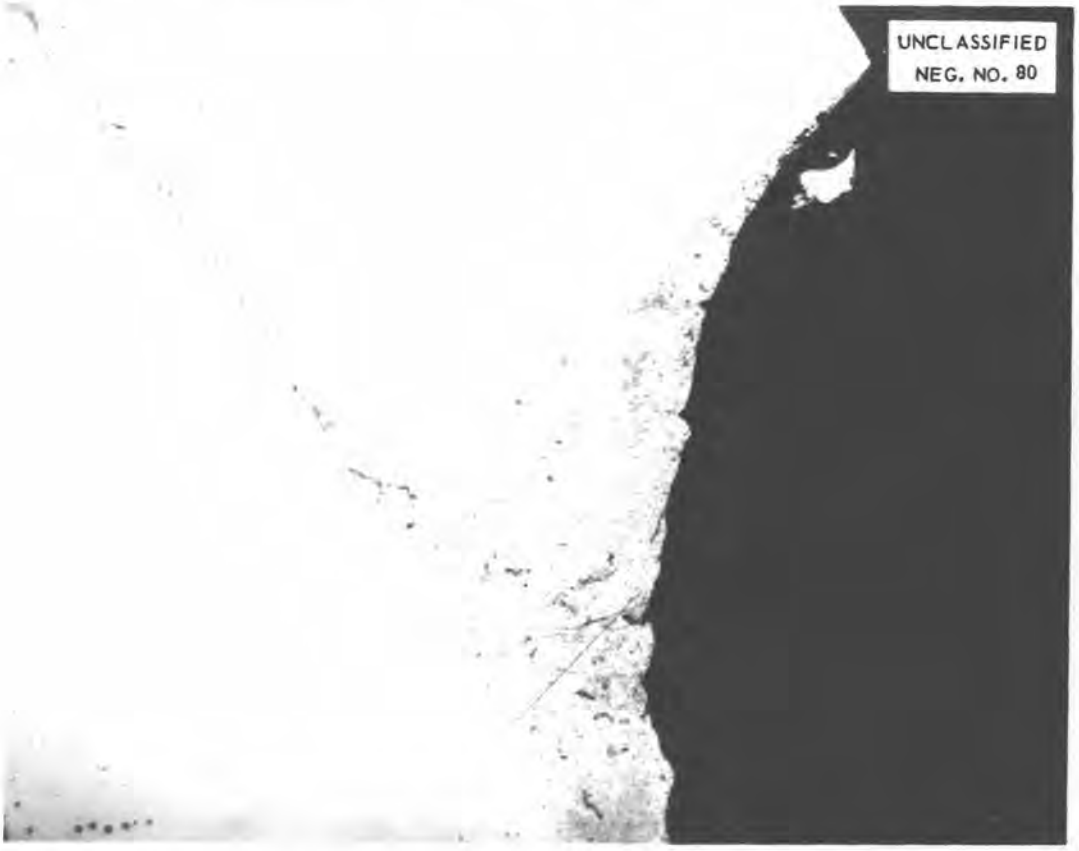

Fig. 43. Section of Sodium Stress-Corrosion Loop at Ni-Pd Braze Joint. 175X.

the beryllium content was below the limit of sensitivity of the analytical method, 0.0005 g of total beryllium per sample, or less than 250 ppm in the sodium bath.

As a check on the condition of the sodium in the capsules, three of the unirradiated capsules were opened under oil, and the oxygen content was determined after the method of Pepkowitz;[8] a layer of oil was substituted for the inert gas or vacuum as protection against the atmosphere. In two of the sodium baths, the oxygen content was 0.1%; in the third bath, it measured 0.18%. The reliability of the determinations is open to question because of the difficulty of separating mercury, water, and oil layers and the difficulty of titrating dilute solutions in the presence of oil droplets. However, it is felt that the determinations serve as an indication of sodium purity.

Visual inspection of the BeO specimens showed no difference between the irradiated and unirradiated material, and neither seemed to have suffered alterations as a result of the heat treatment. The surfaces of all the specimens remained smooth, the corners remained sharp, and no evidence of cracks or pits could be detected (see Fig. 45). The accumulated exposure was about 2×10^{19} nvt (thermal).

RADIATION-INDUCED CHANGES IN THE ENGINEERING PROPERTIES OF METALS

W. W. Parkinson
C. D. Baumann
C. Ellis
O. Sisman

The interest in high-power-density reactors creates a need for extending to the highest available fluxes the already extensive radiation-damage studies on metals. Exposures of 10^{21} fast neutrons/cm^2 can be obtained in two or three months in one of the lattice positions in the C41-C49 row of the MTR. A request to irradiate tensile, impact, and metallographic metal specimens has been approved by the AEC and assigned the MTR designation, ORNL-9.

[8] L. P. Pepkowitz and W. C. Judd, *Anal. Chem.* **22**, 1283 (1950).

DWG. 21121

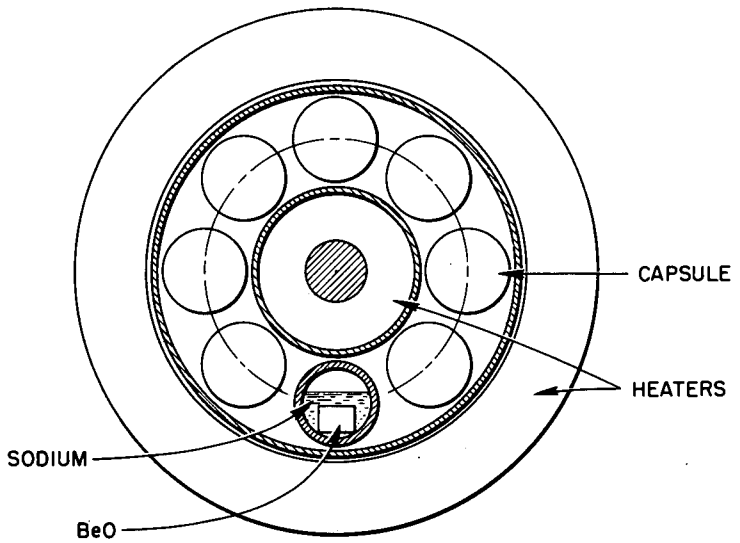

SECTION B—B

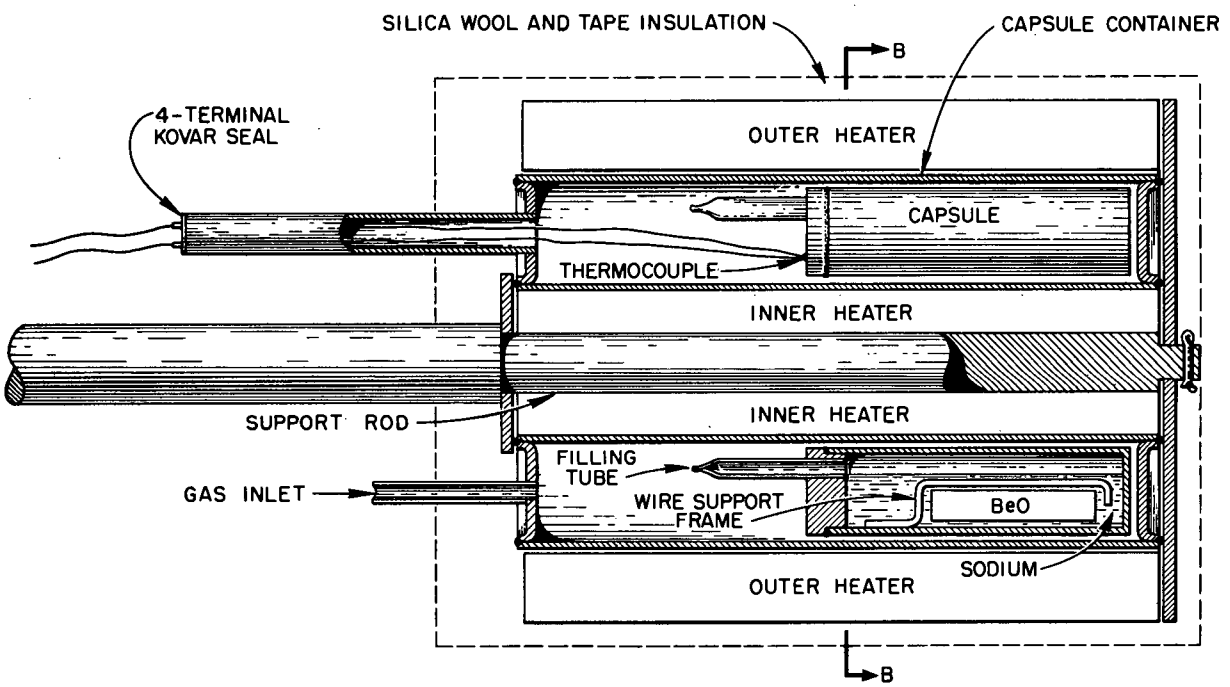

Fig. 44. Container for Na-BeO Corrosion Test.

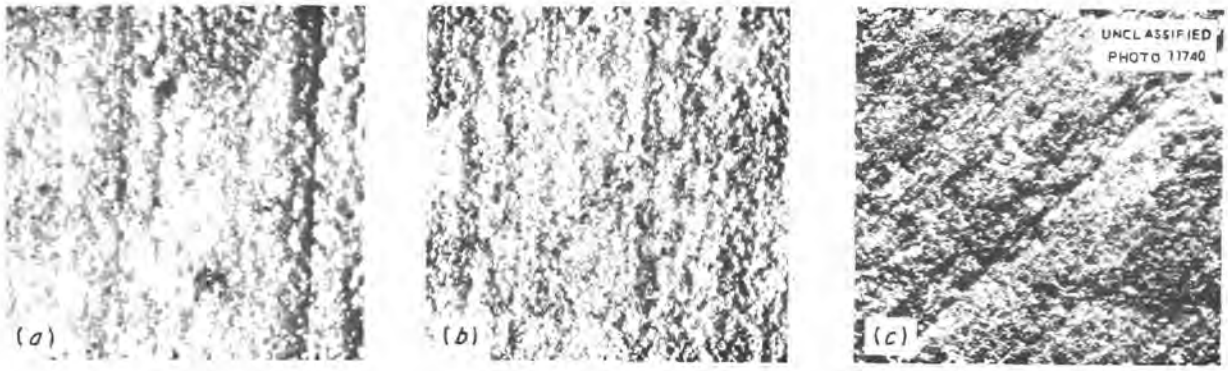

Fig. 45. Typical BeO Specimens. (*a*) Untreated, (*b*) heat treated in sodium, unirradiated, (c) irradiated in sodium at 1500°F. 40X. Reduced 25.5%.

The nuclear heating in one of the lattice positions mentioned above is the major problem in the room-temperature irradiation of metal specimens. The most simple means of removing the heat generated by the reactor emanations (possibly 10 watts/g) is to utilize the reactor cooling water if specimens subject to corrosion can be protected. Several methods of cladding have been tested for heat transmission, ease of removal of cladding under hot-cell conditions, and water tightness.

Thin lead sheets were pressed around the specimen by using sponge-rubber pads between the platens of a hydraulic press, and the edges of the resulting "sandwich" were closed by soldering. Specimens were clad in aluminum sheets in the same manner and were closed by either welding or soldering the edges. Aluminum tubing was also used to clad specimens by spinning it tightly on the specimen. Specimens metallized with a rather thick coat of spray-welded aluminum were found to be adequately leak tight and abrasion resistant. The last two types of cladding create problems in removal by hot-cell manipulators; therefore some modification will be necessary.

Heat transmission characteristics of the four types of cladding mentioned above were tested by cladding a $\frac{5}{8}$-in.-dia specimen of aluminum or stainless steel in which a 75-watt cartridge heater was inserted. Temperatures were measured, inside and at the surface of the specimen in running water, as a function of the heat input. With several simplifying assumptions, an "equivalent air gap" between the cladding and the sample was calculated. By using this gap, the surface and the axial temperatures of a $\frac{1}{4}$-in. stainless steel rod were estimated in a nuclear heating field of 10 watts/g and a cooling water stream at 100°F. The calculated gap values and estimated temperatures are tabulated in Table 2.

Apparently, only the last two cladding methods will be suitable for heat-treatable iron alloys.

A holder for suspending the specimens in an LB piece has been designed and was tentatively approved after discussions with MTR personnel.

TABLE 2. CALCULATED GAP VALUES AND ESTIMATED TEMPERATURES FOR CLAD SPECIMENS

CLADDING MATERIAL AND METHOD	EQUIVALENT AIR GAP BETWEEN CLADDING AND SPECIMEN (in.)	SPECIMEN SURFACE TEMPERATURE (estimated, °F)	SPECIMEN AXIAL TEMPERATURE (estimated, °F)
Lead, pressed on by use of rubber pads	0.0030	710	730
Aluminum, pressed on by use of rubber pads	0.0022	550	570
Aluminum, spun on	0.00027	155	174
Aluminum, spray welding (metalizing)	0.00010	120	139

FUSED SALTS

FUSED-SALT CAPSULE TESTS IN THE LITR

W. R. Willis M. J. Feldman
C. C. Webster A. E. Richt
G. W. Keilholtz

A study of the corrosion of Inconel capsules by ARE fuel No. 30 at 815°C has been made as a function of irradiation time; the results are shown in Table 3. The general type of corrosion in the controls can be called subsurface void or globular corrosion to differentiate from the intergranular type noted in many of the irradiated capsules. While both corrosive actions may take place at the grain boundary, the resulting corrosion evidence differs in appearance. The appearance of the control samples is similar to that of the unirradiated corrosion capsules metallographically examined by the Y-12 Corrosion Group.

An additional point pertinent to this study is that, in general, the Y-12 group believes that maximum corrosion is reached between 60 and 120 hr in the static-type corrosion tests and that the time vs. corrosion curves show a saturation effect. Although the number of samples studied in this series is not large enough for a similar curve to be drawn, the general conclusion is that the irradiated samples do not follow the behavior of the unirradiated samples.

While the number of samples per test time and the time interval of the tests are not large, two important tendencies can be reported. First, the corrosion saturation noted by the Y-12 group and, to some extent, that found in the control runs 29Z-76, 30Z-77, 31Z-78, and 32Z-79 do not apply to the irradiated capsules. The differences in the surface-to-volume ratio of the types of capsules compared have not been taken into consideration.

The second point, and one more difficult to evaluate metallographically, is that the amount of corrosion in the irradiated capsules is much larger than that in the unirradiated capsules. The method of reporting corrosion in terms of depth of corrosive penetration does not lend itself to an evaluation of the amount of corrosion in this particular case. In general, the corrosion in unirradiated tests has been of a globular or spotty intergranular type, while the corrosion noted on the irradiated samples appears as a continuous network of intergranular attack. The samples showed maximum corrosion in the salt section, with decreasing attack in the intermediate and the vapor sections. There was no evidence of very large grains to indicate any overshooting of temperature.

With the exception of one sample (19Z-66, 810 hr), the set of irradiated capsules analyzed displayed a

TABLE 3. CORROSION OF INCONEL CAPSULES BY ARE FUEL NO. 30 AT 815°C

CAPSULE	TIME (hr)	PENETRATION OF METAL (mils)		
		Salt Region	Interface	Vapor Region
LITR Tests (230 watts/cc)				
21Z-68	53	0 to 0.5	*	None
12Z-59	140	1	1	1
25Z-72	270	1	0.5	None
15Z-62	565	2 to 3	1 to 2	1
18Z-65	685	3 to 4	3 to 4	1 to 2
19Z-66	810	1	*	1
Control Tests (0 watts/cc)				
29Z-76	100	None	None	*
30Z-77	300	1 to 2	1	*
31Z-78	520	1	1	*
32Z-79	700	1	*	*

*Not photographed.

rough time-corrosion dependence, approximately 0.5 mil/100 hr (see Table 3).

FUSED-SALT CAPSULE TESTS IN THE MTR

J. G. Morgan
W. R. Willis
H. E. Robertson
P. R. Klein
C. C. Webster
G. W. Keilholtz

Chemical examination of the salt contained in the LITR corrosion capsules showed that the concentration of uranium varied in an irregular manner. There is definite evidence that, under the conditions of the corrosion tests, ZrF_4 was vaporizing from the salt. From the manner in which the data scattered, it also appeared that the salt-sampling technique was not satisfactory.

To avoid these difficulties, the MTR corrosion capsules were designed with as small a vapor space over the liquid as possible. The temperature of this area is close enough to the salt temperature so that no ZrF_4 will vaporize from the salt. A new solid-salt sampling technique was devised so that the danger of any composition change in molten salt during sampling was eliminated and so that certain definite sections of the salt column could be examined. The technique consisted in coring the sample by drilling progressively larger sections of the salt column from the capsule. A precision drill press was modified for remote operation in the hot cells.

Since the new techniques were initiated, five capsules have been analyzed for segregation data. Four of these capsules were irradiated in the MTR, and one was a special control test with a similar thermal history. The samples taken from the capsules were analyzed by two methods: chemical analyses by both potentiometric and polarographic techniques and mass spectrometry.

The data obtained from these tests are shown in Table 4 and are given graphically in Fig. 46. Samples in the 500 series originally contained 26.3 wt % uranium and were tested in capsules with an internal diameter of 55 mils; the 400 series contained 13.3 wt % uranium and were also tested in 55-mil capsules; the 200 series contained 8.68 wt% uranium and were tested in 100-mil capsules. In experiments in which several corings were taken from the capsule, those samples labeled A were the corings from the center of the salt column, those

TABLE 4. ANALYSES OF IRRADIATED FUEL

SAMPLE	TIME OF IRRADIATION OR CONTROL TEST (hr)	POWER DISSIPATION IN FUEL (watts/cc)	THERMAL FLUX (nv × 10^{14})	ORIGINAL URANIUM CONTENT (%)	THEORETICAL URANIUM CONTENT AFTER BURNUP (%)	URANIUM CONTENT, MASS SPECTROMETER (%)	URANIUM CONTENT, CHEMICAL ANALYSIS (%)
75 A	510	0.00	0.0	8.68	8.68		8.46
B	510	0.0	0.0	8.68	8.68	8.26	8.85
C	510	0.0	0.0	8.68	8.68	8.67	8.69
D	510	0.0	0.0	8.68	8.68	8.75	8.86
E	510	0.0	0.0	8.68	8.68	8.37	8.71
F	510	0.0	0.0	8.68	8.68	8.90	8.68
G	510	0.0	0.0	8.68	8.68	8.97	8.42
H		0.0	0.0	8.68	8.68	8.31	8.70
219 A	330	2300	2.4	8.68	7.55	6.96	6.50
B	330	2300	2.4	8.68	7.55		7.50
C	330	2300	2.4	8.68	7.55	7.49	8.20
410	419	4400	2.4	13.3	11.12	11.57	11.20
501	120	9600	2.4	26.3	24.7	24.28	
502	273	9600	2.4	26.3	23.4	22.97	

labeled B were the next samples out from the center, etc. All concentrations given were calculated to total uranium concentration, as found in chemical analyses.

The theoretical concentrations were calculated from the following equation which was derived from considerations of the uranium burnup:

$$\% \, U = 100 \left[1 - \frac{1}{1 + \frac{N_0^{28}}{N_0^{25}}} \cdot \frac{\sigma_f^{25}}{\sigma_f^{25} + \sigma_c^{25}} \left(1 - \frac{e^{-\sigma_a^{25} \phi t}}{M} \right) - \frac{1}{1 + \frac{N_0^{25}}{N_0^{28}}} \left(1 - e^{-\sigma_a^{25} \phi t} \right) \right] ,$$

where

$$M = \frac{N_0^{25}}{N_0^{28}} \cdot \frac{N_f^{28}}{N_f^{25}} .$$

Figure 46 shows the data with the concentration of uranium reduced to the fraction of the original concentration so that all data could be shown in one graph. Of the data available, only the 219 series of samples show results which could be considered, in any way, as unusual. At present, extensive testing of the salt is under way in the LITR and the MTR. Since these tests can be performed in large-diameter capsules, it is expected that samples may be obtained that show the uranium concentration in various portions of the capsule, as well as the total uranium balance in the capsule.

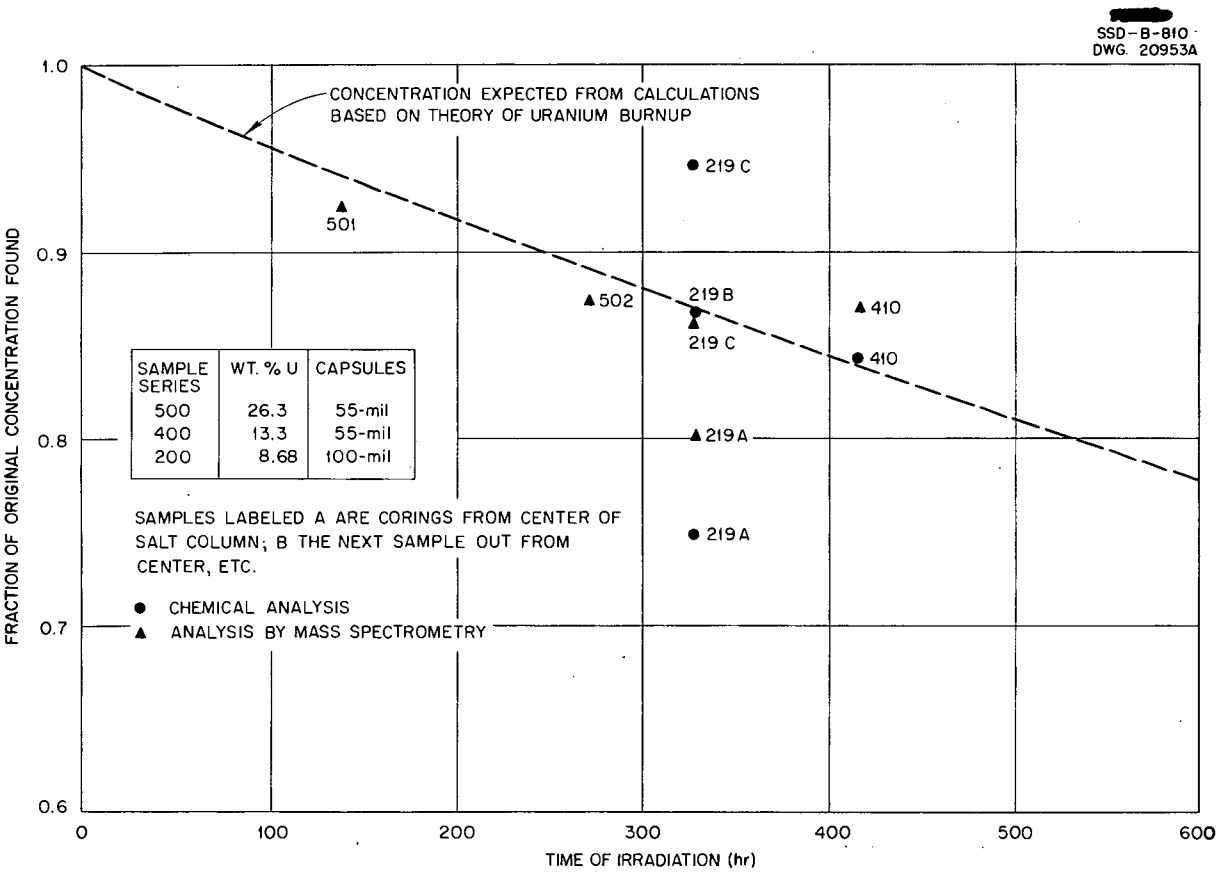

Fig. 46. Uranium Concentration vs. Corrosion Time in the MTR.

MTR CAPSULE CALCULATIONS

P. R. Klein

A simplified model has been used in solving the transient-temperature distributions in the MTR capsules during the startup period when the MTR power rises by steps. The fuel-Inconel interface is assumed to remain at a constant temperature, and the physical properties of the salt are assumed to remain unchanged. The solution was found by using the Laplace transform on the differential equation of heat conduction. The calculation shows that, if the assumptions made are true, the MTR power may be increased after as short a period as desired without waiting for steady-state conditions to exist between power increments and that no overheating will be produced in the capsules.

The theoretical flux distributions in MTR capsules have been calculated; due consideration has been given to the influence of the container material in a capsule with a 100-mil-dia fuel column. The one-velocity model has been used throughout. The flux at the center of the fuel is found to be approximately 10% below the flux value, as measured by unencased cobalt. In fuel No. 30, the flux remains constant to within 0.2% throughout the fuel. At the Inconel-moderator interface, the flux perturbation amounts to approximately 8%.

The temperature distribution and the power distribution in a typical MTR salt were computed by using a radial density gradient. It was first assumed that the neutron flux across the diameter of the fuel column remained constant. It was further assumed that the thermal conductivity of the fuel is independent of temperature and that the only mechanism of heat removal operative is that of conduction. End effects of the salt column are neglected. Under these conditions, the temperature distribution is in a closed form. The error introduced by the use of the "r^2 law" for the determination of the temperature gradient is found to be 3%, which

indicates that the law serves as a very good approximation. The power generation across the capsule is found to change by 11%. The variation of the average power from the power generation near the outside of the fuel is found to be 5%. In cases where the flux varies appreciably over the fuel column, the temperature distribution is given by an infinite series expression.

THERMAL FLUX IN FACILITY A-38 OF THE MTR

M. T. Robinson P. R. Klein

The thermal-neutron flux in facility A-38 of the MTR has been remeasured as a check on earlier work.[1] Two 30-min irradiations on specimens of cobalt foil were carried out, and the samples were returned to ORNL where they were weighed just prior to being counted. Counting was done on the high-pressure ionization chamber of the Chemical Technology Division. The activity of the samples was determined 5 and 18 days after the irradiation, and the result obtained was 1.30 ± 0.03 rutherfords/mg·hr. If the capture cross section of Co^{59} is taken to be 34.8 ± 2.0 barns[2] and the half life of Co^{60} is taken to be 5.10 ± 0.15 years, the thermal-neutron flux in facility A-38 is 2.36 (±0.16) × 10^{14} neutrons/cm^2·sec. The half life of Co^{60} was obtained by weighting each value in the literature by the inverse square of its uncertainty and by taking the average. The flux value obtained is about 15% lower than the value obtained previously, and about half this discrepancy is due to the use of a lower value for the Co^{60} half life in the present experiment. The remaining difference is attributable to differences in calibration between the ORNL ion chamber and the ion chamber used at the MTR site.

ANALYSIS OF FLUORIDE FUELS FOR Cs^{137}

M. T. Robinson

An attempt has been made to use the fission product 33-year Cs^{137} as an internal dosimeter during MTR irradiations of fused-fluoride fuels. After the irradiated salt has been removed from the capsule and dissolved for uranium analysis, a measured quantity of Cs^+ is added to an aliquot of the solution. Insoluble $CsClO_4$ is precipitated by the addition of perchloric acid and alcohol, and the precipitate is dried, weighed, and mounted on an aluminum counting card. From the weight of $CsClO_4$ recovered, the yield of the procedure is calculated. The samples are counted with a bell-type, thin-window G-M tube at a distance of about 2 cm from the sample. With the use of an ORNL model 1010 scaler, a sufficient number of counts were taken so that random errors were no more than 1% of the counting rate. The number of fissions represented by the Cs^{137} in the sample was calculated by comparison with standard samples counted at Argonne National Laboratory; an absolute calibration of the method has been made at ANL. The radiochemical procedures were carried out by the Radiochemical Laboratory of the Analytical Chemistry Division; counting was done by the Radiochemical Research and Development Group of the same division.

The results obtained so far indicate that not all the Cs^{137} is retained in the fuel. In a sample of No. 30 fuel irradiated for 116 hr in the MTR (No. 201), about 1% of the Cs^{137} was recovered from the capsule top. In a sample irradiated for 324 hr (No. 204), about 10% of the cesium was found in the capsule top. In neither case was an attempt made to recover cesium quantitatively from the capsule tops. These results probably mean that some loss of Xe^{137} from the liquid fuel occurs before decay to Cs^{137} takes place. The results are not in disagreement with those reported previously[3] because the quantities of xenon involved here are about a million times greater than those used previously.

Analysis of the fuels for Cs^{137} has not yet been found to be satisfactory as an internal monitor, but further checks on the method will be made.

SHIELDED PETROGRAPHIC MICROSCOPE FOR IRRADIATED SAMPLES

M. T. Robinson

The ANP Chemistry Section of the Materials Chemistry Division has found petrographic examination to be of great value in studying the phases present in fluoride fuels. In order to extend this technique to irradiated specimens, a standard Bausch and Lomb petrographic microscope has been adapted for operation within a 3-in.-thick lead

(1) J. G. Morgan, P. R. Klein, and H. E. Robertson, *Solid State Quar. Prog. Rep. Feb. 10, 1953*, ORNL-1506, p. 19.

(2) D. J. Hughes *et al.*, *Neutron Cross Sections*, AECU-2040 (May 15, 1952).

(3) M. T. Robinson and D. D. Davies, *Solid State Quar. Prog. Rep. Aug. 10, 1952*, ORNL-1359, p. 19.

shield. The conventional ocular was replaced by a Bausch and Lomb demonstration eyepiece that permits use of the microscope without danger to the operator. A cutaway side elevation of the equipment is given in Fig. 47, which shows the controls (A and B) for operating the rectangular motions of the mechanical stage and the friction drive for the rotational motion of the stage. Installation of the equipment has been completed.

ELECTRICAL CONDUCTIVITY OF FLUORIDES

M. T. Robinson J. C. Pigg
J. G. Morgan

In an attempt to find an in-pile measurement capable of detecting radiation effects in fused salts, a series of experiments has been planned on the electrical conductivity of such materials. It was necessary to design a suitable circuit, capable of measuring low resistances (0 to 10 ohms), in which a.c. and long leads will be used. Existing a-c methods are of limited application because of the range and lead requirements, while d-c methods cannot be used because of chemical polarization effects in the cell. A very simple circuit has been designed and constructed which appears to meet the requirements. W. G. James, W. Adams, and G. Ritscher of the Instrumentation and Controls Division have aided in this work. The resistance-comparator circuit is shown in Fig. 48. Power is supplied by a Hewlett-Packard model 205 AG audio-frequency signal generator, and detection is accomplished by a balanced high-gain amplifier feeding directly into the vertical plates of an oscilloscope. On the low range (0 to 1.1 ohms), measurements are reproducible to ±0.0005 ohm; on the high range (0 to 11.1 ohms), reproducibility is ±0.002 ohm. While the equipment is most satisfactory at 1 kc, reasonably good results can be obtained from 500 cps to 5 kc.

The conductivity cell intended for use with this equipment consists of an Inconel capsule with a coaxial well. The capsule body serves as one current lead and the well serves as the other. The potential probes are spot-welded to the inside of the well and to the outside of the capsule. The two electrodes are separated by a spacer of forsterite (Mg_2SiO_4) brazed to the well and the capsule cap with an alloy of 97% silver and 3% zirconium. The cap is pressure tight at 100 psi. This arrangement allows the fused electrolyte to be in contact only with Inconel and does not sacrifice the pressure tightness or convenient geometry of ordinary irradiation capsules.

HIGH-TEMPERATURE PROPERTIES OF POTASSIUM MONOFLUOROPHOSPHATE

M. T. Robinson G. E. Klein

Monofluorophosphates exhibit a very low viscosity at the operating temperature of the ARE; if they could be used in a reactor there would be a considerable saving in the required pumping power. A few tests have been made of the high-temperature stability of K_2PO_3F and of its compatibility with container materials. The lattice constants of the room-temperature modification have been determined. The report of Ray[4] that K_2PO_3F and K_2SO_4 are isomorphous has been verified by x-ray diffraction; however, it was found that the salts Na_2PO_3F and $(NH_4)_2PO_3F$ were not isomorphous with the corresponding sulfates. Patterns of the sodium and ammonium salts have not been analyzed, but cell constants for K_2PO_3F and K_2SO_4 are given below:

	β-K_2SO_4	K_2PO_3F
a_0, Å	7.534	7.587
b_0, Å	10.12	10.20
c_0, Å	5.800	5.924
Z	4	4
$d_{calc.}$, g/cm^3	2.615	2.551
$d_{meas.}$, g/cm^3	2.622	2.495
Space group	$D_{2h}^{16} - Pnma$	$D_{2h}^{16} - Pnma$

Potassium monofluorophosphate has been tested as follows:

1. in a graphite crucible at 5×10^{-4} mm pressure of air for 2 hr at 800°C,
2. in a porcelain crucible at 1 atm pressure of air for 17 hr at 1000°C,
3. in an Inconel capsule at 1 atm pressure of air for 24 hr at 900°C,
4. in a graphite crucible with chromium metal chips at 10^{-5} mm pressure of helium for 2 hr at 900°C and 1.5 hr at 1000°C.

In the first test, no decomposition was observed, and except for a small quantity of moisture, no volatile product was collected.

[4] P. C. Ray, *Nature* 126, 310 (1930).

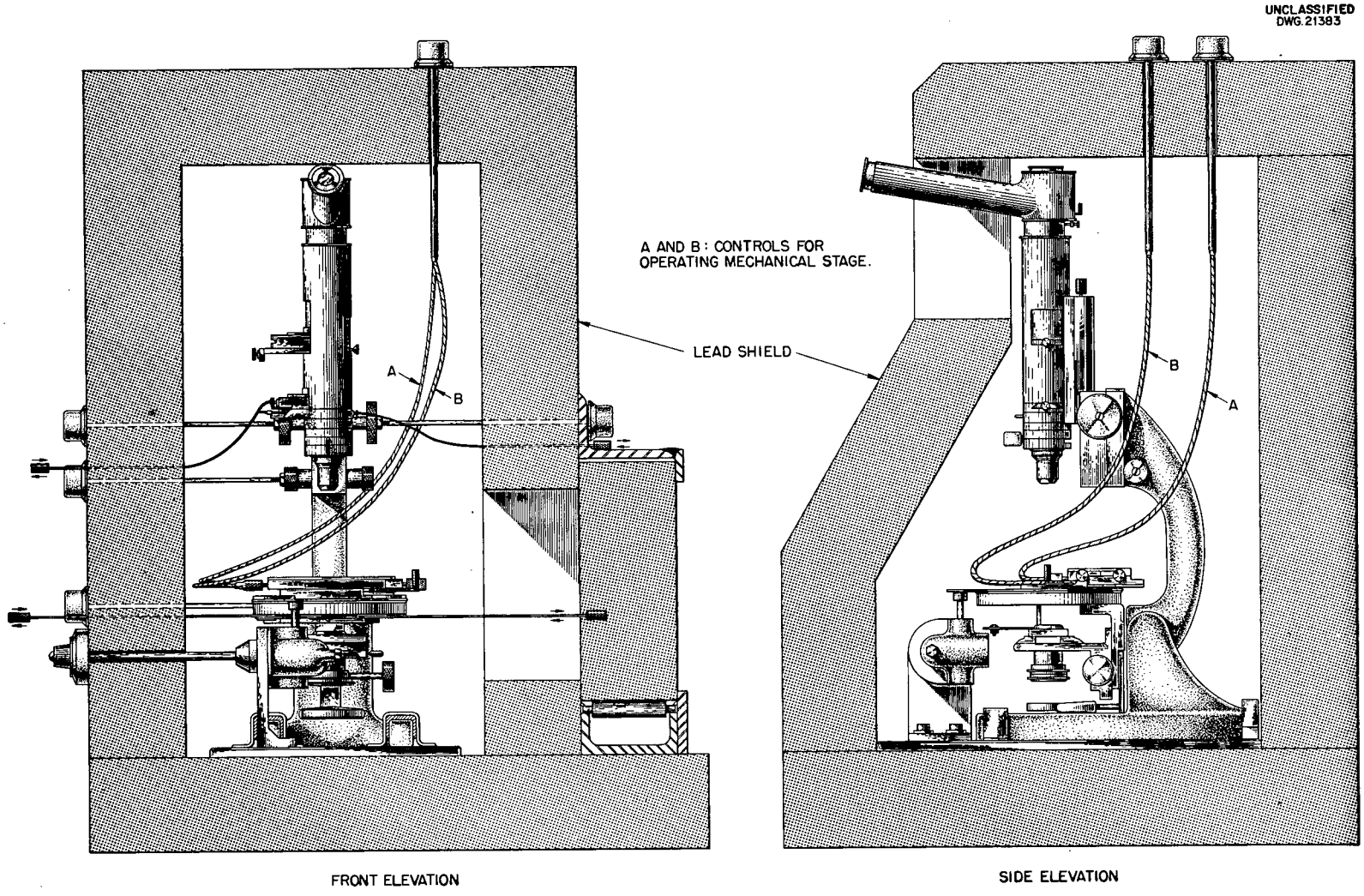

Fig. 47. Shielded Petrographic Microscope.

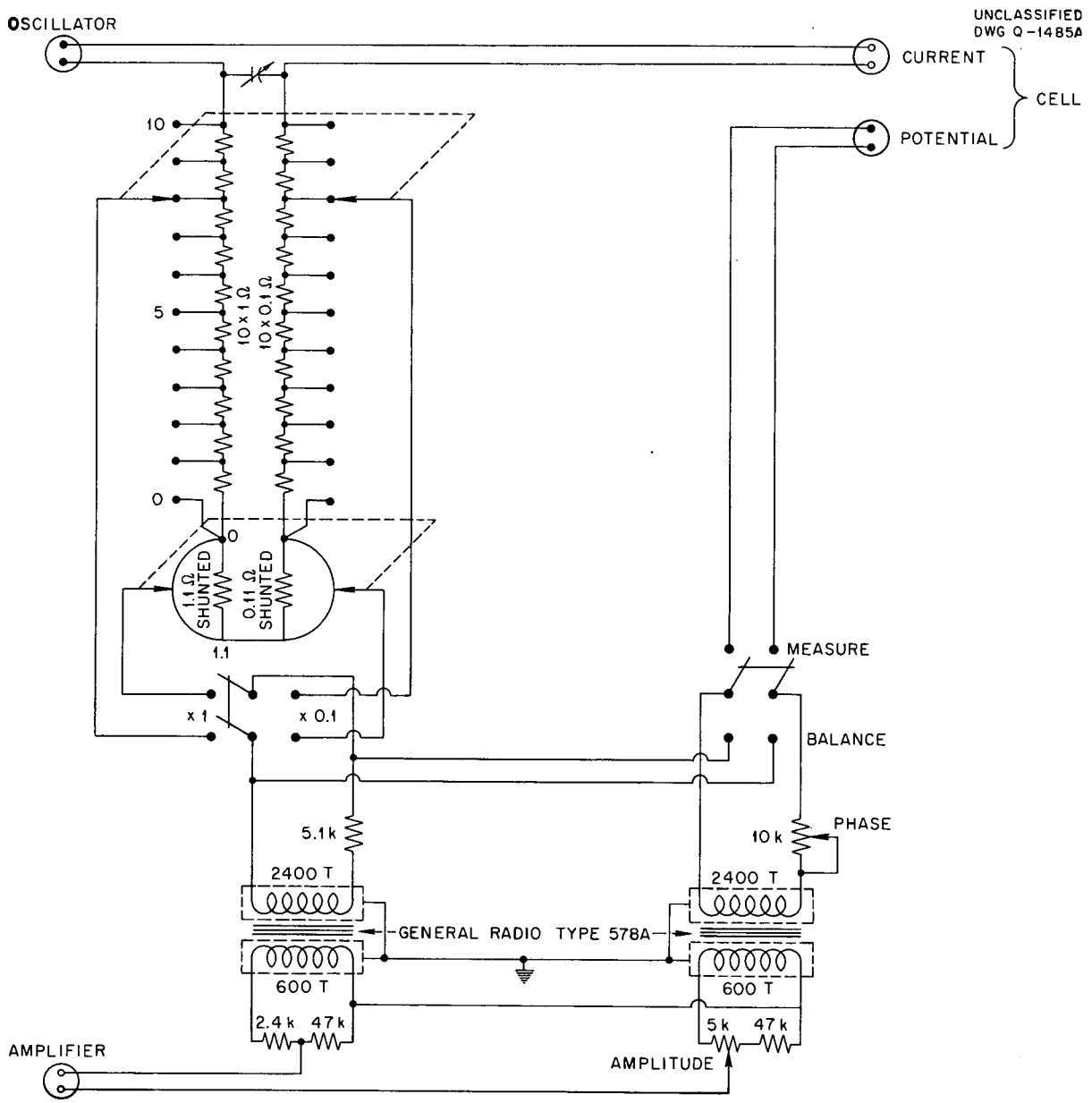

Fig. 48. A-C Resistance Comparator.

In the second test, the salt attacked the porcelain very strongly, and the product was unidentifiable.

In the third test, there was evidence that part of the metal had fused (m.p. of Inconel = 1400°C); this part was chromium free. The remainder of the capsule was only lightly corroded, and the salt was still largely K_2PO_3F, although it contained an unidentified green compound.

The fourth test gave a green salt product containing Cr_2O_3 and K_3PO_4 and also unidentified materials that were different from those in tests 2 and 3. A white substance, solid at the temperature of liquid N_2 and gaseous at room temperature, was collected that was presumed to be PF_3. Most of the K_2PO_3F was recovered as a white sublimate from the walls of the furnace tube.

It appears likely that a reaction such as

$$9K_2PO_3F(l) + 2Cr(s) = 3PF_3(g) + Cr_2O_3 + 6K_3PO_4$$

is responsible for the extensive and rapid reaction of K_2PO_3F with chromium metal. The use of Inconel or stainless steels with this material appears to be undesirable.

SPECIAL PROJECTS

ANNEALING OF IRRADIATED GRAPHITE-UO_2 MATERIALS

R. H. Kernohan

Test results for graphite bars that contained 5 wt % uranium in the form of UO_2 nodules of varying sizes and that had been irradiated for one month in the ORNL graphite reactor were given in previous reports.[1] The weight, dynamic modulus of elasticity, electrical resistivity, and relative thermal conductivity of the bars were measured before and after irradiation.

Annealing studies in which the changes in electrical resistivity were used to indicate the extent of recovery from neutron and fission damage were made during the report period. A process of step-annealing in which each specimen or bar was heated for 1 hr at each temperature, beginning with 150°C and going up by 25-deg steps to 425°C, was used in the study. After each heating step, each specimen was removed from the annealing furnace, allowed to cool, and its resistivity was measured and corrected to 20°C (see Table 5). Since data taken in the vicinity of 400°C indicated that very little further annealing was occurring, the specimens were given a long-time anneal (18 hr) at 425°C. Measurements following the long anneal indicate, within the limits of error, only slight changes; these measurements are shown in column 6 of Table 5. A further anneal at 750°C for 12 hr was then given the specimens; results are shown in column 7 of Table 5. Difficulties usually inherent in measuring resistivity of graphite probably account for much of the variation in the last three columns of this table. Also, measurements given in column 5 were made in a different resistivity device than those listed in the other four columns.

Following the anneal of the specimens listed in Table 5, all other irradiated specimens were annealed for 18 hr at 425°C and their resistivities were measured. Since there were variations from specimen to specimen in the preirradiation values of resistivity and since some basis of comparison of specimens and specimen types was needed, it

[1] R. H. Kernohan, *Solid State Quar. Prog. Reps. for Jan. 31, 1952*, ORNL-1261, p. 41; *May 10, 1952*, ORNL-1301, p. 30; *Nov. 10, 1952*, ORNL-1429, p. 38; *Feb. 10, 1953*, ORNL-1506, p. 33.

TABLE 5. RESISTIVITIES OF GRAPHITE-UO_2 BARS

SPECIMEN	SIZE OF UO_2 NODULES (μ)	RESISTIVITY, ρ*				
		Before Irradiation	After Irradiation	After Step Anneal	After 18 hr at 425°C	After 12 hr at 750°C
R-2	No UO_2	1432	1892	1502	1519	1505
S-12	586	1437	1843	1547	1555	1543
T-6	334	1399	1712	Not measured	1511	1500
U-7	94	1404	1819	1598	1628	1624
V-7	<44	1509	2771	2429	2468	2407

*ρ in μohm-cm corrected to 20°C.

was decided to normalize all resistivities from their preirradiation value to the value 1000. The reciprocal of the normalized resistivity or the normalized conductivity was then calculated. Thus, in Table 6, the original or preirradiation value of the electrical conductivity of each specimen is taken as 1000 mhos/cm. The true values are lower than this normalized value and range from 660 to 715 mhos/cm. The values in Table 6 are the normalized conductivities after irradiation and after the subsequent anneal at 425°C. Since the value for the R specimens does not return to 1000, it is obvious that not all the neutron damage has been annealed out. Presumably some neutron damage is still retained in all the specimens.

A comparison of the observed and the theoretical fission damage to the various types of specimens is shown in Table 7. Figure 49 is a graph of the normalized conductivity values vs. the reciprocal particle size of the UO_2. The particle sizes of the UO_2 were microscopically determined, except in the case of the V-type specimens whose particles passed through a U. S. Standard 325-mesh sieve. The fabricators of the specimens believe that the average particle size for the V specimens would be in the neighborhood of 20 μ or less, rather

TABLE 6. NORMALIZED ELECTRICAL CONDUCTIVITY OF GRAPHITE-UO_2 BARS

SPECIMEN	SIZE OF UO_2 NODULES (μ)	CONDUCTIVITY,* σ'	
		After Irradiation	After Annealing
R-1	No UO_2	828	955
R-2	No UO_2	757	943
R-6	No UO_2	770	932
Average		785	943
S-5	586	883	929
S-9	586	820	930
S-12	586	779	924
Average		827	928
T-2	334	854	923
T-6	334	817	926
T-17	334	808	918
Average		826	922
U-4	94	765	863
U-7	94	772	862
U-11	94	806	876
Average		781	867
V-3	<44	501	579
V-7	<44	545	612
V-8	<44	604	681
Average		550	624

*Conductivity before irradiation = 1000.

than 22 μ as shown in Fig. 49. It is perhaps because of this wide range in size that there is a wide range in normalized conductivity values for the V specimens. In other words, the specimens are not truly homogeneous. The variations in size and in conductivity values make the location of a good point for the V-type specimens on the graph very difficult.

It is well known that a large part of the neutron damage anneals out of pure graphite at about 250°C, whereas the remainder anneals out around 1100°C.

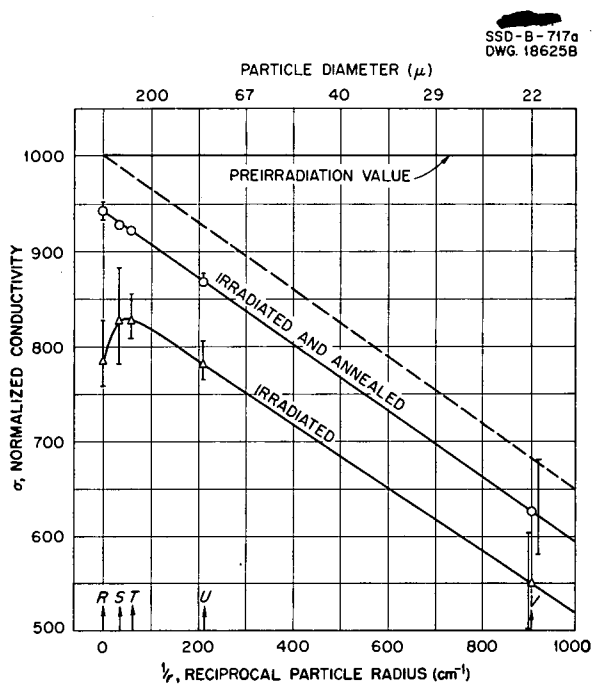

Fig. 49. Reciprocal Particle Size vs. Normalized Conductivity of Graphite-UO_2 Specimens.

From the values of conductivity for the R specimens, it would appear that about three-fourths of the effect from the damage has been removed by annealing at 425°C and that about one-fourth remains. All the specimens were subject to neutron damage. The dotted curve which is drawn parallel to the top solid curve of Fig. 49 and which intersects the preirradiation value curve (1000) at $1/r = 0$ indicates conductivity values if all neutron damage were annealed out and only fission damage remained. The value of the ordinates between the dotted curve and the horizontal curve (1000) representing the preirradiation value is a measure of the fission damage remaining in the specimens.

The extent of fission damage can also be considered from a theoretical point of view. For mathematical purposes, it can be assumed that each UO_2 nodule is a sphere of radius R containing fissionable atoms whose fragments will have a range of r in UO_2. The geometrical probability that a fragment will escape the surface of the sphere and thus enter the graphite matrix is then

$$p = \frac{3}{4}\frac{r}{R} - \frac{1}{16}\left(\frac{r}{R}\right)^3 .$$

However, this approach is inadequate for several reasons. The value of r in UO_2 is not known, but, from available information, the range would appear to be about 6 microns. The exact value of the radius of the V-type specimens is not known, and this approach also neglects the range-energy relationship of fission fragments.

In spite of the objections mentioned above, a comparison of the ordinate values, f', between the dotted and the horizontal lines of Fig. 49 with the geometric escape probability, p, for a fragment

TABLE 7. COMPARISON OF OBSERVED AND THEORETICAL FISSION DAMAGE

SPECIMEN TYPE	PARTICLE DIAMETER (μ)	OBSERVED ORDINATE VALUE, f'	THEORETICAL ESCAPE PROBABILITY, p*	$p/f \times 10^3$
S	586	13	0.0154	1.18
T	334	21	0.0269	1.28
U	94	75	0.0957	1.28
V	22**	320	0.399	1.25

*Assumed fission-fragment range of 6 μ in UO_2.

**Average.

range of 6 μ (see Table 7) shows that there is a fairly good correspondence.

PHYSICAL-PROPERTY TESTS ON THORIUM

R. H. Kernohan R. E. Adams[2]

Six specimens of pure thorium metal fabricated under the direction of R. E. Adams and E. J. Boyle of the Metallurgy Division were tested for physical properties. All specimens were tested in remotely controlled measuring apparatus for density, dynamic modulus of elasticity, electrical resistivity, and relative thermal conductivity, and they will be sealed in suitable containers and irradiated in the MTR. Table 8 is a summary of the measurements taken; a repetition of the measurements will be made after irradiation.

TRANSFORMATIONS OF Cd-Au SINGLE CRYSTALS

D. S. Billington R. H. Kernohan
T. A. Read[3] T. C. Wollan

The alloy consisting of 49.0 at. % cadmium and 51.0 at. % gold transforms, in the region just above room temperature, from the tetragonal to the cubic phase. This transformation occurs when the alloy is heated to between 45 and 55°C and is apparently diffusionless. When the cubic phase is cooled, the reverse transformation to the tetragonal phase occurs around 30°C.

Two single crystals of this alloy in the form of ⅛-in.-dia rods, 2½ in. long were prepared by M. S. Wechsler and T. A. Read of the Columbia University School of Mines. The transformations were followed by means of electrical-resistance measurements, and the measurements made at Columbia could easily be reproduced in the remote resistivity apparatus in the ORNL hot cells.

One of the specimens, J-5, was irradiated for one week in hole 51 of the ORNL graphite reactor. This facility is water cooled; consequently the specimen was irradiated in the low-temperature tetragonal phase. The integrated neutron flux was approximately 5×10^{17} neutrons/cm^2. Since the transformation occurs at such a low temperature and so easily, it was considered that neutron bombardment might easily change the nature or temperature of the transformation.

The results after irradiation, shown in Fig. 50, do not differ at all from preirradiation results, and it may be concluded that the transformation is not affected. (The specimen was run through the heating cycle one day, allowed to remain in the cubic phase overnight, and cooled the next day. The fact that the ends of the heating-cooling curves do not coincide may be attributed to stress-relaxation effects.) Plans are now being made to irradiate the specimen while it is in the cubic, or high-temperature, phase.

ABNORMAL AFTEREFFECTS IN ALUMINUM

D. S. Billington R. H. Kernohan
T. C. Wollan

Studies of the untwisting of iron, zinc, and cadmium wires that have been twisted beyond their elastic limits have provided evidence that an

[2] Metallurgy Division.
[3] Columbia University School of Mines.

TABLE 8. PREIRRADIATION MEASUREMENTS ON THORIUM RODS

ROD NUMBER	WEIGHT (g)	LENGTH (in.)	DIAMETER (in.)	DENSITY (g/cc)	ELECTRICAL RESISTIVITY (μohm-cm)	MODULUS OF ELASTICITY (psi)
1	16.1495	2.7480	0.1981	11.673	18.37	9.79×10^6
2	16.7065	2.7469	0.2013	11.672	18.38	10.03×10^6
3	16.7211	2.7446	0.2015	11.669	18.41	9.78×10^6
4	16.8096	2.7652	0.2012	11.665	18.33	10.05×10^6
5	16.8131	2.7543	0.2017	11.666	18.37	9.96×10^6
6	16.7652	2.7550	0.2015	11.667	18.43	9.44×10^6
Average				11.669	18.38	9.84×10^6

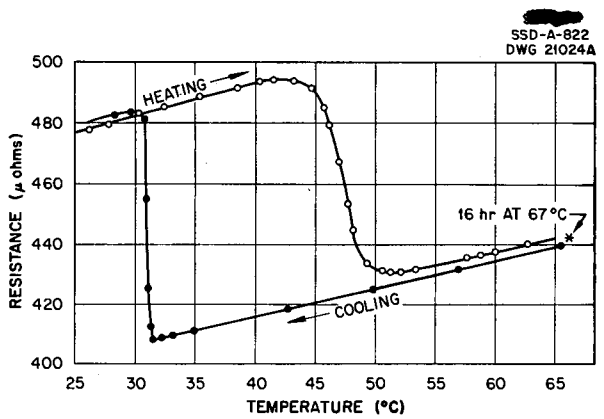

Fig. 50. Resistance vs. Temperature of an Irradiated Cd-Au Crystal.

oxide film on the surface of a metal can constitute a barrier to the escape of dislocations that approach the surface from within the metal. The escape of dislocations is made possible by etching away the oxide film and is revealed as an abrupt decrease in the rate of untwisting. In fact, a twisting effect or abnormal aftereffect may occur if the movement of dislocations released by etching is greater than the normal redistribution of locations causing the untwisting. The twisting or abnormal aftereffect has been observed by Barrett,[4] Phillips and Thompson,[5] Coffin and Weiman,[6] and by others.

Studies of the abnormal aftereffect could provide basic information on plastic flow, as well as information on surface films and stress corrosion. Stress corrosion may be of particular interest in that it can be enhanced or diminished by neutron bombardment. Studies of abnormal aftereffect on irradiated stainless steel wires might also furnish pertinent data for those interested in homogeneous reactors.

A device was constructed that consisted of a glass tube in which a wire specimen could be mounted. The wire was fixed at the bottom end, and a galvanometer mirror was attached to the top end; a gripping mechanism for twisting the wires was also included.

In order that the reliability of the device could be checked, specimens made from 2-in.-long, 0.035-in.-dia 2S aluminum wires which had been annealed were twisted in the device and measured. All specimens were surrounded with water when they were twisted through 360 deg and were held for 30 sec in the position of maximum strain before being released. At the end of 6 min, during which time the rate of untwisting had been established, the water environment around three of the specimens was replaced with an etchant (2% HF, 10% HCl, and H_2O). An abrupt twisting was observed and then the normal untwisting again occurred. The course of untwisting of each of the three wires (see Fig. 51) with all specimens normalized to the 3-min starting level indicates that the abnormal aftereffect is fairly reproducible. Thus far, attempts to discover any changes in rate of untwisting of stainless steel wire have not been successful.

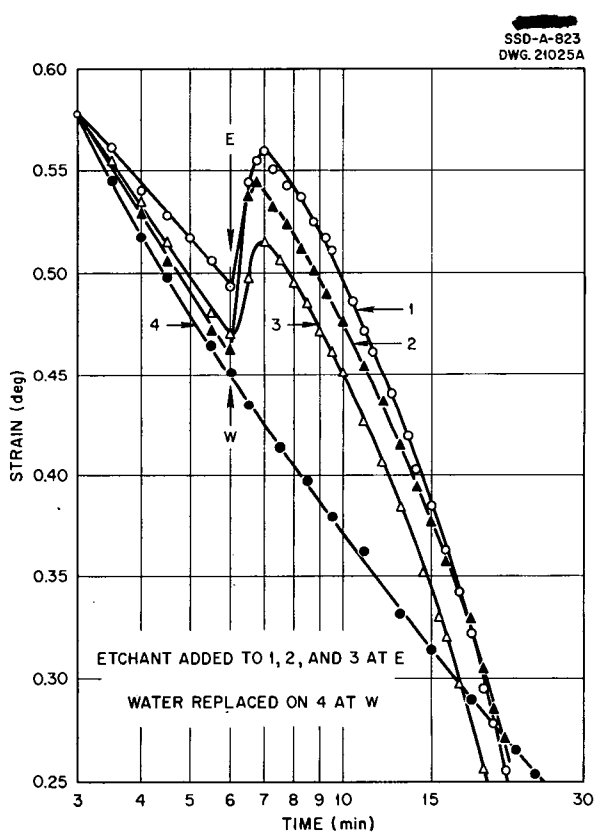

Fig. 51. Strain Aftereffects in 2S Aluminum.

(4) C. S. Barrett, *Acta Met.* 1, 2 (1953).

(5) D. J. Phillips and N. Thompson, *Proc. Phys. Soc. (London)* B63, 839 (1950).

(6) F. D. Coffin and A. L. Weiman, *J. Appl. Phys.* 24, 282 (1953).

CURIE TEMPERATURE OF Ni-Be ALLOY

D. S. Billington R. H. Kernohan
A. B. Lewis

The Curie temperature, or the temperature at which a ferromagnetic material loses its magnetic property, is a function of the impurity contained in the material. This is particularly true for the alloy Ni-Be. Pure nickel has a Curie temperature in the neighborhood of 360°C, whereas an alloy containing only 2.5 wt % beryllium has a Curie temperature of about 35°C. Furthermore, the alloy Ni-Be, when rapidly quenched from 1100°C, is supersaturated with beryllium atoms and can be age-hardened by heat treatment in a manner similar to that used on the alloy Cu-Be. Thus, the beryllium content can be varied by heat treatment and can be indicated easily by changes in the Curie temperature.

Since it was realized that the position of beryllium atoms may be influenced by fast-neutron bombardment, a study was begun on the variation of Curie temperature in Ni-Be alloys. Much previous work on this alloy was done by Gerlach.[7]

A vacuum casting of Ni-Be was produced by W. McNeish of the Metallurgy Division and was subsequently shaped by alternate steps of heat treatment and swaging into ⅛-in. rods by H. Inouye of the Metallurgy Division. The final analysis was 2.3 wt % beryllium and 97.7 wt % nickel.

Several methods for accurate measurement of Curie temperature were tried, the most successful being the Anderson bridge method for measuring inductance. A method was also devised for studying hysteresis patterns on a cathode-ray oscilloscope. For the Anderson bridge, a 4-in. long coil of 1400 turns was wound on a ceramic core whose inner diameter was just large enough to hold the ⅛-in.-dia, 4-in.-long Ni-Be rods. The Curie temperature is indicated as an abrupt change in the value of inductance when the coil and the specimen are heated in an oven. Figure 52 shows the result of a run on a Ni-Be rod which had been solution annealed for 1 hr at 1070°C and rapidly quenched. The Curie temperature may be taken as 61°C. Furthermore, an a-c bridge must also be balanced with respect to resistance, as well as inductance, and the lower curve represents the effective resistance of the coil as measured by the bridge. The resistance measurement also gives an indication of the Curie temperature, as can be seen in Fig. 52.

A run was also made on the as-swaged material. The Curie temperature was in the neighborhood of 130°C, but the point could not be accurately repeated because of stress-relaxation effects. Gerlach also established that this point was indefinite for the work-hardened alloy.

Studies will be continued on the Curie temperature of Ni-Be as a function of age-hardening heat treatment and irradiation.

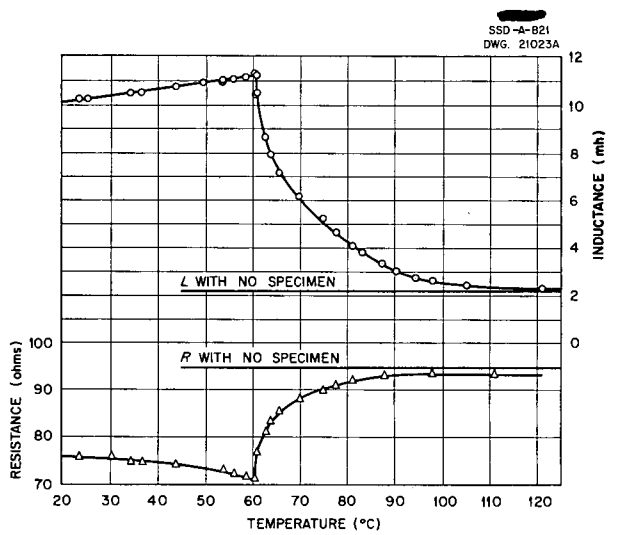

Fig. 52. Curie-Temperature Curve of Solution-Annealed Ni-Be Alloy.

EFFECT OF REACTOR IRRADIATION ON THE THERMAL CONDUCTIVITY AND OTHER PROPERTIES OF STRUCTURAL MATERIALS

A. Foner Cohen L. C. Templeton

A survey of in-pile thermal-conductivity experiments performed at various temperatures from approximately 250 to 830°C indicates no change in thermal conductivity as a result of irradiation when structural materials are exposed in either the ORNL graphite reactor[8] for periods up to several months or in the LITR for several hundred hours.[9] The experimental conditions were such that a change

(7) W. Gerlach, *Z. Metallkunde* **28**, 80 (1936); **28**, 183 (1936); **29**, 124 (1937); **30**, 77 (1938).

(8) Power level approximately 3700 kw – fuel channel near center of reactor.

(9) Power level 1500 kw – facility used was HB-3.

in conductivity of, say, 10% would have been very obvious. The materials used in the experiments included types 316 and 310 stainless steel, Inconel, and high-purity nickel which were exposed in the ORNL graphite reactor and Inconel and high-purity nickel which were exposed in the LITR.

Postirradiation tests on the same specimens which had been measured during irradiation in the ORNL graphite reactor were made at a later date at approximately 150°C and were compared with tests on unirradiated specimens of the same geometry. These before-after tests verify the in-pile results.

The specimens irradiated in the LITR were later machined to a size suitable for postirradiation measurements of the thermal conductivity. Results of such measurements at 150°C agreed within the accuracy of measurement (better than ±3%) with those on unirradiated control specimens of similar geometry. Two Inconel specimens and one high-purity nickel specimen comprised the irradiated samples. The conclusion is, therefore, that LITR irradiation of Inconel and nickel for periods of several hundred hours does not affect the thermal conductivity.

In addition, a small Inconel sample irradiated in the MTR at approximately 300 to 400°C for 406 hr at a flux intensity of approximately 2.7×10^{14} neutrons/cm^2·sec was measured at 150°C after removal and compared with an unirradiated specimen. No indication of change in the thermal conductivity was observed within the accuracy of measurement (better than ±10%).

In the case of the specimens irradiated in the ORNL graphite reactor, postirradiation tests were performed at room temperature to determine whether the electrical conductivity or Young's modulus was affected by the irradiation. The control specimens were given heat treatments approximating those of the irradiated specimens. The electrical resistivity measurements indicate no changes in the electrical conductivity as a result of irradiation on types 310 and 316 stainless steel, Inconel, or high-purity nickel; the accuracy of the method was better than ±1%. Within the accuracy of measuring Young's modulus (± few per cent), no effect of irradiation was found in high-purity nickel, types 310 and 316 stainless steel, or Inconel.

THERMAL CONDUCTIVITY OF DIELECTRICS AT LOW TEMPERATURES

A. Foner Cohen

Construction of the cryostat[10] for use between 2 and 90°K has been completed. The associated vacuum systems and means for measuring vapor pressures of the cryostat liquids have been designed and built and were tested at 80°K with satisfactory results.

Construction of an exhaust system to be used when liquid hydrogen is used in the experiments is being completed. Techniques for the measurement of the thermal conductivity of dielectrics, as well as metals and semiconductors, before and after irradiation are currently being tried at the temperature of liquid nitrogen.

---

(10) A. Foner Cohen, *Solid State Quar. Prog. Rep. Aug. 10, 1952*, ORNL-1359, p. 27.

Part II

UNCLASSIFIED PROJECTS

CONTENTS

PART II

SUMMARY 59

SOLID STATE REACTIONS 62
- Low-Temperature Irradiation of *p*-Type Germanium 62
- Behavior of *n*-Type Germanium Bombarded at Low Temperatures 65
- Acceptor States in Bombarded Germanium 68
- Gold-doped Germanium 70
- Magnetic Susceptibility of Germanium 71
- Neutron Irradiation of Indium Antimonide 75
- Low-Temperature Irradiation of Cu-Be Alloy 77
- Rectifier Bombardment 79
- Radiation Effects in Ionic Crystals 80
- A-C Resistance Comparator 84

ENGINEERING PROPERTIES 86
- Radiation Stability of Plastics and Elastomers 86
- Dynamic Properties of Irradiated Elastomers 88
- X-Ray Diffraction Patterns of Plastics 96

SPECIAL PROJECTS 98
- Irradiation of Quartz 98
- Irradiation of Miscellaneous Materials 100
- Use of K_β Radiation for the X-Ray Analysis of Reflections Unresolved in the K_α Region 101
- Neutron Irradiation of LiF Crystals 101

SUMMARY

SOLID STATE REACTIONS

Low-Temperature Irradiation of *p*-Type Germanium. *p*-Type germanium samples were irradiated at −90 to −160°C in the hole 52 cryostat of the ORNL graphite reactor. It was found that the bombardment effects in *p*-type germanium are markedly influenced by the temperature of irradiation. Irradiation below −80°C is characterized by the introduction of defects that decrease the conductivity by the trapping of holes. Measurements of the conductivity as a function of temperature indicate that the apparent depth of these hole traps is 0.11 (±0.01) ev. When specimens irradiated below −140°C are warmed, they show a further decrease in conductivity until the temperature reaches −122°C. This behavior is assumed to be associated with a subtle rearrangement of disorder to a more stable form that has a higher concentration of hole traps associated with it. Further warming produces annealing of the bombardment-induced conductivity decrease. The latter process is presumably caused by the removal or rearrangement of unstable disorder. The disorder retained by the crystal after it is heated to room temperature is associated with acceptor states and can be removed only by annealing at 450°C.

Behavior of *n*-Type Germanium Bombarded at Low Temperatures. Irradiation of *n*-type germanium at temperatures below −100°C causes a decrease in conductivity similar to that observed at room temperature; the rate of electron removal is higher at the low temperatures by a factor of 1.5.

During warming, the conductivity behavior of *n*-type germanium differs markedly from the behavior of *p*-type material. The curve for conductivity vs. temperature for *n*-type germanium contains two peaks – one at 134°K (~−140°C) and the other at 165°K (~−110°C). This oscillatory behavior may be caused by (1) a disorder arrangement that does not alter the number of traps but which increases the trap depth or (2) a disorder rearrangement that increases the number of traps.

Only a small portion of the bombardment-induced conductivity anneals out of the *n*-type samples when they are subjected to a heating-cooling cycle. This is also in contrast to the behavior of the *p*-type material.

Acceptor States in Bombarded Germanium. It has been shown that it is possible to use a Gaussian distribution of acceptor levels with a superimposed narrow Gaussian distribution representing a discrete energy level to explain the temperature dependence of carrier concentrations arising from bombardment-induced acceptor states in *p*-type germanium.

Gold-doped Germanium. Acceptor states produced by doping germanium with gold lie about 0.15 ev above the top of the filled band, and an appreciable concentration of acceptor states produced by fast-neutron bombardment lies about 0.1 ev above the filled band. It has been found that the effect of the gold acceptors in gold-doped, *p*-type germanium can be canceled by introduction of a sufficient number of bombardment-produced acceptors.

Magnetic Susceptibility of Germanium. The magnetic susceptibility of germanium cubes was measured at 70 to 300°K. The Hall coefficient and the conductivity of plates cut from material adjacent to the cubes were measured and assumed to be representative of the cubes. The cubes exhibited an increasing diamagnetic behavior with decreasing temperature; there is a temperature dependence in the high-temperature portion of the curves.

Of the three samples irradiated, only one exhibited a measurable change in magnetic susceptibility; this was indicated by a reduction in the temperature dependence of the contribution by the unionized impurities and the current carriers at low temperature.

Neutron Irradiation of Indium Antimonide. A sample of *n*-type InSb was irradiated in hole 52 of the ORNL graphite reactor at reactor ambient temperature to determine the rate of decrease of conductivity and the possibility of conversion from *n*- to *p*-type material. Material of higher purity than that now available will be required to determine whether the conversion does take place. The initial rate of removal of electrons is almost four times the initial rate of removal from *n*-type germanium.

For *p*-type InSb, the conversion to *n* type occurs at about −40°C and indicates an activation energy of about 0.40 ev. Irradiation in hole 52 at reactor ambient temperature with excursions to low temperatures indicated a behavior almost exactly like that previously noted for *p*-type germanium.

Low-Temperature Irradiation of Cu-Be Alloy. At low temperatures, direct reading of the resistance of Cu-Be alloy under irradiation was inaccurate

because of temperature fluctuations and noise-level increase. The temperature was therefore periodically varied, and a determination was made of the temperature coefficient of resistance which was not affected by irradiation; the resistance change was then obtained from successive *R* vs. *T* curves.

The slope of the relative resistance curve for a specimen irradiated at 30°C was about 2.5 times larger than that for a specimen irradiated at −150°C.

A sample that had been irradiated at −150°C was warmed to 50°C to determine the time required to anneal the disorder stored at low temperature; 4 hr was sufficient for the change.

These experiments are believed to indicate that lattice disorder produced during low-temperature irradiation causes only a small amount of resistance increase, whereas the greater portion of radiation-induced resistance increase depends on a process that is presumably microdiffusion, and microdiffusion requires a thermal activation.

Rectifier Bombardment. Construction has been completed on a function plotter that permits the tracing in about ½ min of a complete forward and reverse characteristic curve of a rectifier. Previously, the fixed-bias type of measurements required correlation of data from different units and extrapolation of data taken on the same unit. The function plotter has been used for studying the changes in an IN38A Sylvania glass-sealed germanium tube during bombardment. The forward characteristic shows little change in the first 20 min, but the reverse current changes in 20 min by an order of magnitude for a given voltage change. There are some indications that the sample should become ohmic after 115 min of bombardment, but it is still clearly nonlinear after 260 min of bombardment.

Radiation Effects in Ionic Crystals. Electrical conductivity measurements were made on potassium chloride crystals irradiated with a Co^{60} source. The temperature of the crystals was increased by intervals of 25 to 30°C and held for periods of time up to 2 hr for studying the annealing of the irradiation effect. Both decreases and increases were observed at various temperatures. These transitions were observed in the same sequence when samples were raised at once to a high temperature. Reasons for the changes are not yet understood.

A-C Resistance Comparator. An a-c bridge circuit has been developed for measuring the resistance of polarizable liquids. The bridge operates with any signal in the frequency range of 500 cps to 5 kc.

ENGINEERING PROPERTIES

Radiation Stability of Plastics and Elastomers. Plastics and elastomers have been exposed to sufficient gamma and reactor radiation to produce extensive changes in their physical properties. The energy absorption required to produce a given change in most properties is about the same for both reactor radiation and Co^{60} gamma radiation.

Radiation-stability measurements were made on additional plastics. Triallyl cyanurate polymer, Styron 371, Styron 637, and Melmac 592 proved to have intermediate resistance to change under bombardment. Material with quaternary carbon atoms exhibits poor stability.

A group of elastomers formulated by the Materials Laboratory of the Wright Air Development Center was tested. The chief difference between many of these elastomers and the formulations previously tested was that the former had a lower percentage of carbon black. The radiation stability of both groups of formulations is about the same and indicates that the polymer rather than the filler largely governs the radiation stability of the formulation.

Dynamic Properties of Irradiated Elastomers. The dynamic properties of elastomers are being measured by the vibrating-reed method. The dynamic mechanical properties are those that govern the response to sinusoidal stresses. The specimen is clamped at one end and placed in forced vibration. The amplitude-frequency relation is observed, and the resonance frequency and the band width are used to calculate the internal friction and Young's modulus. Measurements have been made on natural rubber and on synthetic styrene-butadiene formulations.

X-Ray Diffraction Patterns of Plastics. Two peaks in the x-ray patterns of polyethylene correspond to peaks found for paraffin hydrocarbons. Polyethylene has a structure similar to that of the paraffins, except that the polyethylene has amorphous regions between minute crystallites. Irradiation destroys the crystalline peaks and increases the prominence of a halo at about 4.6 Å. The x-ray pattern changes little with exposures beyond 2.4×10^{18} nvt. This is taken to indicate that crystallinity is largely destroyed by an exposure of less than 2.4×10^{18} nvt. The x-ray

pattern for nylon is affected similarly by irradiation.

SPECIAL PROJECTS

Irradiation of Quartz. The single-crystal quartz lattice remains coherent under bombardments up to 1.19×10^{20} nvt but disrupts into highly disordered polycrystalline material when irradiated by 1.35×10^{20} nvt. Although the initial rate of density change under bombardment is small, permanent damage is probably introduced in the crystal at an early stage.

Experiments indicate that neither gamma-ray nor neutron bombardment appreciably changes the oscillating frequency of y-cut quartz crystals but that, upon fast-neutron bombardment, the activity of the quartz crystals is lowered to a point at which it will no longer drive an oscillator circuit. It is believed that, in the case of neutron bombardment, the activity rather than the frequency should be studied further.

Irradiation of Miscellaneous Materials. Studies of diamond lattice expansion have been extended to bombardments of 2.2×10^{20} nvt; the density change approaches saturation at a 3.39% decrease. Single-crystal x-ray studies are now in progress.

Cubic SiC shows a density decrease of 2.51% when bombarded by 1.35×10^{20} nvt. The same bombardment decreases the density of cubic TiC by 1.15%.

The lattice constants of silicon, germanium fluorite, and calcite remained unchanged by irradiations up to 10^{20} nvt.

Use of K_β Radiation for the X-Ray Analysis of Reflections Unresolved in the K_α Region. Many cases in which the $K_{\alpha_1\alpha_2}$ doublet cannot be resolved in an x-ray pattern can be studied by the use of K_β radiation. The K_β radiation produces a peak about 20% broader than the K_α peaks, but the K_{β_1} is approximately 80 times as intense as the K_{β_2} radiation and is therefore separated appreciably from the K_{β_2} peak even when extreme line broadening renders the K_α reflections useless.

Neutron Irradiation of LiF Crystals. Single crystals of LiF were irradiated, and the changes were observed by means of x-ray and density measurements for the purpose of checking a possible difference between the measurements caused by lattice defects. Thin crystals were found to be more suitable for irradiation because there is less neutron attenuation than in thick crystals. After corrections for attenuation in the thin crystals were made, the x-ray parameter changes exceeded density parameter changes by less than 20%.

The irradiated crystals were subjected to sucessive anneals between 275 and 560°C, and, again, the x-ray parameter changes exceeded density changes by less than 20%.

The width of the x-ray line at one-half maximum broadened markedly with increasing irradiation and in the early stages of annealing; as annealing was conducted at higher temperatures, the line narrowed to its original sharp condition. This phenomenon appeared to have been caused by internal lattice strain. Irradiation also caused a strong dissymmetry in the individual components of the x-ray line.

SOLID STATE REACTIONS

LOW-TEMPERATURE IRRADIATION OF *p*-TYPE GERMANIUM

J. W. Cleland J. H. Crawford, Jr.
J. C. Pigg

A number of germanium samples (composed of material that was originally *p* type and material that was converted from *n* type to *p* type by room-temperature exposure) have been irradiated in the hole 52 cryostat of the ORNL graphite reactor. Exposures have been made from –90 to –160°C, and the experiments have demonstrated that fast-neutron bombardment introduces a considerable amount of disorder that is thermally unstable, even in this temperature range. Forster and Fan[1] have observed similar annealing effects in germanium bombarded with deuterons.

The curve for conductivity vs. bombardment time for a typical run on *p*-type germanium is shown in Fig. 53; the temperature throughout the run is shown by the dashed curve. At the beginning of the run, as the sample is cooled, the conductivity increases because of the temperature dependence of the hole mobility. In the constant-temperature range (–135°C for this run), the conductivity decreases with bombardment, and the slope of the curve indicates an approach to saturation. The constant low-temperature part of a similar curve for σ vs. bombardment time for a sample exposed at –114°C is shown in more detail in Fig. 54. The upper curve is for conductivity plotted against bombardment time; the points are experimental,

(1) J. H. Forster, H. Y. Fan, and K. Lark-Horovitz, *Phys. Rev.* 91, 229 (1953).

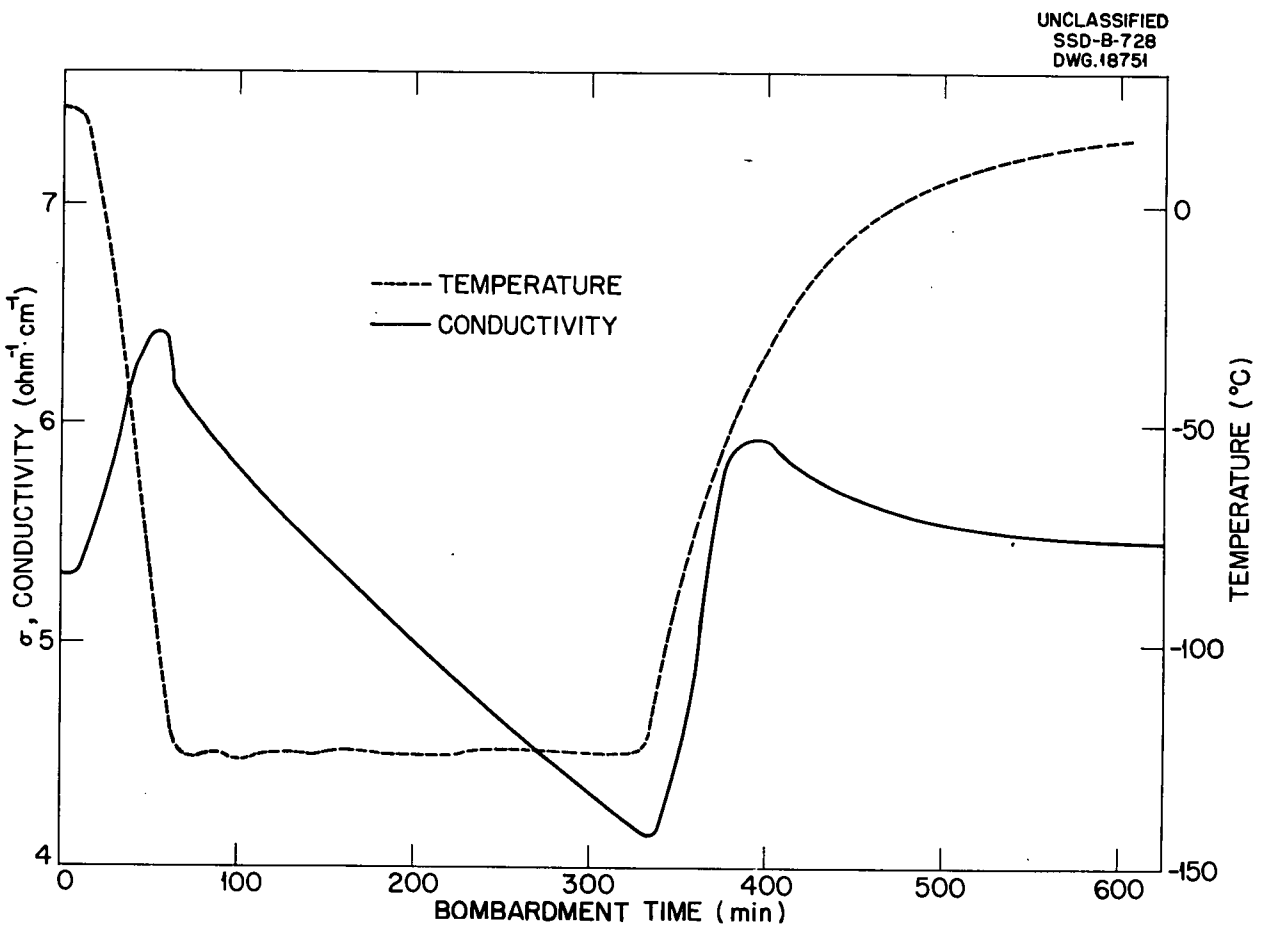

Fig. 53. *p*-Type Germanium Conductivity vs. Bombardment Time During Temperature Cycling.

while the solid line is calculated on the assumption that the bombardment-induced conductivity decrease approaches saturation by a first-order process. The equation for this behavior is

$$\Delta\sigma = \frac{K}{k'}\left(1 - e^{-k't}\right) ,$$

where K is the initial slope of the curve and k' is the first-order rate constant. These parameters were determined directly from a straight-line plot of the curve for log $\Delta\sigma/\Delta t$ shown in the lower portion of Fig. 54 in which log K is the intercept and k' is the slope of the line. The results for a number of samples are compiled in Table 9, and indicate that, in the temperature range where temperature control is sufficiently good to permit such an analysis (–135 to –90°C), the conductivity decrease does appear to anneal by a first-order process. The data in this temperature range are neither sufficiently precise nor extensive to permit the activation energy for the process to be calculated. In fact, evidence from pulse-annealing experiments indicates the existence at lower temperatures of a second-rate process which leads to a decrease instead of an increase of conductivity. If these data fall in a temperature range wherein the two processes coexist, it would not be possible to determine the activation energy of the process in question by this method.

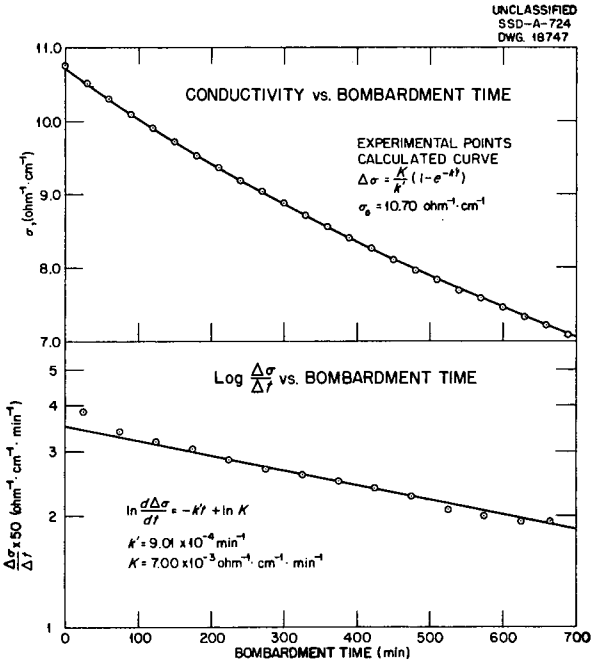

Fig. 54. Effect of Bombardment on Conductivity of *p*-Type Germanium at –114(±1)°C.

When the sample that was used for obtaining the data in Fig. 53 is warmed, the conductivity increases rapidly to a maximum at –40°C and then decreases to a room-temperature value slightly higher than that at the start of the run. This increase in the room-temperature conductivity is just what would be expected for the same period of irradiation at that temperature. Although the rapid conductivity increase may be due, in part, to the thermal release of holes trapped in the bombardment-produced defects, subsequent recooling of the sample shows that all the conductivity decrease induced by low-temperature irradiation has annealed during the warming period. The rate of conductivity increase during the heating cycle is shown in Fig. 55; $\Delta\sigma/\Delta t$ is plotted as a function of time, and the temperature during the cycle is indicated by a dashed line. The curve shows a single

TABLE 9. CURVE DATA FOR *p*-TYPE GERMANIUM

SAMPLE	RUN	EXPOSURE TEMPERATURE (°C)	K (ohm^{-1}·cm^{-1}·min^{-1})	k' (min^{-1})
45-S-12-B	1	–134	9.88×10^{-3}	3.74×10^{-3}
45-S-11-A	1	–100	4.86×10^{-3}	1.29×10^{-3}
	2	–114	7.00×10^{-3}	0.90×10^{-3}
	3	– 90	3.56×10^{-3}	3.12×10^{-3}
44-R-22	1	–114	8.59×10^{-3}	1.20×10^{-3}

maximum that is characteristic of a single-rate process. Since the effect of lattice disordering on the mobility of charge carriers is generally small compared with the effect on the carrier concentration, it can be assumed, as a first approximation, that all the conductivity decrease produced by low-temperature irradiation of *p*-type germanium is caused by the trapping of holes. The increase in conductivity during warming is due to one or both of two processes (suitably modified to account for the temperature dependence of hole mobility): (1) the thermal release of holes from traps or (2) the annealing, by some mechanism, of the hole-trap defects which releases holes. Although recooling the specimen reveals that all the conductivity decrease, and hence the hole traps, has been removed during the heating cycle, the first process is by no means ruled out. A defect which behaves as a hole trap is stabilized by the approximate extent of the trapping energy when the trap is occupied. Consequently, it is possible that the annealing process is by one of two steps: the thermal release of holes from traps or the subsequent annealing of those traps which have lost the stabilizing effect of the trapped hole. If such behavior is the case, the curve for $\Delta\sigma/\Delta t$ vs. t will not reflect the rate of annealing of hole-trap defects but, rather, the rate of thermal release of holes. This point is considered in more detail in connection with pulse-annealing experiments which yielded the necessary information for deciding between processes (1) and (2).

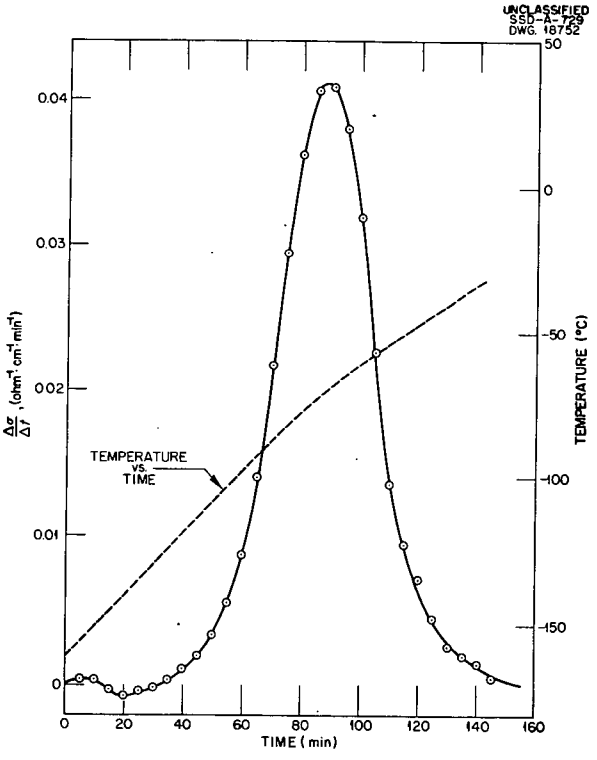

Fig. 55. *p*-Type Germanium $\Delta\sigma/\Delta t$ vs. Time During Warmup After 640-min Exposure at −150°C.

If samples are irradiated for considerable periods at temperatures below −140°C, quite different behavior is observed during the warmup, even though the curve for σ vs. bombardment is apparently the same as that observed above this temperature. Initially, as the temperature begins to rise, there is a further sharp conductivity decrease which is faintly evident in the first part of the Fig. 55 curve. In order to investigate this behavior more thoroughly, several pulse-annealing experiments were performed. The results of one such experiment, carried out simultaneously on two *p*-type samples after they had been irradiated for 18 hr at approximately −160°C, are shown in Fig. 56. The temperature was pulsed during a reactor shutdown in order to eliminate complications caused by irradiation, and, as indicated by the solid line, was pulsed to successively higher temperatures and returned, after each pulse, to the reference temperature, −166°C. These curves indicate conclusively that there are two distinct processes associated with the annealing of fast-neutron-induced disorder. After each pulse, the conductivity shows a definite decrease until −122°C is reached. Pulsing to higher temperatures produces an increase which is the characteristic annealing behavior of disorder introduced above −140°C.

Although its nature is not clearly understood at present, the low-temperature process may be a result of either a potential barrier around the lip of the hole trap, which makes trapping an activated process, or a rearrangement of disorder. Of these two processes, the latter is the more attractive. Except for certain extreme ranges of concentration, the first would be a second-order process, while the second is expected to be first order. Although the data are not sufficiently precise for an accurate analysis, examination of the annealing behavior during the third pulse shown in Fig. 56 seems to indicate first-order decay for both specimens. In addition, the alteration of the energy

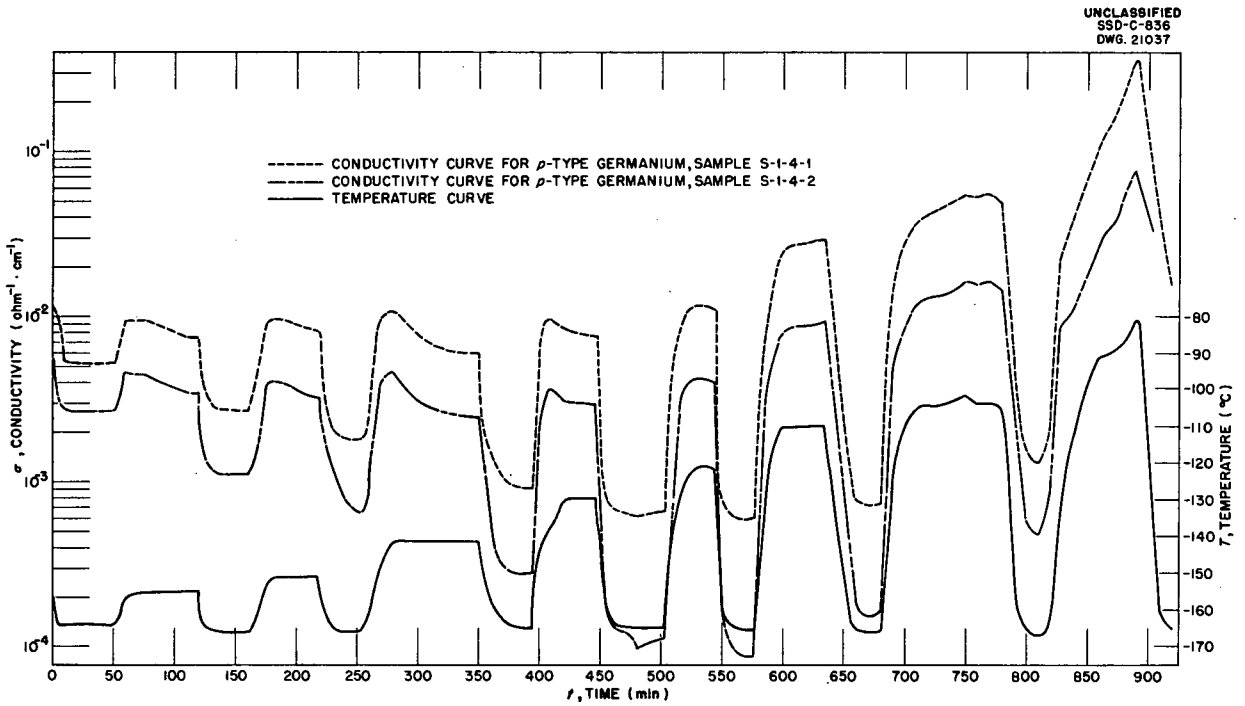

Fig. 56. Results of Pulse-Annealing Experiment.

spectrum of free holes toward higher energies by reactor radiations, even though slight, makes occurrence of the activated trapping process less likely. Experiments are being planned for improving the pulse-annealing data by providing more suitable temperature control.

Inspection of Fig. 56 reveals that a reversible process, presumably ionization of trapped holes, plays a predominant role in the σ vs. T behavior during pulsing. The warmup and cool-down data between pulses have been examined in detail. In every case, plots of log σ vs. $1/T$ yield a straight line whose slope corresponds to an apparent ionization energy or trap depth ϵ_{ap} of 0.11 ± 0.01 ev. If the concentration of traps N_t is comparable to the original hole concentration n_b^0, this value is half the true ionization energy or trap depth ϵ_t. On the other hand, if $N_t \gg n_b^0$, $\epsilon_{ap} \equiv \epsilon_t$.[2] In either case, a hole-trap defect decreases its energy by > 0.1 ev when it is occupied. In the temperature range under consideration, this would correspond to appreciable stabilization. Returning to the question raised earlier in connection with the curve for $\Delta\sigma/\Delta t$ (Fig. 55), in view of the stabilization effect and the evidence from pulse-annealing experiments for a large reversible contribution to the pulse height, it would seem that the character of this curve is predominantly due to thermal release of holes [process (1)], at least in the low-temperature region. Hence, it is expected that little can be learned concerning the annealing kinetics of hole-trap defects from curves of this sort. A better method of study is the pulse-annealing technique.

[2] N. F. Mott and R. W. Gurney, *Electronic Processes in Ionic Crystals*, 2d ed., chap. 5, Clarendon Press, Oxford, 1948.

BEHAVIOR OF *n*-TYPE GERMANIUM BOMBARDED AT LOW TEMPERATURES

J. W. Cleland J. H. Crawford, Jr.
J. C. Pigg

A number of *n*-type germanium samples have been irradiated in the hole 52 cryostat at temperatures below −100°C. The conductivity decreases with bombardment in a manner similar to that observed

at room temperature, and this indicates that electron trapping by bombardment-introduced acceptors is the predominant effect. The initial rates of electron removal per incident fast neutron were calculated from the initial slopes of the curve for conductivity vs. bombardment and the initial electron concentration by using relative fast-neutron flux values determined from the initial-slope method at ambient temperature.[3] These values, together with the initial electron concentration, n_e^0, and the exposure temperature, T_e, are listed in Table 10. The rate of removal is higher at these low temperatures than at room temperature[3] by a factor of about 1.5. It is interesting to note that the James–Lark-Horovitz model of multiple defect-energy level[4] predicts two electron traps per vacancy-interstitial pair; one of these is quite shallow (~0.05 ev) and therefore relatively ineffective except at low temperatures. It is possible that the enhanced rate of removal of conduction electrons may be due, in part, to such a trap distribution. However, examination of thermal-cycling data indicates that the excess decrease may have been annealed.

The conductivity behavior of *n*-type germanium during warming after low-temperature irradiation is in marked contrast to the behavior of *p*-type material. Curves for conductivity vs. temperature for samples B-19-7-2 (during irradiation) and S-1-4-1 (during reactor shutdown) are shown in Figs. 57 and 58, respectively. The curves are characterized by two maximums – one at 134°K and the other at 165°K. The quantitative agreement of the position of the maximums and minimums of the two curves with respect to temperature is rather striking. After the second maximum, the conductivity falls to a minimum at approximately 200°K and then increases rapidly with increasing temperature. The presence of similar maximums was also indicated in the exposure of samples Sb-6 and S-1-4-2 but was less pronounced because: (1) only a small portion of the conduction electrons in Sb-6 was trapped as a result of the high initial electron concentration, and their behavior was obscured by the temperature dependence of mobility, and (2) S-1-4-2 was bombarded almost to its minimum conductivity and therefore behaved more like intrinsic or slightly *p*-type material.

The reason for this unusual oscillatory behavior is not clear. However, it is probably caused by two or more processes. These processes must result in two successive decreases in electron concentration separated by a rather narrow temperature interval. There are at least three distinct possible processes for each of these maximums (although possible, mobility effects are not probable and are not considered here): a disorder rearrangement that does not alter the number of traps but increases the trap depth, a disorder rearrangement that increases the concentration of traps, and temperature-dependent electron trapping rates caused by a potential barrier at the lip of the trap. For reasons discussed in connection with the low-temperature

[3] J. W. Cleland, J. H. Crawford, and J. C. Pigg, "Estimation of the Effective Fast Flux in Hole 52N," *Solid State Quar. Prog. Rep. Feb. 10, 1953*, ORNL-1506, p. 43.

[4] H. M. James and K. Lark-Horovitz, *Z. physik. Chem.* 198, 107 (1951).

TABLE 10. RATES OF REMOVAL OF CONDUCTION ELECTRONS AT LOW TEMPERATURES

SAMPLE	n_e^0 (cm^{-3})	T_e (°C)	$\left(\frac{dn_e}{d\phi t}\right)_{t=0}$ (cm^{-1}·neutrons^{-1})
Sb-6	1.10×10^{18}	−157	−6.4
B-19-7-2	1.36×10^{17}	−157	−4.8
S-1-4-2	2.36×10^{16}	−153	−4.8
S-1-4-1	3.25×10^{16}	−153	−4.0
			Average −5.0

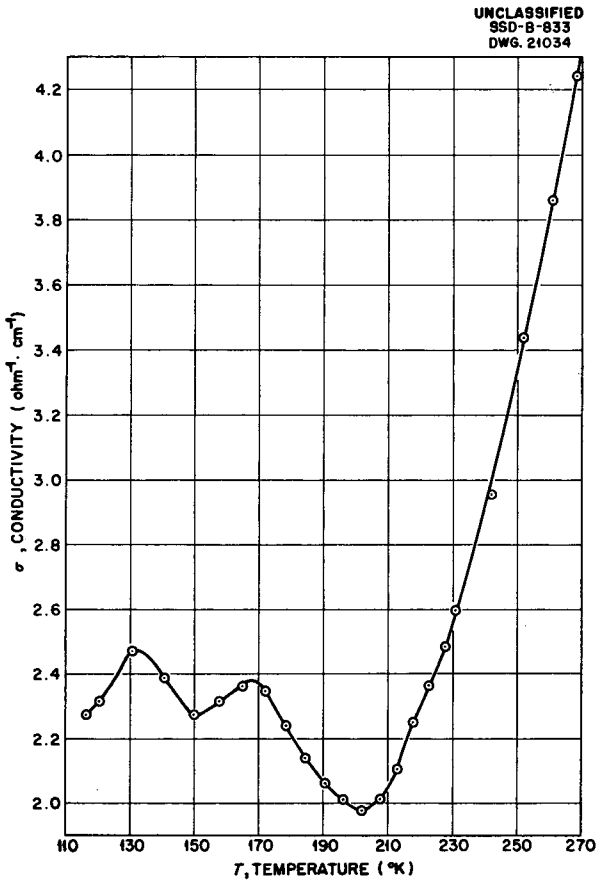

Fig. 57. Conductivity vs. Temperature for *n*-Type Germanium Sample B-19-7-2 After 2520-min Exposure at −155°C.

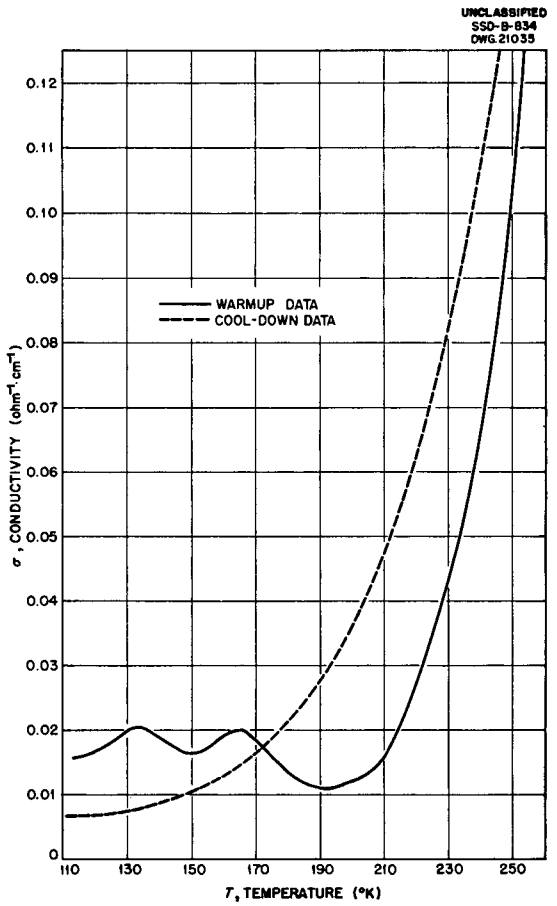

Fig. 58. Conductivity vs. Temperature for *n*-Type Germanium Sample S-1-4-1 After 1125-min Exposure at −157(±2)°C.

process observed in the case of *p*-type germanium, the third possibility is not considered as being very probable. Further experiments are required for an explanation of this behavior.

After sample S-1-4-1 was warmed to room temperature, it was recooled; the curve for σ vs. T for this operation is included in Fig. 58. The conductivity during cooling is higher than the conductivity during the warmup subsequent to the completion of the process producing the second maximum. It is interesting to note that the value at 110°K, after the temperature excursion, is lower by more than a factor of 2 than the value before the heating cycle. Further temperature variation indicates that, after the warmup, the curve for σ vs. T is reversible, at least at temperatures below 180°K. Plots of log σ vs. $1/T$ for the cooling data are shown in Fig. 59. When the residual conductivity, caused by electrons in excess of the trap concentration and represented by point A on the curve, is subtracted from the rest of the data, the corrected curve is obtained; the slope of the corrected curve yields a value of approximately 0.13 ev for the apparent trap depth. It should be pointed out that no correction is made for the temperature dependence of mobility; such an omission would lower the slope slightly.

Studies of the heating-cooling cycle data indicate that, in marked contrast to the conductivity behavior of low-temperature irradiated *p*-type germanium, only a small portion of the bombardment-induced conductivity decrease anneals out. In addition, the oscillatory behavior of conductivity observed early in the warmup run has no obvious counterpart in *p*-type germanium. These effects will be studied in more detail by pulse-annealing techniques.

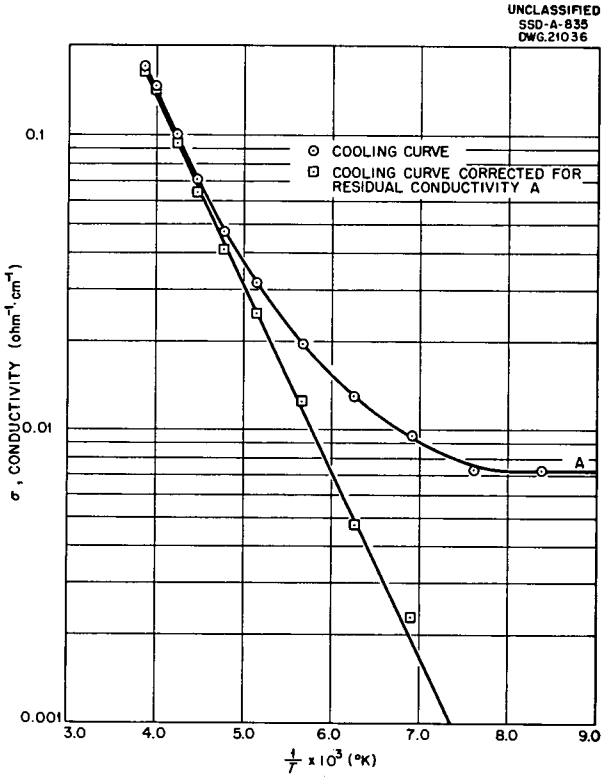

Fig. 59. Conductivity vs. Reciprocal Temperature for *n*-Type Germanium Sample S-1-4-1 After It Was Irradiated for 1125 min at −157(±2)°C and Warmed to Room Temperature.

ACCEPTOR STATES IN BOMBARDED GERMANIUM

I. M. Katz[5]

The behavior of hole concentration and mobility in bombarded *p*-type germanium (determined from Hall coefficient and resistivity measurements) as a function of temperature and period of exposure was discussed in a previous report.[6] Attempts to analyze these data on the basis of certain chosen energy-level distributions were also reported. The data could not be explained on the basis of either one or two discrete acceptor levels. The use of a square-wave distribution with a discrete level superimposed leads to reasonable success. The following is an account of the application of another type of energy-level distribution – a wide Gaussian distribution with an appropriate narrow or discrete level superimposed.

If $g(\epsilon)$ is a distribution of electron states and if $F(\epsilon,T)$ is the probability that an energy level at ϵ is occupied at temperature T, then the fraction of all states that is occupied is

$$(1) \qquad n(T) = \frac{\int_{-\infty}^{\infty} g(\epsilon)\, F(\epsilon,T)\, d\epsilon}{\int_{-\infty}^{\infty} g(\epsilon)\, d\epsilon} .$$

Fermi-Dirac statistics give, for electrons,

$$(2) \qquad F(\epsilon,T) = \frac{1}{1 + e^{\mu(\epsilon - \zeta)}} ,$$

where

ζ = Fermi level,

$\mu = 1/kT$, in which k is the Boltzmann constant and T is the absolute temperature.

For many forms of the distribution function, $g(\epsilon)$, Eq. 1 does not yield an expression in closed form. The normal distribution which is of interest is such a case. For this distribution, an approximation[7] for Eq. 2 which may be of use is

$$(3) \qquad F(\epsilon,T) \sim f(\epsilon,T) = \frac{1}{\sqrt{2\pi}} \int_{-\infty}^{(\zeta - \epsilon)/\sigma} e^{-x^2/2}\, dx ,$$

where $\sigma = \sigma(T, \zeta - \epsilon)$.

The dependence of σ upon $\zeta - \epsilon$ is investigated by calculating the value of σ that makes $F(\epsilon,T) = f(\epsilon,T)$ for some chosen value of $\zeta - \epsilon$. In these calculations, it is useful to note that Eq. 3 may be written

$$(4) \qquad f(\epsilon,T) = \frac{1}{2} \pm \frac{1}{2} P\left(\frac{\zeta - \epsilon}{\sqrt{2}\,\sigma}\right), \qquad \zeta \gtrless \epsilon,$$

where

$$(5) \qquad P(x) = \frac{2}{\sqrt{\pi}} \int_0^x e^{-t^2}\, dt$$

and is the well-known probability integral.

[5] Reactor School student with Solid State Division during summer of 1953.

[6] J. W. Cleland, J. H. Crawford, and J. C. Pigg, "Mobility and Hole Concentration in Bombarded P-Type Germanium," *Solid State Quar. Prog. Rep. Feb. 10, 1953*, ORNL-1506, p. 43.

[7] The author is indebted to M. L. Nelson of the Mathematics Panel for suggesting this approximation.

Since the Fermi function and its approximation, $f(\epsilon,T)$, have the same symmetry about the value $\frac{1}{2}$, it can be seen that σ is an even function of $\zeta - \epsilon$.

For large values of $\zeta - \epsilon$, many significant figures are required for $P(x)$ in order to calculate σ. With a method of trial and error, a value for σ at large $\zeta - \epsilon$ can be obtained by matching the slopes of Eqs. 2 and 3. Graphs of $\sigma(\zeta - \epsilon,T)$ for several values of the temperature are shown in Fig. 60. Two important facts are demonstrated: σ undergoes no rapid variations; σ does not become large anywhere in a range of reasonable values of $\zeta - \epsilon$.

Now it can be seen that if the integrand of Eq. 1 is significantly large only over a finite range of $\zeta - \epsilon$, then there will be some ϵ_1 for which $\sigma(\zeta - \epsilon_1)$ would adequately represent the value of σ for the integrand over the entire range of integration. Thus, for example, with a narrow Gaussian distribution centered at ϵ_0, $\sigma(\zeta - \epsilon_0)$ would approximate with good accuracy the value of σ for the entire integrand. The value of $\epsilon = \epsilon_1$ to choose can be determined by an examination of the shape of the integrand; this makes σ most accurate where the integrand is largest.

The approximation in Eq. 3 can now be used to find an expression for $n(T)$ for the case of a Gaussian distribution

$$(6) \qquad g(\epsilon) = \frac{1}{\sqrt{2\pi}\,\Delta\epsilon} e^{-\frac{1}{2}[(\epsilon - \epsilon_0)/\Delta\epsilon]^2} .$$

Now

$$(7) \qquad n(T) = \frac{1}{2\pi} \int_{-\infty}^{\infty} e^{-\frac{1}{2}[(\epsilon - \epsilon_0)/\Delta\epsilon]^2} \int_{-\infty}^{(\zeta - \epsilon)/\sigma} e^{-\frac{1}{2}x^2}\, dx \, \frac{d\epsilon}{\Delta\epsilon} .$$

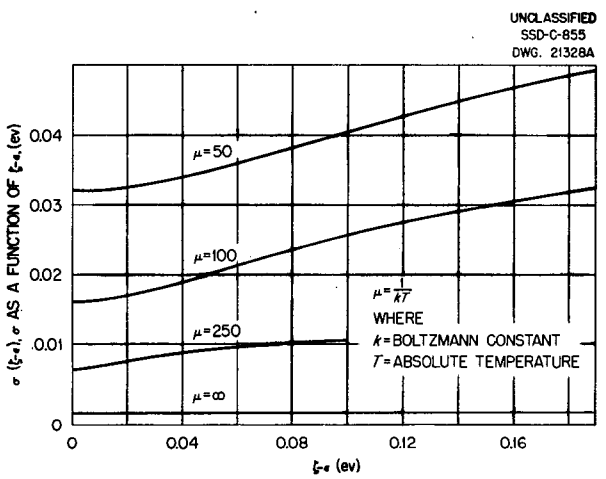

Fig. 60. Dependence of σ on $\zeta - \epsilon$ for Various Values of μ.

By a rotation of the coordinates x and ϵ, Eq. 7 can be transposed into a product of two integrals with the result that

$$(8) \qquad n(T) = \frac{1}{\sqrt{2\pi}} \int_{-\infty}^{(\zeta - \epsilon_0)/\sqrt{\sigma^2 + \Delta\epsilon^2}} e^{-x^2}\, dx .$$

Let $\omega = x/2$. Then

$$(9) \qquad n(T) = \frac{1}{\sqrt{\pi}} \int_{-\infty}^{(\zeta - \epsilon_0)/\sqrt{2(\sigma^2 + \Delta\epsilon^2)}} e^{-\omega^2}\, d\omega ,$$

and hence

$$(10) \qquad n(T) = \frac{1}{2} \pm \frac{1}{2} P\left[\frac{\zeta - \epsilon_0}{\sqrt{2(\sigma^2 + \Delta\epsilon^2)}}\right], \qquad \zeta \gtrless \epsilon_0 .$$

Equation 10 was checked against results obtained by graphical integration of Eq. 1 for the three cases in which $\zeta - \epsilon_0 = 0.007$, 0.02, and 0.041, with $\Delta\epsilon = 0.0022$. In each case, agreement was obtained to within 1%.

Equation 10 has been used to investigate the temperature dependence of hole concentrations in bombarded samples of p-type germanium. In these calculations, it is assumed that all donors are ionized and that all impurity acceptor states are filled for all temperatures considered. Each defect-produced acceptor state filled by an electron corresponds to a hole; hence the number of filled states equals the number of holes.

Hole concentrations are calculated from Hall-effect measurements by means of the equation

$$n_h(T) = \frac{7.37 \times 10^{18}}{R(T)} , \tag{11}$$

where $R(T)$ is the Hall coefficient. If the chemically introduced acceptors are subtracted, the remainder is the defect-produced hole concentration, n_h.

It should be noted here that Eq. 10 is transcendental in form, since ζ depends upon n_h through the partition function

$$\zeta = KT \ln \frac{2(2\pi m^* KT)^{3/2}}{n_h h^3} , \tag{12}$$

where m^* is the effective hole mass and is taken to be equal to the free-electron mass. Hence, Eq. 10 will not easily be solved for n_h. The data are used as a "first guess" in calculating ζ and then $n(T)$, which is examined to see whether its temperature dependence compares with the data.

For a single, narrow, Gaussian distribution, Eq. 10 does not show the same temperature dependence as that given by the data, regardless of where the Gaussian distribution is centered in the forbidden band.

An attempt was made to match the data with a linear combination of distribution functions of the form

$$g(\epsilon) = (1-\beta)\, g_1(\epsilon, \epsilon_{01}, \Delta\epsilon_1) + \beta g_2(\epsilon, \epsilon_{02}, \Delta\epsilon_2) ; \tag{13}$$

this was unsuccessful for small $\Delta\epsilon_1$ and $\Delta\epsilon_2$ and for the several values of β, ϵ_{01}, or ϵ_{02} that were tried. Another attempt was made with $\Delta\epsilon_1$ wide and $\Delta\epsilon_2$ narrow. The use of a wide Gaussian distribution calls for further consideration of the function $\sigma(\zeta - \epsilon)$. If $\Delta\epsilon^2 >> \sigma^2$, then σ need not be known very accurately for use in Eq. 10, and a value obtained by extrapolation of the curves in Fig. 60 would be sufficient. An expression that may be of use is obtained by equating the slopes of Eqs. 2 and 3 at $\zeta - \epsilon = 0$; this gives

$$\sigma = \frac{4}{\sqrt{2\pi}} \frac{1}{\mu} . \tag{14}$$

For $\Delta\epsilon \sim \sigma$, care must be taken to choose a σ which best represents $\sigma(\zeta - \epsilon)$ for the entire range of integration, as described above.

Data from a 52.33-hr irradiated sample were fitted, to within the experimental error, with the following values of the parameters (see Fig. 61):

$$\begin{aligned} \epsilon_{01} &= 0.375 , \\ \Delta\epsilon_1 &= 0.235 , \\ \epsilon_{02} &= 0.09 , \\ \Delta\epsilon_2 &= 0 , \\ \beta &= 0.05 . \end{aligned}$$

These values were varied individually until a fit was no longer obtained; this gave a range of possible values and also demonstrated the sensitivity to such variation. The results are:

$$\begin{aligned} 0.22 &< \Delta\epsilon_1 < 0.25 , \\ 0 &< \Delta\epsilon_2 < 0.01 , \\ 0.08 &< \epsilon_{02} < 0.10 , \\ 0.04 &< \beta < 0.075 . \end{aligned}$$

It is not shown that these are the only values of the parameters which will give a fit to the data. However, that the values may be significant is indicated because they also produced a fit to data from a 92.33-hr sample. Only a slight decrease in $\Delta\epsilon_1$ and in β was required to match a curve from a 334.8-hr sample. Further calculations will be necessary to identify the effect upon these parameters of varying the integrated flux to which the sample is exposed.

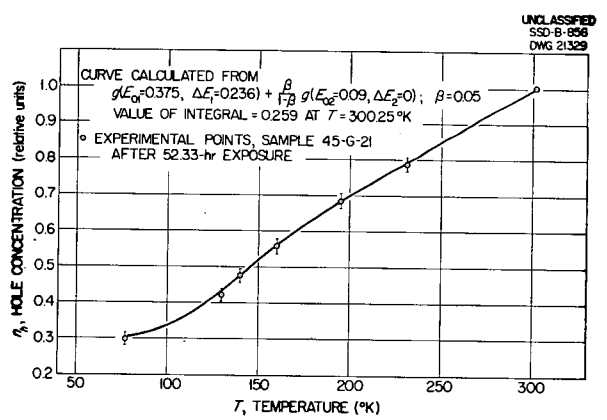

Fig. 61. Hole Concentration vs. Temperature for Irradiated Germanium.

GOLD-DOPED GERMANIUM

J. W. Cleland J. H. Crawford, Jr.
E. S. Schwartz

The acceptor states produced by doping germanium with gold lie about 0.15 ev above the top

of the filled band,[8] while recent studies (cf. "Acceptor States in Bombarded Germanium," this report) indicate that an appreciable concentration of acceptor states produced by fast-neutron bombardment, although widely distributed in energy, lies approximately 0.1 ev above the top of the filled band. It should therefore be possible to cancel the effect of the gold acceptors by the introduction of a sufficient number of bombardment-produced acceptors.

The Hall coefficient and the resistivity of a gold-doped, *p*-type germanium sample[9] were determined as a function of temperature (see Fig. 62). The sample was then exposed to a total fast-neutron flux of 2.7×10^{17} nvt; the increase in conductivity indicated an approach to saturation similar to that observed for other *p*-type germanium samples. The resistivity as a function of temperature after irradiation is also shown in Fig. 62, and it is clearly indicated that the concentration of bombardment-produced acceptor states introduced by this period of exposure completely cancels the effect of the acceptor states caused by the gold.

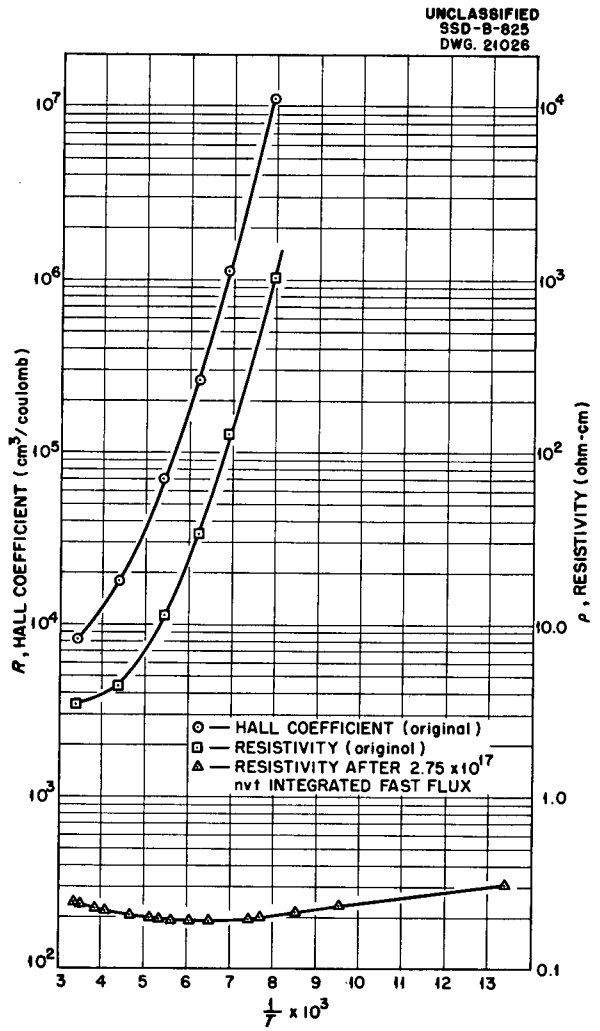

Fig. 62. Hall Coefficient and Resistivity vs. Reciprocal Temperature of Gold-doped *p*-Type Germanium.

MAGNETIC SUSCEPTIBILITY OF GERMANIUM

D. K. Stevens J. H. Crawford, Jr.
J. W. Cleland

The magnetic susceptibility (χ) of eight single-crystal cubes of germanium has been measured as a function of temperature in the range from 70 to 300°K. The Hall coefficient and the electrical conductivity of plates[10] cut from ingot material adjacent to the cubes were studied,[11] and the information obtained is assumed to be representative of these properties in the cubes. Table 11 lists the samples by Purdue melt number and shows the type, carrier concentration before and after bombardment, and irradiation time in hole 51 of the ORNL graphite reactor.

The conductivity of a companion plate was continuously monitored during irradiation, and the Hall coefficient and the resistivity of this plate were remeasured as a function of temperature after the plate was removed from the reactor. Sample Sb-7, originally *n*-type, was irradiated until the conductivity of the companion plate reached a minimum. The character of the Hall coefficient of this plate after irradiation would indicate that sizable inhomogeneities or impurity concentration gradients exist in this specimen. As a consequence, sample Sb-7 cannot be considered as representative of *n*-type germanium.

Figures 63, 64, and 65 are plots of the magnetic susceptibility vs. temperature data for the eight cubes studied. The location of a given curve with

[8] W. C. Dunlap, Jr., *Phys. Rev.* 91, 208 (1953).

[9] The authors are indebted to Miss Louise Roth of Purdue University for the preparation of the sample used in this experiment.

[10] The cubes and companion plates were prepared by Miss Louise Roth of Purdue University.

[11] Hall coefficient and conductivity studies were carried out by J. W. Cleland.

TABLE 11. IRRADIATION TIME AND CARRIER CONCENTRATION* AT ROOM TEMPERATURE

SAMPLE	BEFORE IRRADIATION		IRRADIATION (hr)	AFTER IRRADIATION	
	Type of Germanium	Carrier Concentration (cm^{-3})		Type of Germanium	Carrier Concentration (cm^{-3})
In-2B	*p*	5.4×10^{17}	47		
In-2B-I				*p*	5.2×10^{17}
In-8	*p*	2.1×10^{17}			
ORB-78	*p*	1.9×10^{14}			
ORD-7D	*n*	1.3×10^{14}			
Sb-5A	*n*	5.9×10^{16}	167		
Sb-5A-I				*p*	8×10^{16}
Sb-6	*n*	1×10^{18}			
Sb-7	n	1.3×10^{18}	118		
Sb-7-I				*n* – *p* (?)**	
Sb-11	*n*	7×10^{17}			

*Calculated from Hall coefficient data obtained on companion crystals.
***n*-Type germanium irradiated to the intrinsic region.

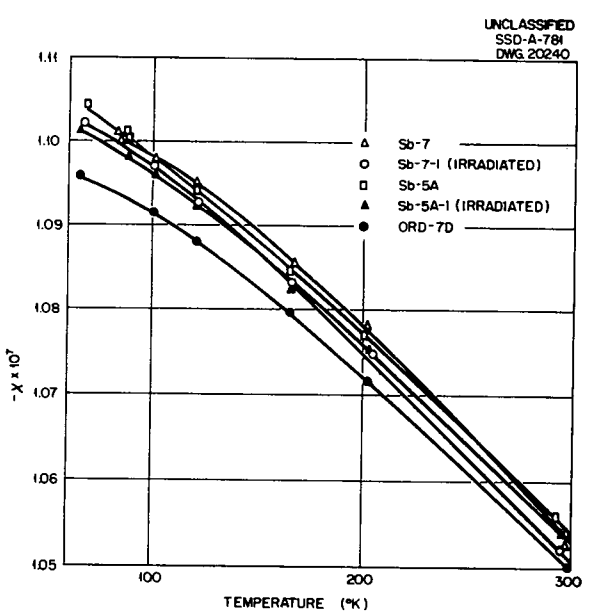

Fig. 63. Magnetic Susceptibility of *n*-Type Germanium Cubes.

respect to the ordinate may be in error by ±0.6%. The relative location of points determining a given curve is in error less than ±0.1%. From these curves, it is apparent in every case that there is an increasing diamagnetic behavior with decreasing temperature and that there is a common temperature dependence in the high-temperature portion of the curves, that is, $\Delta\chi/\Delta T = 2.44 \times 10^{-11}$ cgs units deg^{-1}. In none of the cases studied is there an anomalous hundredfold increase in the diamagnetic susceptibility at 75°K, as reported by Squire.[12]

In an expression similar to that used by Busch and Mooser[13] in their work on alpha tin, the specific susceptibility of an impure germanium semiconductor may be written as the sum of the contributions of (1) the diamagnetic susceptibility of germanium atoms combined in the lattice, χ_A; (2) the paramagnetic susceptibility of the unionized

[12] C. F. Squire, *Phys. Rev.* 58, 202 (1940).

[13] G. Busch and E. Mooser, *Z. physik. Chem.* 198, 23 (1951).

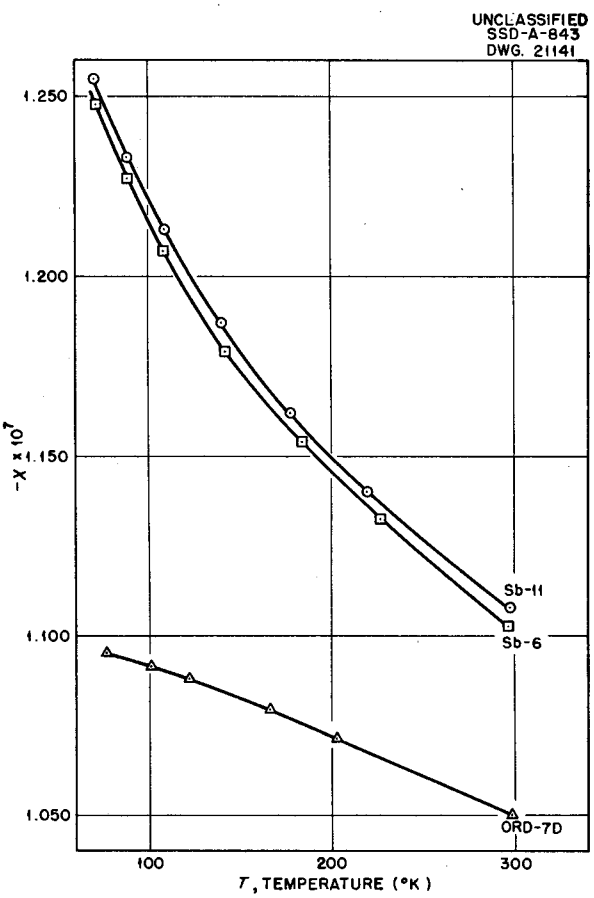

Fig. 64. Magnetic Susceptibility for Unirradiated *n*-Type Germanium Cubes.

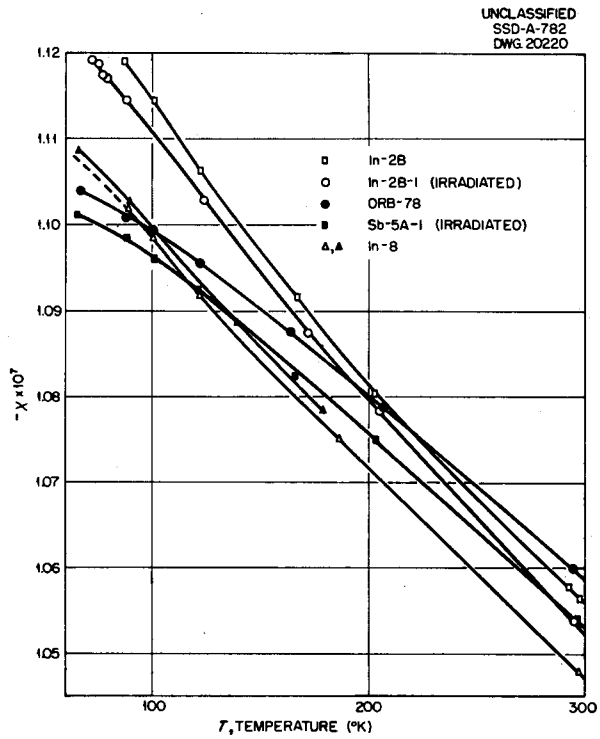

Fig. 65. Magnetic Susceptibility of *p*-Type Germanium Cubes.

impurities with an odd number of electrons, χ_I,

$$\chi_I = \frac{\beta^2}{\rho kT}\left(N_{D_i} - n_i\right) ;$$

(3) the paramagnetic susceptibility of the charge carriers caused by spin, χ_s,

$$\chi_s = \frac{\beta^2}{\rho kT} n_i ;$$

and (4) a diamagnetic contribution arising from the orbital motion of the charge carriers produced by the magnetic field, χ_o,

$$\chi_o = -\frac{\beta^2}{3\rho kT} n_i f_i^2 ,$$

where ρ is the density of germanium, N_{D_i} is the number of ionizable impurities, f is the ratio of the rest mass to the effective mass of the charge carrier ($f = m/m^*$), and n is the number of charge carriers per cubic centimeter. In *n*-type semiconductors, the subscript i refers to electrons, and in *p*-type, the subscript refers to holes. Thus,

$$(1) \quad \chi = \chi_A + \chi_I + \chi_s + \chi_o$$

$$= \chi_A + \frac{\beta^2}{3\rho kT}\left(3N_{D_i} - n_i f_i^2\right) .$$

The last term of Eq. 1 represents the over-all contribution of the charge carriers and unionized impurities with an odd number of electrons to the susceptibility. Above the temperature of liquid nitrogen, practically all the donor or acceptor atoms are ionized, and n_i may be equated to N_{D_i}. Therefore it is evident that unless the mass ratio is less than $\sqrt{3}$, the contribution of the charge carriers to the susceptibility is negative and that for all but excessively large values of this ratio (>10), the contribution would be less than 0.1% (assuming $\chi \sim -10^{-7}$ cgs units) for carrier concentrations of less than 2×10^{15} cm^{-3} at 100°K.

As indicated by their companion Hall plates, samples ORD-7D and ORB-78 are high resistivity *n*- and *p*-type specimens, respectively, with carrier concentrations much lower than 10^{15} cm^{-3}. Since the carrier concentrations in these samples are too low to make a measurable contribution, and since the χ vs. T curves are similar except for a displacement that is within the experimental error, the susceptibility vs. temperature plots are considered to be an exemplification of the germanium lattice contribution, χ_A. This term is seen to be diamagnetic and, in contrast to the assumptions of Busch and Mooser in their work on alpha tin, is temperature dependent.

Subtraction of χ_A from Eq. 1 yields the expression for the contribution of carriers,

$$\Delta\chi = \chi - \chi_A = \frac{\beta^2}{3\rho kT}(3N_{D_i} - n_i f_i^2) ,$$

which when differentiated with respect to $1/T$, gives

$$\frac{d(\Delta\chi)}{d\left(\frac{1}{T}\right)} = \frac{\beta^2}{3\rho k}\left[(3N_{D_i} - n_i f_i^2) - \frac{1}{T} f_i^2 \frac{d(n_i)}{d\left(\frac{1}{T}\right)}\right] .$$

At high temperatures, where ionization of the impurities is complete and there is no degeneracy, the expression may be simplified to

$$\frac{d(\Delta\chi)}{d\left(\frac{1}{T}\right)} = \frac{\beta^2 n_i}{3\rho k}(3 - f_i^2) .$$

Figures 66 and 67 are plots of $\Delta\chi$ vs. $1/T$ for data obtained from point-by-point subtraction of the ORD-7D and ORB-78 curves of χ vs. T from the curves for the *n*- and *p*-type specimens, respectively. It is evident from these plots that the contribution of the unionized impurities and the current carriers tends to make the material diamagnetic because of the orbital motion imparted to the electrons and the holes by the magnetic field and the low effective mass of these charge carriers. Tables 12 and 13 list the slopes of the curves and the mass ratios calculated by using the carrier concentrations obtained from the Hall data of the companion plates.

TABLE 12. CALCULATED MASS RATIOS OF HOLES IN GERMANIUM AT ROOM TEMPERATURE

SAMPLE	$\frac{d(\Delta\chi)}{d(1/T)}$	$f_i = \frac{m}{m^*}$
In-2B	-2.84×10^{-7}	4.1
In-2B-I	-2.48×10^{-7}	3.9
In-8	-1.48×10^{-7}	4.6

TABLE 13. CALCULATED MASS RATIOS OF ELECTRONS IN GERMANIUM AT ROOM TEMPERATURE

SAMPLE	$\frac{d(\Delta\chi)}{d(1/T)}$	$f_e = \frac{m}{m^*}$
Sb-6	-12.30×10^{-7}	5.9
Sb-11	-12.35×10^{-7}	6.9

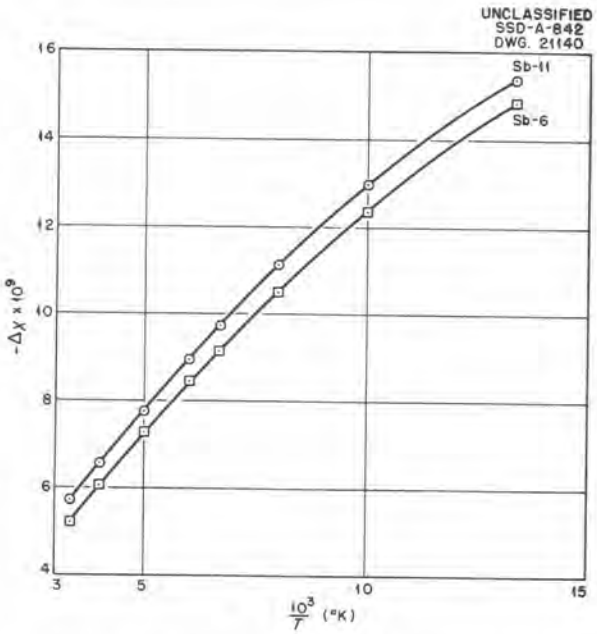

Fig. 66. $\Delta\chi$ vs. Reciprocal Temperature of *n*-Type Germanium.

Page 74 Column 1 Line 31 for contribution of the unionized impurities and the current carriers tends to make the material diamagnetic

read total contribution of the unionized impurities and the current carriers is diamagnetic

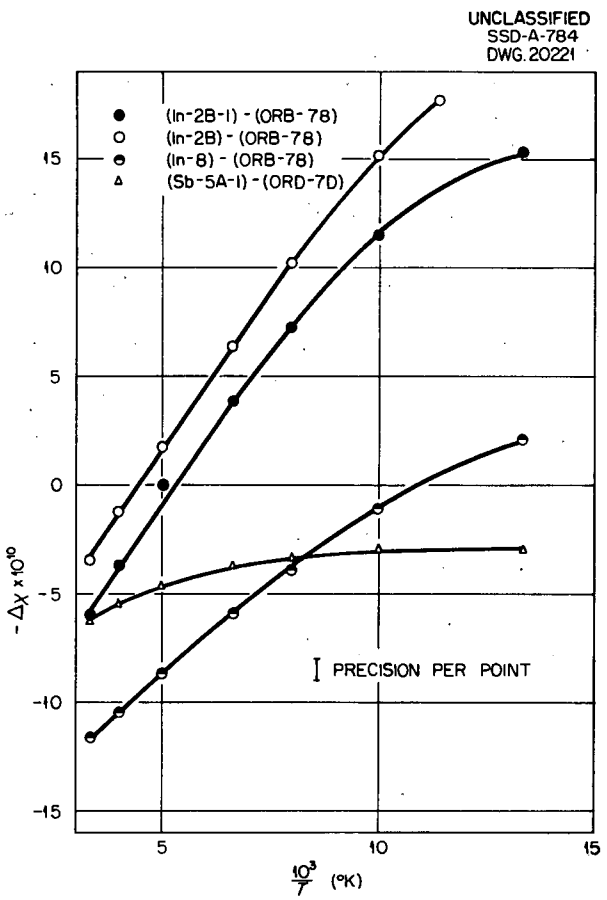

Fig. 67. $\Delta\chi$ vs. Reciprocal Temperature of *p*-Type Germanium.

As pointed out previously, the character of the Hall data of Sb-7 after irradiation indicates that sizable impurity gradients or inhomogeneities exist in this sample, and, as a consequence, the sample is not considered exemplary of *n*-type germanium. The magnetic data suggest that the carrier concentration in Sb-5A before irradiation is lower than that indicated by the companion crystal.

Of the three samples irradiated, only In-2B exhibited a measurable change in the magnetic susceptibility. The effect is seen as a reduction in the temperature dependence of the contribution by the unionized impurities and the current carriers at low temperature, in conformity with expectations. More irradiations are needed before sound interpretations can be made.

The data already assembled are being subjected to further analysis; sample Sb-11 is being irradiated and Sb-6 is to be irradiated. Further work on *p*-type and high-resistivity specimens is planned.

NEUTRON IRRADIATION OF INDIUM ANTIMONIDE

J. W. Cleland J. H. Crawford, Jr.
E. S. Schwartz

Intermetallic compounds such as InSb, GaSb, and AlSb have recently been extensively investigated.[14] Because of their similarity to other semiconducting materials of the diamond-type lattice, experiments designed to correlate the effects of reactor irradiation on these materials with effects previously observed in germanium and silicon have been undertaken. A preliminary report of the effect of reactor-ambient-temperature irradiation of a low-resistivity, *n*-type InSb sample has already been made.[15]

The Hall coefficient and the resistivity of a typical low-resistivity, *n*-type InSb sample are shown in Fig. 68. In an attempt to determine the rate of decrease of conductivity and the possibility of conversion from *n*-type to *p*-type material, a sample was exposed in the low-temperature facility of the ORNL graphite reactor at reactor ambient temperature, approximately 30°C. The curve for conductivity vs. nvt is shown in Fig. 69. It is obvious from these data that irradiation produces electron traps that decrease the conductivity, but this effect tends to produce saturation long before any conversion from *n* to *p* type could take place in material of such low resistivity. It is hoped

(14) H. Welker, *Z. Naturforsch.* 8a, 248 (1953).

(15) W. H. Sullivan and F. T. Howard, *ORNL Status and Progress Report, April 1953*, ORNL-1545, p. 26.

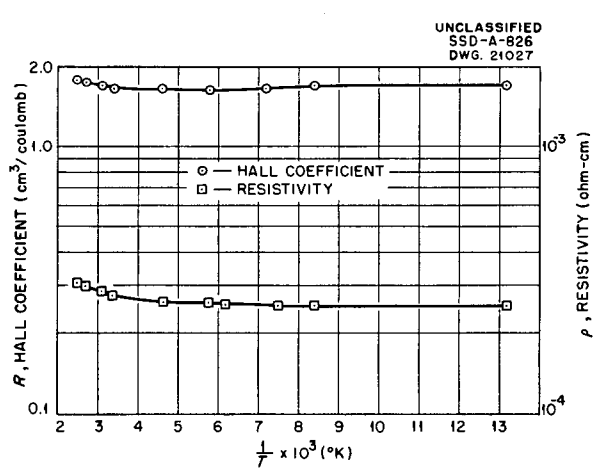

Fig. 68. Hall Coefficient and Resistivity vs. $1/T$ of *n*-Type InSb.

that starting material of higher purity may be obtained for determining whether conversion does take place. Figure 70 indicates the form of the initial portion of the curve for conductivity vs. exposure. It is interesting to note that the initial rate of removal of electrons is almost four times as great as that previously reported for *n*-type germanium.[16]

[16] J. H. Crawford, Jr. and K. Lark-Horovitz, *Phys. Quar. Prog. Rep. March 15, 1950*, ORNL-694, Table I, p. 54.

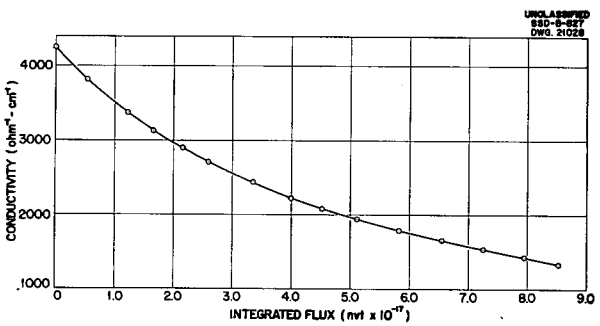

Fig. 69. Conductivity vs. Integrated Fast-Neutron Flux for *n*-Type InSb at Approximately 30°C.

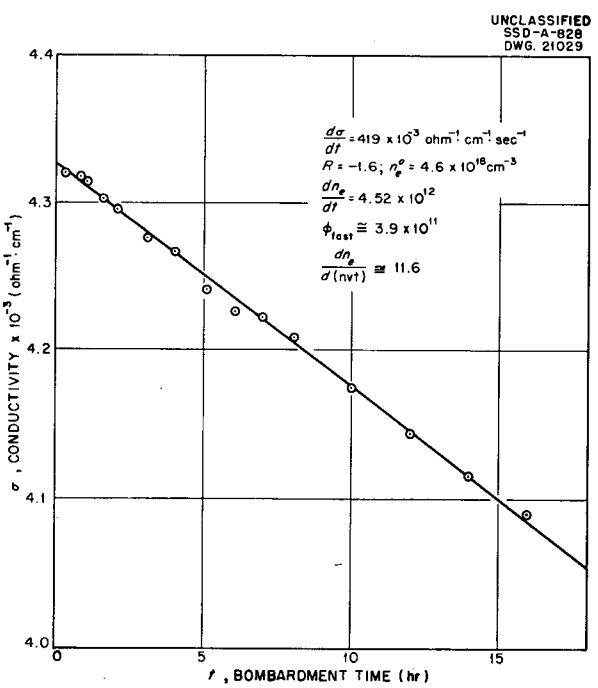

Fig. 70. Conductivity vs. Bombardment at Approximately 30°C for *n*-Type InSb.

The Hall coefficient and the resistivity of a *p*-type InSb sample are shown in Fig. 71. The conversion point from *p* to *n* type occurs at about −40°C, which indicates an activation energy, ΔE, of about 0.40 ev.

The InSb sample was irradiated in the low-temperature facility of the ORNL graphite reactor at reactor ambient temperature (~30°C) for about three weeks, and during this period, several low-temperature exposures were made. Figure 72 shows the curve for conductivity vs. nvt for the total irradiation. The initial slope of the conductivity curve was not calculated because the initial portion of the irradiation was actually carried out at low temperature; however, the conductivity increase and the indication of a slow approach to saturation agree almost exactly with the behavior previously reported for *p*-type germanium.[17]

[17] J. W. Cleland, J. H. Crawford, Jr., K. Lark-Horovitz, and J. C. Pigg, *Phys. Quar. Prog. Rep. June 15, 1950*, ORNL-782, p. 71, esp. 78.

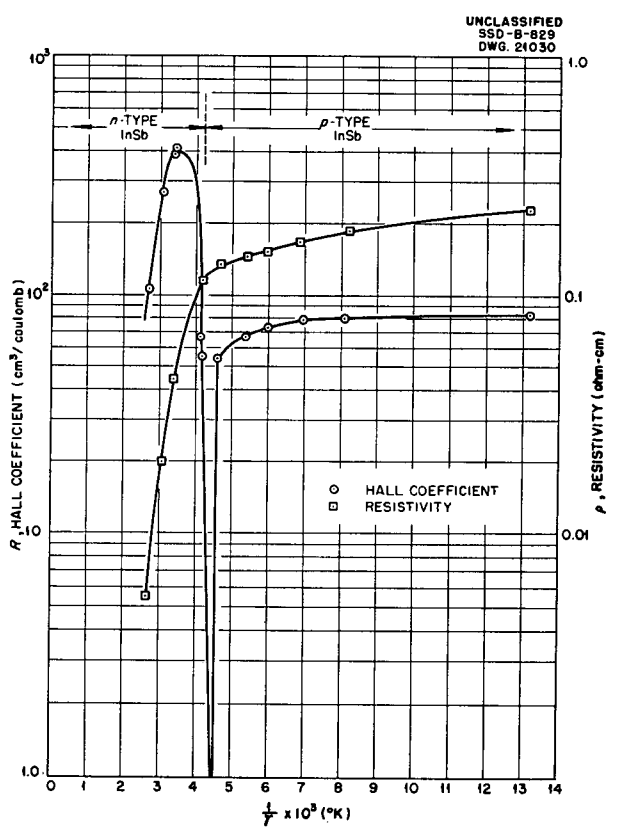

Fig. 71. Hall Coefficient and Resistivity vs. $1/T$ of *p*-Type InSb.

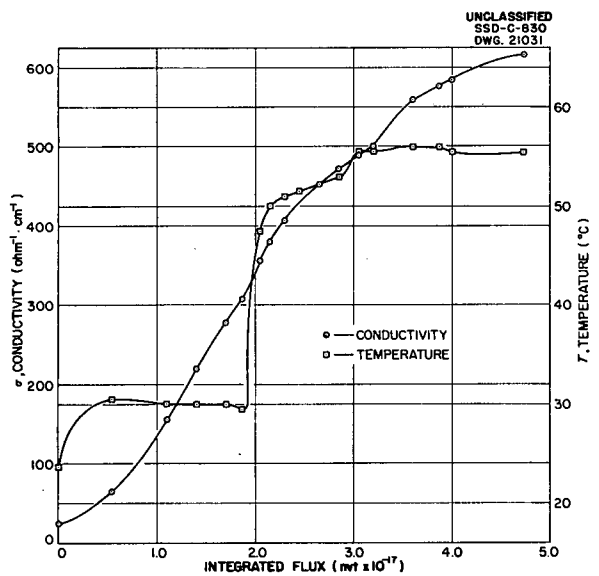

Fig. 72. Conductivity vs. Integrated Fast-Neutron Flux for *p*-Type InSb.

Low-temperature irradiation of *p*-type InSb causes a decrease in conductivity, as shown in Fig. 73. Behavior of this nature has already been reported for both *n*-type and *p*-type germanium,[18] and a discussion of the results is given previously in this report (cf. "Low-Temperature Irradiation of *p*-Type Germanium" and "Behavior of *n*-Type Germanium Bombarded at Low Temperatures").

[18] J. W. Cleland, J. H. Crawford, and J. C. Pigg, *Solid State Quar. Prog. Rep. Aug. 10, 1952*, ORNL-1359, p. 36.

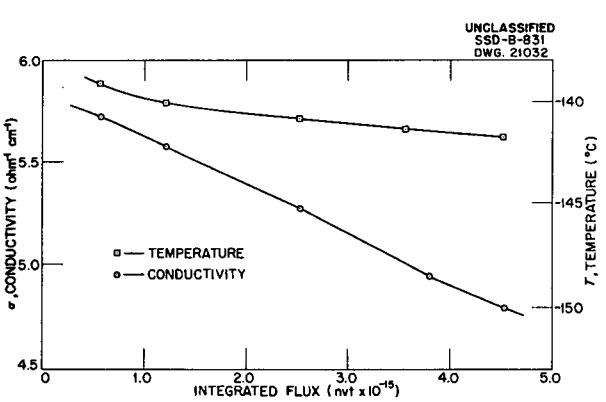

Fig. 73. Conductivity vs. Fast-Neutron Flux for *p*-Type InSb at −140(±2)°C.

The large change in resistivity that occurs for short periods of exposure and the rather surprising change in the shape of the resistivity curve as a function of temperature after a very brief low-temperature irradiation are indicated in Fig. 74. It is hoped that further experiments on InSb and other intermetallic compounds will aid in the interpretation of similar data already being investigated in the case of other semiconducting materials.

LOW-TEMPERATURE IRRADIATION OF Cu-Be ALLOY

J. W. Cleland J. H. Crawford, Jr.
D. S. Billington

The effect of reactor irradiations on the resistivity of solution-quenched and cold-worked Cu–2% Be alloy was described in the last quarterly report.[19] This investigation has been extended to include the measurement of several additional specimens and a more effective method of treating the data.

In the original experiment, the simultaneous irradiation of a solution-quenched specimen and a specimen cold-worked by 50% reduction of a Cu-Be alloy containing 13.5% beryllium was performed. The irradiation was first made at approximately −150°C and then at reactor ambient temperature, 30°C. The resistance was measured continuously with a Brown strip-chart recorder. An alternative method of detecting resistance changes was employed because of the scatter of data caused by temperature fluctuations at low temperatures and because the increase in the amount of noise during irradiation was comparable to the changes observed. Periodically, usually during reactor shutdown periods, the temperature was varied from about −150 to 0°C during the low-temperature exposures and from about −150 to 30°C during the reactor-ambient-temperature exposures. The temperature coefficient of resistance was not affected by the irradiation; hence the resistance change could readily be obtained from successive R vs. T curves, as shown in Fig. 75.

Figure 76 indicates the effect of successive irradiations at about −150°C and at about 30°C for two different specimens that received a total exposure of approximately 10^{18} nvt. The slopes

[19] J. W. Cleland, J. H. Crawford, and E. S. Schwartz, *Solid State Quar. Prog. Rep. Feb. 10, 1953*, ORNL-1506, p. 46.

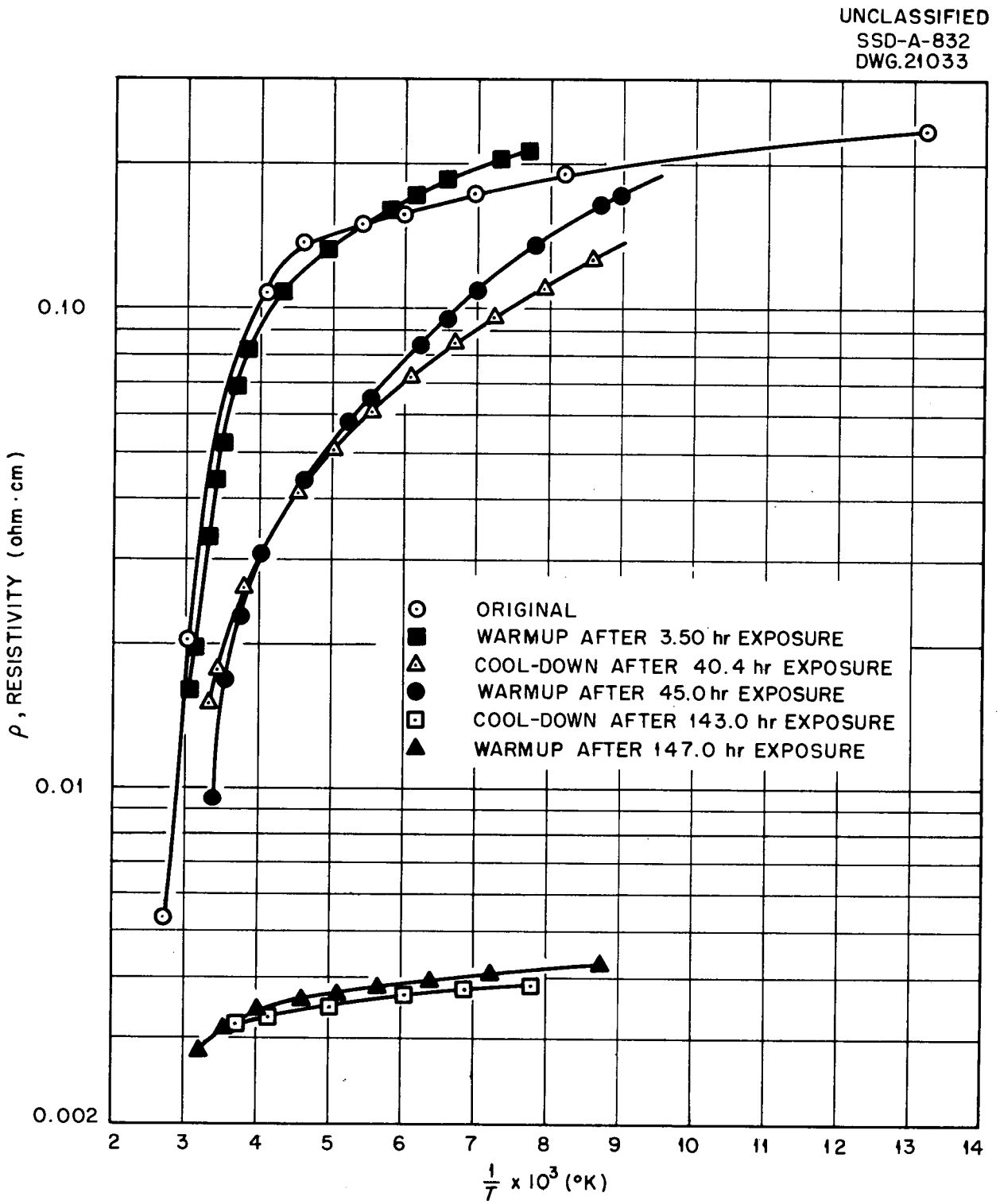

Fig. 74. Resistivity vs. $1/T$ for p-Type InSb After Various Periods of Exposure.

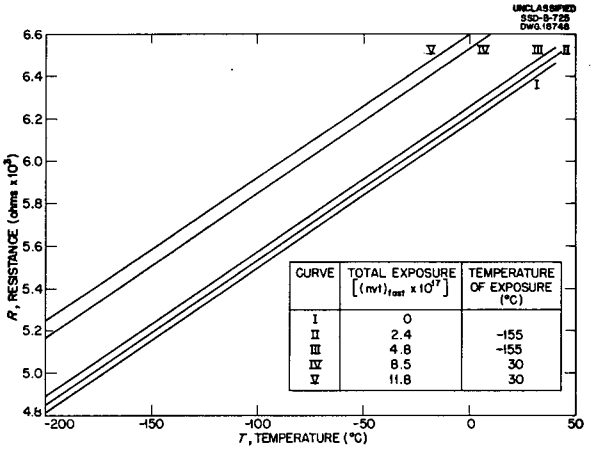

Fig. 75. Resistance vs. Temperature of Solution-Quenched Cu–13.5 at. % Be Alloy After Various Exposures.

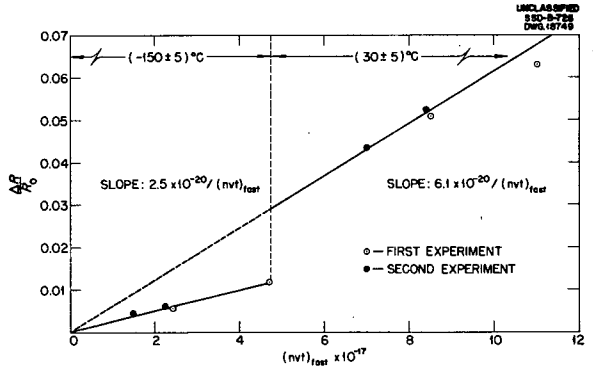

Fig. 76. $\Delta R/R_0$ vs. Integrated Fast Flux for Solution-Quenched Cu–13.5 at. % Be Alloy.

of the relative-resistance curves are quite different for the two temperatures, and the rate of increase is larger by a factor of about 2.5 for the higher temperature.

In an attempt to determine the period of time required for the disorder stored at low temperature to produce the expected resistance change at high temperature, a sample that had been irradiated at –150°C was warmed to 50°C and held at that temperature for about 4 hours. Comparison of the R vs. T curves before and after the warmup showed that 4 hr was sufficient to allow the change to take place.

The cold-worked specimens showed a slightly smaller relative-resistance increase at the low temperatures than did those specimens that were solution-quenched. In addition, the high-temperature irradiations produced no enhancement in the rate of resistance increase in the cold-worked specimens.

The results of these experiments are believed to indicate, as postulated by Murray and Taylor[20] and demonstrated by Blewitt and Coltman[21] for Cu_3Au alloys, that lattice disorder produced during low-temperature irradiation causes only a small amount of resistance increase, whereas the greater portion of radiation-induced resistance increase depends on a process that is presumably microdiffusion, and microdiffusion requires a thermal activation.

RECTIFIER BOMBARDMENT

J. C. Pigg

Experiments with nonlinear semiconductor elements at ORNL have been carried out previously by using a voltmeter-ammeter circuitry technique.[22] This has allowed only a fixed bias or a set of fixed biases to be used. As a result of the fixed-bias type of measurement, the correlation of data from different units and the extrapolations of data taken on the same unit have been required. Since there are variations from unit to unit that are difficult to interpret quantitatively and since nonlinear extrapolations are risky at best, the data left much to be desired.

A function plotter[23] which allows a complete forward and reverse characteristic curve of a rectifier to be traced in about ½ min has been constructed. Changes in a 1N38A Sylvania glass-sealed germanium rectifier have been followed with the function plotter during bombardment 13 ft below the top of the reactor in hole 12 of the ORNL

---

[20] G. T. Murray and W. E. Taylor, *Effect of Neutron Irradiation on Supersaturated Solid Solutions of Beryllium in Copper*, ORNL-1323 (Jan. 29, 1953).

[21] T. H. Blewitt and R. R. Coltman, *Phys. Rev.* 85, 384 (1952).

[22] *Physics Division Progress Reports*, ORNL-159, p. 88; ORNL-228, p. 53; ORNL-366, p. 36; ORNL-481, p. 48; ORNL-577, p. 43; ORNL-694, p. 65; ORNL-782, p. 71; ORNL-865, p. 90; *Physics of Solids Institute; Quar. Prog. Rep. Jan. 31, 1951*, ORNL-1025, p. 13.

[23] J. C. Pigg, *Solid State Quar. Prog. Rep. Feb. 10, 1953*, ORNL-1506, p. 47.

graphite reactor. This location was chosen because past experience[24] has shown that changes in the rectifier characteristic would be small during the time required for the function plotter to plot the curve. Ranges of 0 to 0.5 volt and 0 to 1.5 volts are available; however, only the 0- to 1.5-volt range was used in this experiment.

Figure 77 shows a representative set of curves taken from the data as the sample changed during 260 min of bombardment. The rapid change in the reverse characteristic is quite apparent. The current values for a given voltage change by an order of magnitude in 20 min; the forward characteristic, on the other hand, shows little change during the first 20 minutes. Such differences in the magnitude of the change in the forward and the reverse resistances have been indicated by previous experiments.[25]

The solid curves in Fig. 77 are those obtained as the voltage across the sample is increased. When the voltage is changed from zero to maximum and then back to zero again, a hysteresis loop is produced. The curves are reproducible, however, and subsequent cycling results in retracing of the original curve. Such a curve is shown in Fig. 78, and it can be seen that the hysteresis is in the wrong direction in the reverse curve to be explained either by the heating of the current in the sample or by instrument lags.

Figure 79 shows the change of the forward slope (dotted line in Fig. 78) under bombardment. For the first hour, the change was linear with time. Since the high-voltage forward slope reflects the change in conductivity of the material, this behavior was expected because of the results obtained from experiments previously conducted on bulk single-crystal germanium[24,25,26] and preliminary rectifier experiments. The decreasing slope indicates that carriers are being removed and that the germanium is being changed toward intrinsic material.

Figure 80 shows the change in the back-saturation slope (dotted line in Fig. 78) under bombardment, and by use of these data it is possible to draw a straight line whose slope represents the rate of change of the reverse-saturation slope. However, the present state of the data does not justify such a procedure. The positive slope of the curve in Fig. 80 might indicate the rate of change of barrier height with irradiation.

Figure 81 illustrates the manner in which the ratio of the forward- to reverse-saturation slopes varies as a function of bombardment. The negative slope of the line indicates that the unit is approaching ohmic behavior. Extrapolation of the line in Fig. 81 would indicate that the sample should become ohmic after 115 min of bombardment; however, Fig. 77 clearly shows the rectifier to be nonlinear after 260 min of bombardment.

Because the irradiation facility was not always available, the sample was not bombarded to the ohmic condition. The experiment was conducted primarily as a means of testing the function plotter as a tool for taking data and to indicate the changes needed in the equipment, as well as to indicate the type of data that could be obtained. Modification of the instrument that will allow the extension of rectifier studies will soon be completed.

RADIATION EFFECTS IN IONIC CRYSTALS

C. M. Nelson

Studies of radiation effects have been continued on potassium chloride crystals, and electrical conductivity measurements have been made on crystals irradiated from 7×10^5 to 7×10^8 r with a Co^{60} source. However, when conductivity measurements were made at various temperatures between 25 and 300°C, the irradiation effect was not in proportion to the total radiation. There was some increase in the conductivity, but only with the short irradiations. After bombardment, the crystals ranged from a very slight coloration to a deep magenta color.

In these studies, annealing of the irradiation effect on the conductivity, σ, has been performed on the crystals at temperature intervals of 25 to 30°C for periods up to 2 hours. The first annealing effect is a decrease in σ that takes place at a reasonable rate between 100 and 110°C (see Fig. 82), but with longer irradiation time, this first effect does not appear (see Fig. 83). However, the initial annealing effect, even on long irradiations, is still a decrease in σ which appears to

[24] J. H. Crawford, K. Lark-Horovitz, and J. C. Pigg, *Phys. Quar. Prog. Rep. March 15, 1950*, ORNL-694, p. 64.

[25] K. Lark-Horovitz and J. C. Pigg, *Phys. Quar. Prog. Rep. Sept. 25, 1949*, ORNL-481, p. 47.

[26] J. C. Pigg, J. H. Crawford, and K. Lark-Horovitz, *Phys. Quar. Prog. Rep. Dec. 15, 1949*, ORNL-577, p. 41.

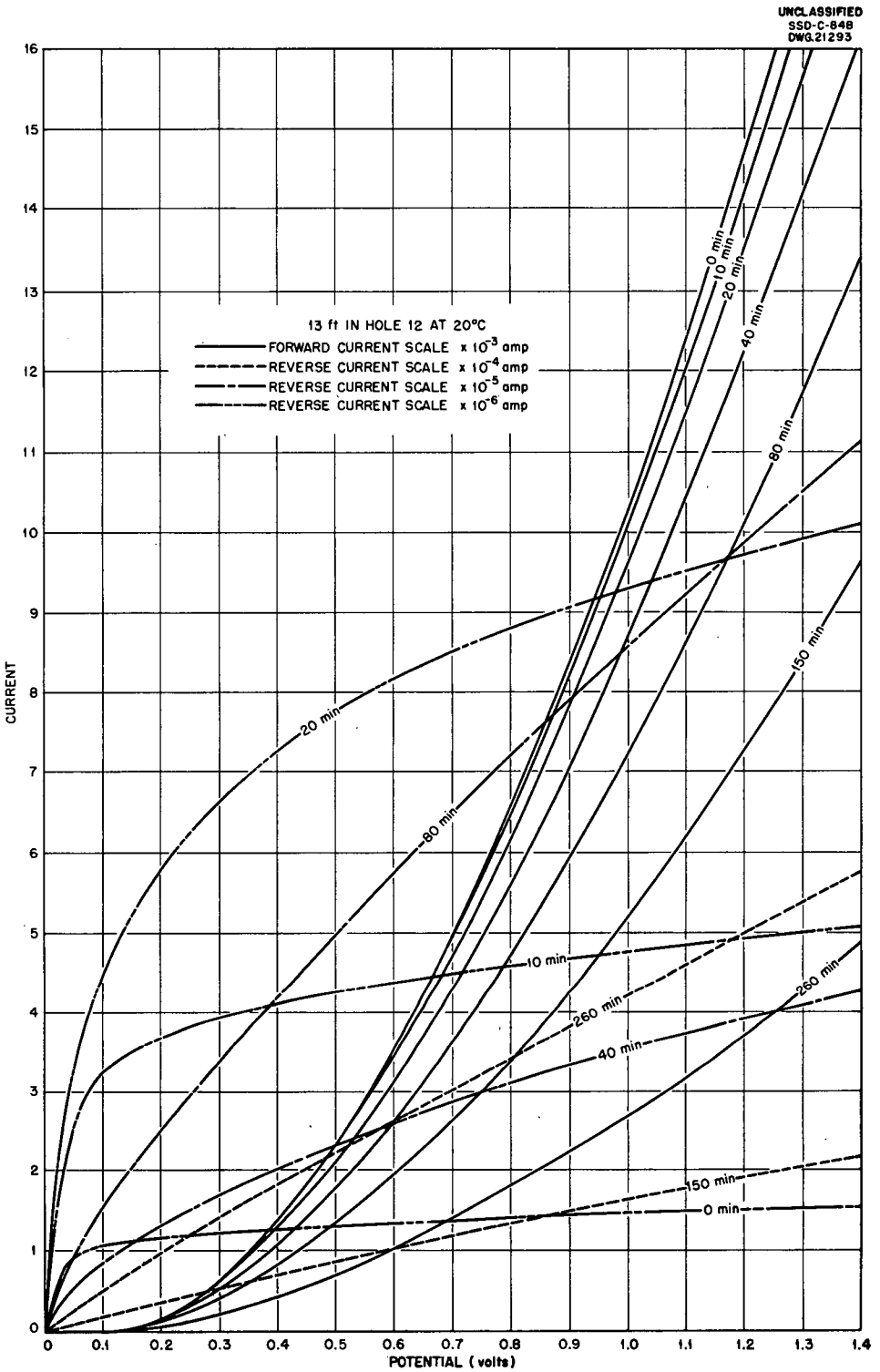

Fig. 77. Rectifier 1N38-A-1 Characteristic Curves as a Function of Bombardment.

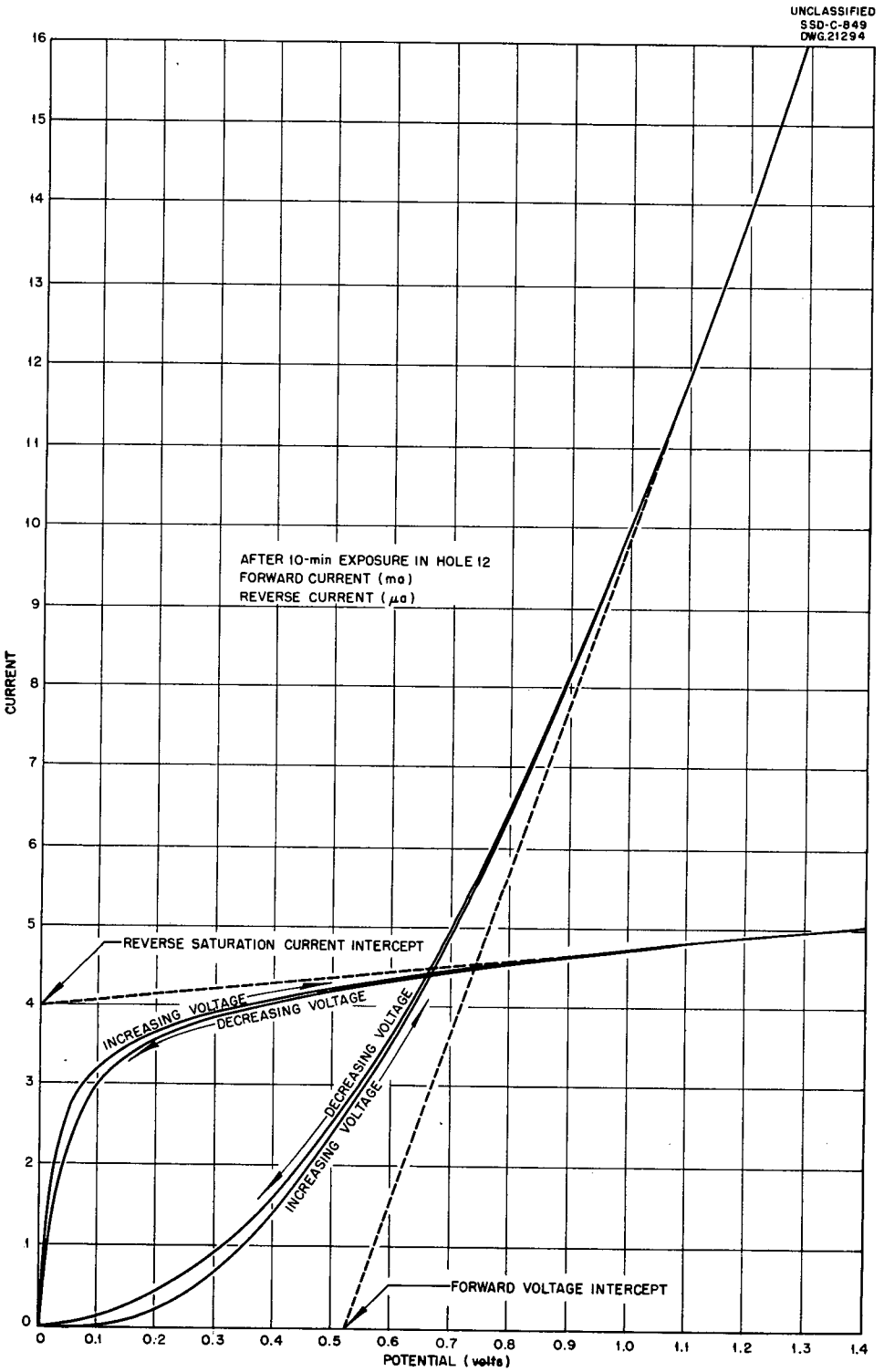

Fig. 78. Characteristic Curve for Point-Contact Rectifier 1N38-A-1 Showing Hysteresis.

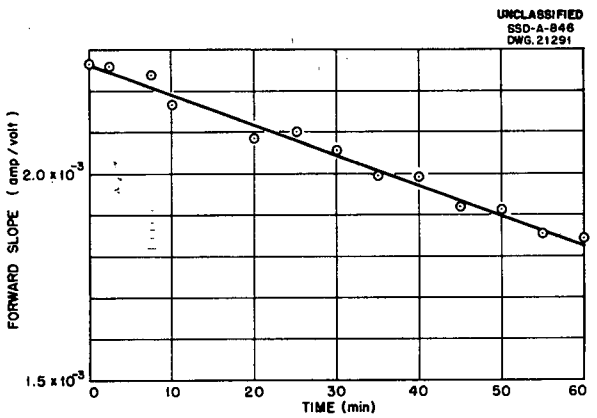

Fig. 79. Forward Slope vs. Bombardment Time for 1N38-A-1.

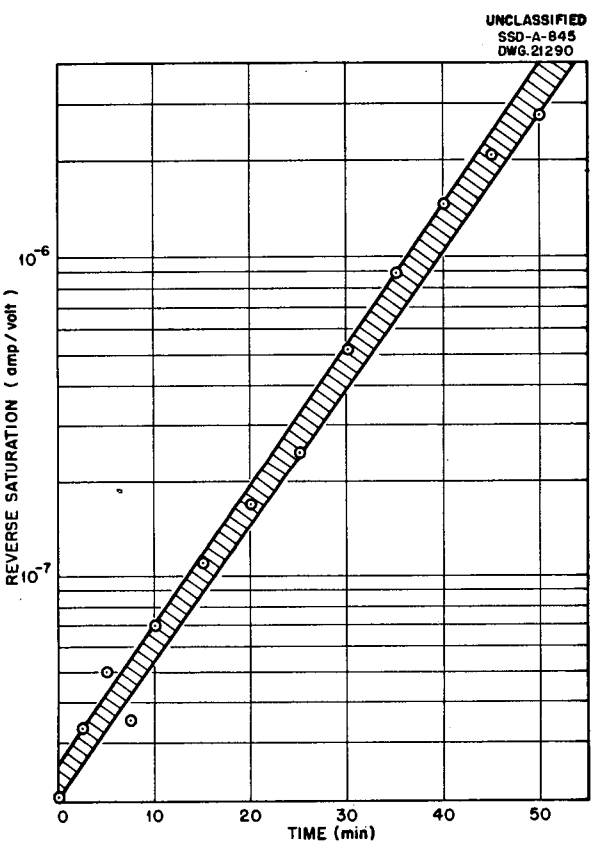

Fig. 80. Reverse Saturation Slope vs. Bombardment Time for 1N38-A-1.

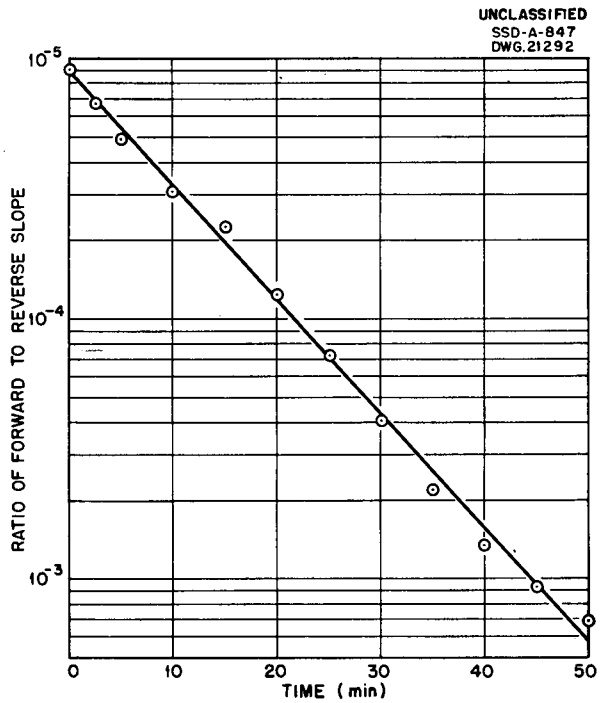

Fig. 81. Ratio of Forward to Reverse Slope vs. Bombardment Time for Sample 1N38-A-1.

be exponential with time at constant temperature. There seems to be a second decrease in σ for short irradiations before an increase occurs, and this second decrease generally takes place around 140°C at a noticeable rate, while an appreciable increase does not appear until around 160°C. A decrease in σ again occurs at between 185 and 190°C, with a subsequent increase at 215°C. Usually, another decrease in σ is observed at higher temperatures (230 or 260°C), followed perhaps by a small increase in σ at 260 to 300°C.

These transitions are apparently sequential, and it has been demonstrated, by a jump to a higher temperature for the annealing experiment, that σ was observed to decrease initially before the increasing and decreasing periods occur. The phenomena have been observed in a number of recent experiments, but the data have not yet been analyzed in detail. A series of samples has been bombarded in the ORNL graphite reactor for periods of from 1 hr to 2 months and will be measured under the same conditions as those used for the Co^{60} irradiated samples. All samples in the series were preannealed in a vacuum at 300°C.

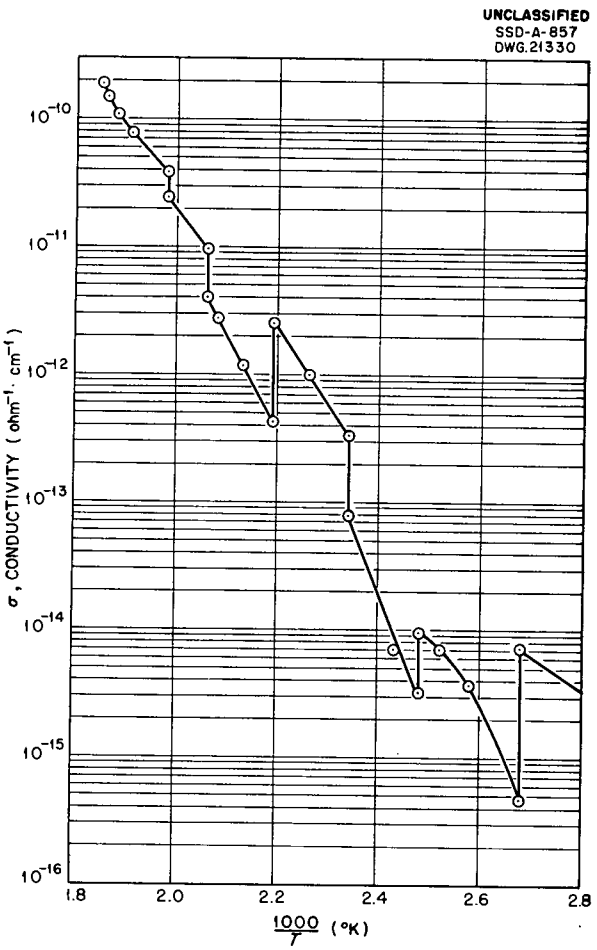

Fig. 82. Electrical Conductivity vs. Temperature of a KCl Crystal After Exposure to 3.6×10^6 r in Hole 7 of the Co^{60} Source.

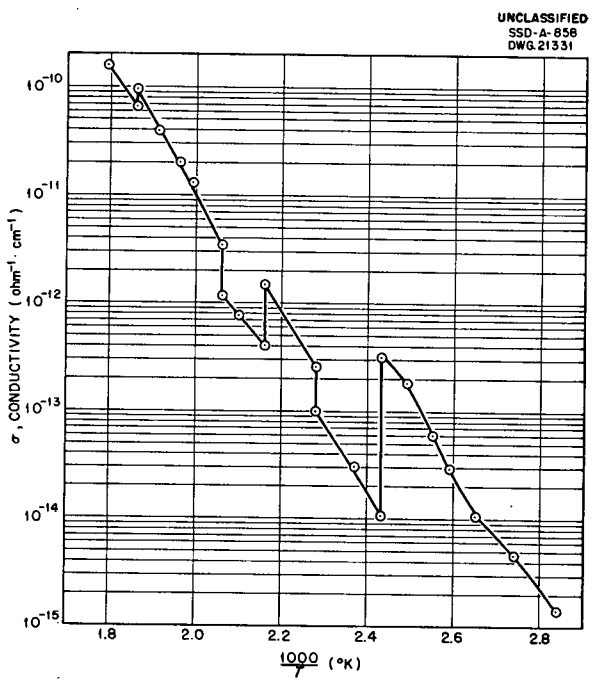

Fig. 83. Electrical Conductivity vs. Temperature of a KCl Crystal After Exposure to 3.2×10^7 r in Hole 7 of the Co^{60} Source.

A-C RESISTANCE COMPARATOR

J. C. Pigg M. T. Robinson
J. G. Morgan

As the result of a need for measuring the resistance of polarizable liquids, an a-c bridge circuit has been developed; a schematic diagram of the circuit is shown in Fig. 84 (see, also, Instrumentation and Controls Division drawing Q-1485, Fig. 48, this report).

An R-C network is connected in series with a conductivity cell containing the sample, and the voltage outputs from the network and the cell are compared by means of a null detection device. R_1 and C_1 are a calibrated resistor and a calibrated capacitor that are adjusted to null the output; the resistivity and the capacitance of the sample may be determined by reading the null values of R_1 and C_1.

When switch 2 is in the balance position, the primaries of T_1 and T_2 are connected across the same resistance, and the secondaries of T_1 and T_2 are connected in opposition. R_3 is adjusted until the trace on the oscilloscope indicates a 180-deg phase difference between the signals from T_1 and T_2. R_4 is then adjusted until a null between the two signals is indicated on the oscilloscope. Switch 2 is then placed in the measure position, and a null output is again obtained by adjusting R_1 and C_1.

By means of switch 1, a range of 0 to 1.1 (±0.0005) ohms or a range of 0 to 11.1 (±0.002) ohms may be selected.

The bridge operates with any signal in the frequency range of 500 cps to 5 kc. This allows a frequency-effect determination on the sample, but the most satisfactory results are obtained for a signal frequency of 1 kc.

UNCLASSIFIED
SSD-A-844
DWG. 21289A

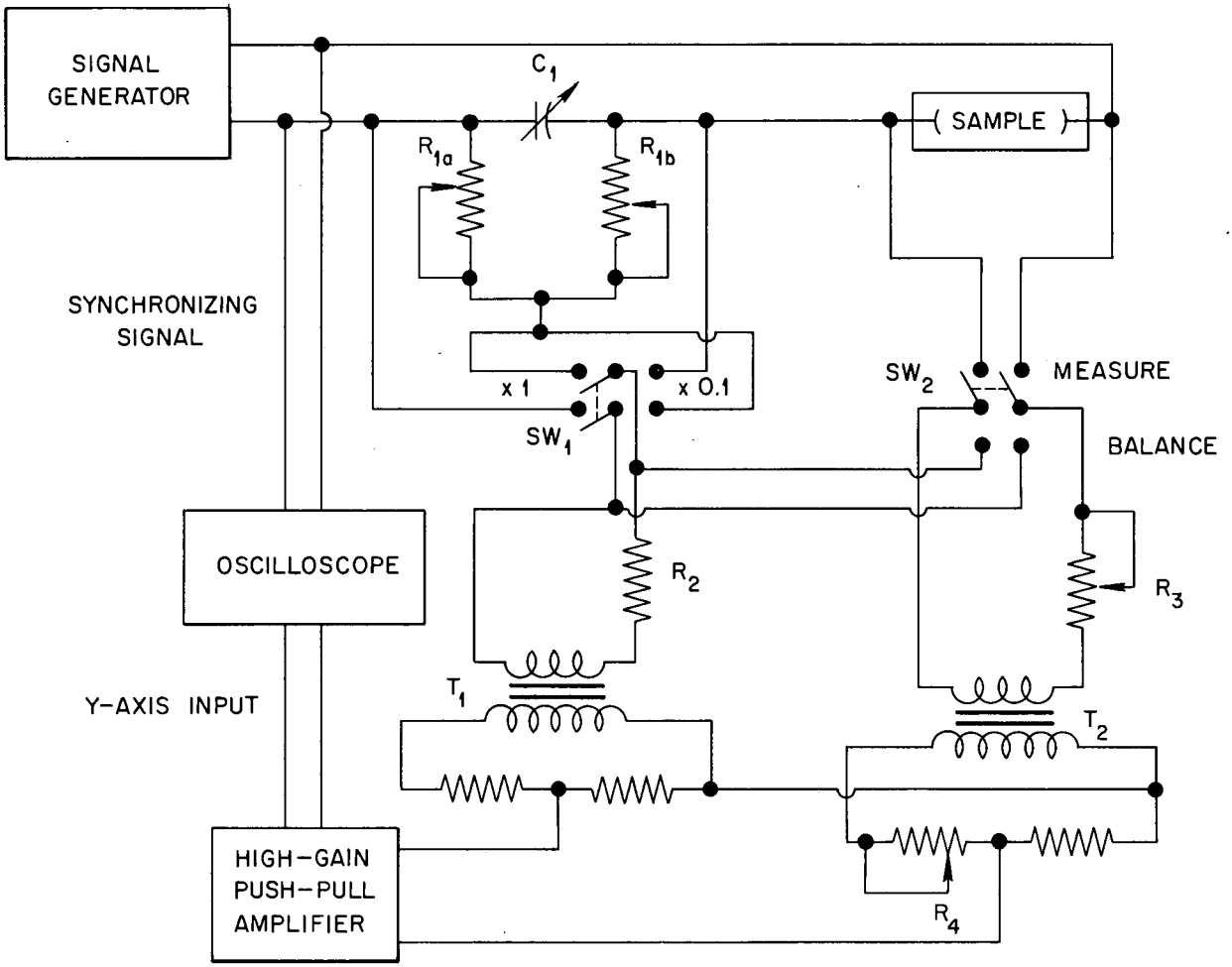

Fig. 84. Diagram of A-C Resistance Comparator Circuit.

ENGINEERING PROPERTIES

RADIATION STABILITY OF PLASTICS AND ELASTOMERS

C. D. Bopp
O. Sisman
W. K. Kirkland
R. L. Towns

Comparisons of the relative damage to plastics and elastomers by gamma and reactor radiation have been given previously[1] for exposures sufficient to cause only small changes in the properties studied. Table 14 shows a comparison of property changes for exposures sufficient to cause extensive damage. There is some uncertainty in the values of the radiation exposure, and the sensitivity of the measurement depends upon the property studied; however, within a factor of 2, the energy absorption required to produce similar changes in most properties is the same for the mixed fast-neutron and gamma radiation in the reactor and for the neutron-free gamma radiation from a Co^{60} source.

The radiation intensity of the Co^{60} source was measured with an ionization chamber. The chamber was calibrated against Victoreen roentgen meters in a uniform field within a cylindrical Au^{198} source at an intensity of about 10^4 rep/hr. In the 10^6 rep/hr field of the Co^{60} source, the voltage across the electrodes of the chamber was varied from 135 to 530 volts with no change in ionization current. The current was therefore taken to be proportional to the intensity of radiation up to the 10^6 rep/hr level. The ionization chamber gave agreement with a dosimetric method in which cerric sulfate was employed. The intensity of radiation in the reactor was calculated by a method which has been described previously.[2] The rep value given in Table 14 for the reactor includes the energy absorbed both from fast-neutron and gamma radiation.

Radiation stability data for additional plastics are given in Table 15. A correlation of radiation stability with chemical structure for all the plastics and elastomers tested to date is included in a forthcoming report.[3] The more resistant of the newly tested plastics include triallyl cyanurate polymer, Styron 371 (light-resistant polystyrene), Styron 637 (heat-resistant polystyrene), and Melmac 592 (mineral-filled melamine formaldehyde plastic). These materials are changed very little after an exposure of about 15×10^{18} nvt. Silicone-varnished glass laminate hardens similarly to the polyethylene tested previously. Mylar polyester film becomes very brittle at about 3×10^{18} nvt; this behavior is like that of the unfilled phenolic polymer tested previously. Polyalphamethyl styrene becomes brittle at about 10^{18} nvt. The poor stability of polyalphamethyl styrene, as compared with unsubstituted polystyrene, is strong evidence of poor stability for polymers with quaternary carbon atoms. The 2,2-parahydroxyphenyl propane polymer shows the best stability of the polymers with quaternary carbon atoms that have been studied. In this polymer, two of the radicals attached to the quaternary carbon atom are phenyl radicals.

The radiation stability was described previously for commercial elastomers[4] and for a group of formulations which were specially compounded[5] in an attempt to obtain improved radiation stability. A third group of formulations compounded by the Materials Laboratory of the Wright Air Development Center was tested largely for confirming the results obtained with the first group. In addition to elastomers, formulations of which were tested in the first group, polybutadiene, Hypalon S2, and FBA[6] were also included in the third group. Fewer irradiations were made in this group because similar results were expected.

The composition of the elastomers is given in Table 16. Polybutadiene, Hypalon S2, and FBA are hardened by radiation at about the same rate as that of the other elastomers. It was possible to make only a few tests on FBA because of the small quantity of this material available. The recipes of plasticized natural compounds are given in Table 17; test results are given in Tables 18 and 19.

---

(1) C. D. Bopp, R. L. Towns, O. Sisman, and W. K. Kirkland, *Solid State Quar. Prog. Rep. Nov. 10, 1952*, ORNL-1429, Table 5, p. 51.

(2) O. Sisman and C. D. Bopp, *Physical Properties of Irradiated Plastics*, ORNL-928, p. 22 (June 29, 1951).

(3) C. D. Bopp and O. Sisman, *Radiation Stability of Plastics and Elastomers*, ORNL-1373 (to be published).

(4) O. Sisman, W. K. Kirkland, C. D. Bopp, and R. L. Towns, *Solid State Quar. Prog. Rep. July 31, 1951*, ORNL-1128, p. 41.

(5) C. D. Bopp, R. L. Towns, O. Sisman, and W. K. Kirkland, *Solid State Quar. Prog. Rep. May 10, 1952*, ORNL-1301, p. 52.

(6) Poly-1,1-dihydroperfluorobutyl acrylate.

TABLE 14. COMPARISON OF DAMAGE PRODUCED BY Co^{60} GAMMA RADIATION AND REACTOR RADIATION

	TENSILE STRENGTH (psi)	ELONGATION (%)	ELASTIC MODULUS (10^5 psi)	DUROMETER HARDNESS	ROCKWELL HARDNESS		SPECIFIC GRAVITY, 25/4°C
					α Scale	R Scale	
Plastics							
Allyl diglycol carbonate polymer (CR-39)							
a	6000	3	3.3		90	112	1.318
b	6000	3	2.7		80	102	1.290
c			1.5		0.6	0.6	2.1
Linen fabric bakelite (phenolic)							
a	12000	4	10		114 to 116	123	1.340
b	6000	0.5	10		112 to 116	122	1.337
c	0.7	0.7					
Unfilled phenolic (Catalin)							
a	5500	1	6.0		109	123	1.300
b	5500	1	4.2		105	119	1.303
c			1.6		1.0	0.3	
Nylon (FM-10001)							
a	8900	40	3.2		86	103	1.135
b	8800	30	2.5		88	106	1.136
c					1.1	1.1	
Royalite							
a	4000	> 10	2.6		70	89	1.113
b	6000	9.1	3.8		78	96	1.124
c	1.2	1.2	1.2		0.7	1.4	0.6
Elastomers							
Natural rubber (32A43)							
a	2600	420		62			1.186
b	1400	100		79			1.196
c	1.2	0.8		0.6			0.8
Neoprene W (32A44)							
a	2900	450		79			1.418
b	1800	20		92			1.428
c		1.2		3			3

TABLE 14. (continued)

	TENSILE STRENGTH (psi)	ELONGATION (%)	ELASTIC MODULUS (10^5 psi)	DUROMETER HARDNESS	ROCKWELL HARDNESS		SPECIFIC GRAVITY, 25/4°C
					a Scale	R Scale	
Elastomers							
Hycar OR-15 (32A45)							
a	1900	250		74			1.229
b	4200	35		97			1.261
c	0.5	0.8		0.7			1.0
GR-S 50 (32A47)							
a	1700	270		69			1.210
b	1600	40		90			1.220
c	1.7	1.7		1.0			0.4
Thiokal ST (3000ST)							
a	800	160		74			1.450
b	700	80		74			1.454
c		2.5					
Silastic 7-170							
a	520	95		59			1.382
b	680	7		93			1.396
c		0.7		0.7			1.4

(a) Before irrodiation.
(b) After 2.8×10^9 rep from Co^{60}.
(c) Ratio of energy absorbed from Co^{60} to the energy absorbed in the reactor for an exposure in the reactor which produces the same value of the physical property as listed in (b).

Many of the formulations of the third group differ from those of the first group chiefly in having a lower percentage of carbon black. The radiation stability of the third group of formulations is similar to that of the formulations of the first group which are based on the same polymers. This indicates that it is the type of polymer which largely governs the radiation stability of the formulation. The six formulations of natural rubber, each of which contains a different plasticizer, show similar stability.

DYNAMIC PROPERTIES OF IRRADIATED ELASTOMERS

C. D. Bopp
O. Sisman
W. K. Kirkland
R. L. Towns

In addition to the properties investigated previously, the dynamic properties of the irradiated elastomers were studied – primarily to estimate the effect of radiation on the heating resulting from the internal friction of cyclic straining (heating is an

TABLE 15. PROPERTIES OF IRRADIATED PLASTICS

PLASTIC	RADIATION EXPOSURE (10^{18} nvt)	SHEAR STRENGTH (psi)	TENSILE STRENGTH (psi)	ROCKWELL HARDNESS		SPECIFIC GRAVITY, 25/4°C
				a Scale	R Scale	
Triallyl cyanurate polymer	0	2,000		111	125	
	10	2,000		111 to 113	125	
Styron 371 and Styron 637	0	6,000		105	122	1.050
	15	6,000		105	122	1.074
Melmac 592	0	7,000		125	123	1.73
	15	4,000		121	120	1.69
Silicone-varnished glass laminate	0	13,500		119	122	
	2.4	10,000 to 13,000		129	128	
	15	2,000		124 to 126	123 to 124	
Mylar polyester film	0		25,000			
	1.2		18,000			
	5		0			
Polyalphamethyl styrene	0	6,000		115	127	1.064
	0.3	3,000		114	126	1.067
	1.8	700		Broke under load		1.078
2,2-Parahydroxyphenyl propane polymer	0	8,000		109	126	
	1.8	6,000		109	124	

important consideration in tire design). The vibrating-reed method was employed, and the apparatus is shown in Fig. 85. An elastomer specimen is clamped at one end and placed in forced vibration as a cantilever. The resonant frequency and the band width of the amplitude-frequency curve are measured. A method of comparing the heating for different elastomers from these measurements has been developed.[7,8,9]

The force associated with the loss (owing to viscous damping) in a material may be written as

(1) $$F_v = \gamma \frac{ds}{dt} ,$$

where

F_v = force per unit area owing to internal friction, dynes/cm^2,

ds/dt = rate of straining, sec^{-1},

γ = viscosity coefficient, g/cm·sec.

Sinusoidal straining may be written as

(2) $$s = s_0 e^{-i\omega t} ,$$

where

s_0 = maximum value of strain, dimensionless,

s = instantaneous value of strain which varies from $-s_0$ to $+s_0$,

t = time, sec,

ω = angular velocity, radians/sec,

e = base of natural logarithms,

$i = \sqrt{-1}$.

From Eqs. 1 and 2,

(3) $$F_v = -i\gamma\omega s .$$

The force owing to elastic deformation of the material is

(4) $$F_e = E_1 s ,$$

where

F_e = force per unit area owing to elastic effects, dynes/cm^2, and

(7) A. W. Nolle, *J. Appl. Phys.* 19, 753 (1948).

(8) M. Horio and S. Onogi, *J. Appl. Phys.* 22, 977 (1951).

(9) J. W. Ballou and J. C. Smith, *J. Appl. Phys.* 20, 493 (1949).

TABLE 16. COMPOSITION OF GROUP 3 ELASTOMERS CURED 20 min AT 310°F

COMPONENTS	PARTS BY WEIGHT											
	Polybutadiene (P1S1C1)	Hycar OR-15 (P1S1C2)	Hycar OS-10 (P1S1C3)	Neoprene GN (P1S1C4)	Neoprene W (P1S1C5)	Butyl Rubber (P1S1C6)	Thiokol ST (P1S1C7)	Silastic 250 (P1S1C8)	Natural Rubber (P1S1C9)	Hycar PA-21 (P1S1C10)	Hypalon S2 (P1S1C11)	FBA (P1S1C12)
Polybutadiene X453	100											
Hycar OR-15		100										
Hycar OS-10			100									
Neoprene GN				100								
Neoprene W					100							
Butyl rubber, GR-I						100						
Thiokol ST							100					
Silastic 250*								100				
Natural rubber**									100			
Hycar PA-21										100		
Hypalon S2											100	
FBA***												100
Zinc oxide	5	5	5	5	5	5	0.5		5			
Stearic acid	1	1.5	1	1	0.5	2	1		3	1		
Sulfur	2	2	3			2			3	0.5		
Methyl treads	0.3											
SRF black	20	20	20	20	20	20	40		20	20	20	
Altax		1.75										
Captax			1						1		3	
Neozone "A"				2	2							
ELC magnesium oxide				4	2	3						
Permalux				0.5								
NA22					0.5							
Triuram M						1						
Polyac						1						5
GMF							1.5					
Triamine base										3		
Litharge											40	
Staybelite resin											2.5	
Lead peroxide												20

*Cured 15 min at 300°F.

**Standard smoked sheet.

***Poly-1,1-dihydroperfluorobutyl acrylate.

TABLE 17. COMPOSITION OF VARIOUS PLACTICIZED NATURAL RUBBER COMPOUNDS CURED 20 min AT 310°F

COMPONENT	PARTS BY WEIGHT					
	L.P. Oil (P1S2C1)	Dioctyl Phthalate (P1S2C2)	Dioctyl Sebacate (P1S2C3)	Tributoxy Ethyl Phosphate (P1S2C4)	TP90B (P1S2C5)	Plasticizer "SC" (P1S2C6)
Smoked sheet	100	100	100	100	100	100
Stearic acid	1	1	1	1	1	1
Zinc oxide	5	5	5	5	5	5
Sulfur	3	3	3	3	3	3
Captax	1.5	1.5	1.5	1.5	1.5	1.5
SRF black	30	30	30	30	30	30
L.P. oil	30					
Diactyl phthalate		30				
Dioctyl sebacate			30			
Tributoxy ethyl phosphate				30		
TP90B					30	
Plasticizer "SC"						30

E_1 = elastic modulus (Young's modulus), dynes/cm^2.

The total force is

(5) $F = F_e + F_v$

$$= E_1 s - i\gamma\omega s = E_1 s - iE_2 s = E^* s \quad ,$$

where

F = total force per unit area, dynes/cm^2,
E^* = $E_1 - iE_2$ = complex modulus, dynes/cm^2,
E_2 = $\gamma\omega$ = viscous modulus, dynes/cm^2.

For the vibrating reed, the approximate relations may be derived according to

(6) $$\frac{E_1}{\rho} = B_n \frac{l^4}{t^2}\left[\nu_0^2 + \frac{1}{2}(\Delta\nu)^2\right] \quad ,$$

(7) $$\frac{E_2}{\rho} = B_n \frac{l^4}{t^2}\,\nu_0 \Delta\nu \quad ,$$

where

ρ = density, g/cm^3,
B_n = 38.4 for the fundamental mode of vibration,
l = length of the reed, cm,
t = thickness of the reed, cm,
ν_0 = resonant frequency, cps,
$\Delta\nu$ = band width of the resonance curve at $1/\sqrt{2}$ times the maximum amplitude, cps.

A different method which is, perhaps, a more rigorous analysis[8] yields the same relations, except that the factor of ½ in Eq. 6 is replaced by ⅛. Since $\Delta\nu$ is small compared with ν_0 for most of the measurements given here, the choice between ½ or ⅛ has little effect (⅛ is used in the calculations made here).

For a comparison of the heating of different materials, the following relations may be used (they are given in slightly different form in ref. 9):

(8) $$P_F = 2\pi\nu F_c^2 \frac{E_2}{E_1^2} \quad ,$$

(9) $$P_s = 2\pi\nu s_c^2 E_2 \quad ,$$

TABLE 18. RADIATION-PRODUCED CHANGES IN THE PHYSICAL PROPERTIES OF GROUP 3 ELASTOMERS

ELASTOMER	IRRADIATION EXPOSURE (10^{18} nvt)	TENSILE STRENGTH (psi)	ELONGATION (%)	SHORE DUROMETER HARDNESS	SPECIFIC GRAVITY, 25/4°C	VOLUME RESISTIVITY (ohm-cm)
Polybutadiene	0	670	360	49	1.040	10^{14}
(P1S1C1)	0	590	355	49	1.040	10^{14}
	0.25	460		67	1.045	10^{14}
	0.54	280	20	79	1.055	10^{10}
	1.3	1200	< 2	98	1.087	10^{9}
Hycar OR-15	0	1270	310	59	1.122	10^{11}
(P1S1C2)	0	1540	360	59	1.122	10^{11}
	0.25	1600	110	76	1.131	10^{11}
	0.54	2600	45	97	1.146	10^{11}
	1.3	7800	< 2	100	1.177	10^{13}
Hycar OS-10	0	1240	375	52	1.119	$> 10^{14}$
(P1S1C3)	0	1360	390	52	1.119	$> 10^{14}$
	0.25	1600	180	67	1.121	6×10^{13}
	0.54	800	70	77	1.128	2×10^{12}
	1.3	3600	25	100	1.144	5×10^{12}
Neoprene GN	0	2520	475	62	1.363	2×10^{11}
(P1S1C4)	0	2460	475	62	1.363	2×10^{11}
	0.25	990	45	85	1.372	4×10^{9}
	0.54	1900	20	99	1.386	10^{8}
	1.3	3300	< 2	100	1.390	10^{8}
Neoprene W	0	3330	700	53	1.346	2×10^{11}
(P1S1C5)	0	2800	650	53	1.346	2×10^{11}
	0.25	Sample lost				
	0.54	Sample broken		98	1.360	2×10^{10}
	1.3	7200	< 2	100	1.384	10^{10}
Thiokol	0	1100	195	70	1.464	10^{8} to 10^{10}
(P1S1C7)	0	1000	175	70	1.464	10^{8} to 10^{10}
	0.25	630	90	75	1.464	10^{10}
	0.54*	400	60	72	1.462	10^{9}
	1.3	450	70	73	1.469	10^{7}
Silastic 250	0	160	330	19	1.205	10^{14}
(P1S1C8)	0	150	320	19	1.205	10^{14}
	0.25	160	7	81	1.214	10^{14}
	0.54*	Sample broken		93	1.204	10^{12}
	1.3	230	< 2	97	1.253	10^{14}
Natural rubber	0	2250	460	47	1.045	$> 10^{14}$
(P1S1C9)	0	2210	450	47	1.045	$> 10^{14}$
	0.25	430	65	67	1.049	10^{14}
	0.54*	400	30	80	1.053	10^{14}
	1.3	110	< 2	92	1.072	10^{12}

TABLE 18. (continued)

ELASTOMER	IRRADIATION EXPOSURE (10^{18} nvt)	TENSILE STRENGTH (psi)	ELONGATION (%)	SHORE DUROMETER HARDNESS	SPECIFIC GRAVITY, 25/4°C	VOLUME RESISTIVITY (ohm-cm)
Hycar PA-21	0	610	235	45	1.217	6×10^{11}
(P1S1C10)	0	720	275	45	1.217	6×10^{11}
	0.25	340	60	55	1.222	10^{11}
	0.54*	300	30	70	1.226	3×10^{10}
	1.3	500	3	80	1.240	5×10^{10}
Hypalon S2	0	2410	250	78	1.488	6×10^{13}
(P1S1C11)	0	2550	250	78	1.488	6×10^{13}
	0.25	1800	38	90	1.495	4×10^{12}
	0.54*	1500	6	96	1.500	2×10^{13}
	1.3	3000	< 2	100	1.504	2×10^{13}
FBA**	0			58	1.793	
(P1S1C12)	0			58	1.793	
	0.25			94	1.806	
	0.54			99	1.745	

*Exposed to moisture during irradiation as a result of water leaking into the sample can.
**Poly-1,1-dihydroperfluorobutyl acrylate.

where

P_F = power dissipated per unit volume for cyclic stressing, ergs/sec·cm^3,
P_s = power dissipated per unit volume for cyclic straining, ergs/sec·cm^3,
F_c = maximum value of the cyclic force per unit area, dynes/cm^2,
s_c = maximum value of the cyclic strain, dimensionless,
ν = frequency of application of the stress or strain, cps.

Equation 8 is used for comparing materials on the basis of cyclic loading; Eq. 9 is used if the comparison is made on the basis of cyclic straining. For the case of cyclic loading, the heating is proportional to E_2/E_1^2; for cyclic straining, the heating is proportional to E_2. In the use of tires, the heating will lie between these two extremes. Strictly, E_2 and E_1 should be determined at the frequencies for which the heating is to be calculated. The frequency used in the measurements taken here varied from 80 to 400 cps, depending on the material. It has been found empirically that E_1 and E_2 are roughly constant over this range and up to much higher frequencies.[7]

In Figs. 86 and 87, the frequency-amplitude relations are given for the natural rubber (P1S1C9) and Hycar OS (P1S1C3) formulations whose compositions are given in Table 16. The specimen dimensions and the values of E_1 and E_2 calculated from Eqs. 6 and 7 are given in Table 20. Two additional elastomer formulations, natural rubber formulation 32A43 and GR-S formulation 32A47, are also included in Table 20. The compositions of the last two formulations[10] differ chiefly from the first two in that they include more carbon black (the chemical structural formula of Hycar OS is similar to that of GR-S). It is intended to make a study of the dynamic properties of the other elastomers listed in Table 16, but the elastomers given in Table 20 were selected for study first because they are employed in the manufacture of tires.

Figure 86 shows little change in the band width (at $1/\sqrt{2}$ of the maximum amplitude) before hardening and loss of extensibility have advanced to the point where the material is no longer recognizable

[10] O. Sisman, C. D. Bopp, R. L. Towns, and W. K. Kirkland, *Physics of Solids Institute; Quar. Prog. Rep. April 30, 1951*, ORNL-1095, p. 75.

TABLE 19. RADIATION-PRODUCED CHANGES IN PLASTICIZED NATURAL RUBBER COMPOUNDS

PLASTICIZER	IRRADIATION EXPOSURE (10^{18} nvt)	TENSILE STRENGTH (psi)	ELONGATION (%)	SHORE DUROMETER HARDNESS	SPECIFIC GRAVITY, 25/4°C	VOLUME RESISTIVITY (ohm-cm)
L.P. oil	0	1310	560	30	1.308	$> 10^{14}$
(P1S2C1)	0	1330	560	30	1.308	$> 10^{14}$
	0.25	440	97	55	1.039	10^{14}
	0.54	160	20	67	1.044	10^{14}
	1.3	Sample broken		83	1.059	10^{10}
Dioctyl	0	715	420	30	1.048	10^{14}
phthalate	0	890	460	30	1.048	10^{14}
(P1S2C2)	0.25	330	90	52	1.054	10^{14}
	0.54	200	30	65	1.059	10^{14}
	1.3	130	10	80	1.072	10^{14}
Dioctyl	0	915	510	28	1.046	10^{14}
sebacate	0	930	540	28	1.046	10^{14}
(P1S2C3)	0.25	260	60	57	1.049	10^{14}
	0.54	Sample broken		70	1.055	10^{14}
	1.3	140	7	86	1.067	10^{14}
Tributoxy ethyl	0	1150	440	31	1.094	10^{9}
phosphate	0	Sample slipped out of grips		31	1.094	10^{9}
(P1S2C4)	0.25	280	55	59	1.108	10^{9}
	0.54	320	27	76	1.115	10^{10}
	1.3	300	5	92	1.130	10^{10}
TP90B	0	1360	370	54	1.180	10^{5}
(P1S2C5)	0	1260	340	54	1.180	10^{5}
	0.25	700	50	78	1.181	10^{5}
	0.54	300	10	87	1.186	10^{5}
	1.3	410	3	95	1.203	10^{5}
Plasticizer	0	1220	390	40	1.110	10^{11}
"SC"	0	1240	390	40	1.110	10^{12}
(P1S2C6)	0.25	510	57	68	1.113	10^{11}
	0.54	260	22	80	1.121	10^{12}
	1.3	110	3	91	1.130	10^{10}

as an elastomer (see Table 18). The resonant frequency, however, increases for radiation exposure periods when the material still retains some extensibility. The driving amplitude on the clamped end of the reed was the same for all specimens given in Fig. 86. For materials which have E_1/E_2 values greater than about 5, the amplitude of vibration of the free end of the reed at the resonant frequency may be shown to be proportional to E_1/E_2 if the driving amplitude is kept constant. That this is approximately the case for the Fig. 86 specimens may be shown by comparing the peak heights with the E_1/E_2 values given in Table 20. When the driving amplitude on the clamped end was varied, no amplitude dependence was found for either the resonant frequency, ν_0, or the band width, $\Delta\nu$, for the specimens in Fig. 86.

Figure 87 shows an increase in peak height with increase in E_1/E_2. It is not to be expected that the relation will be one of direct proportionality,

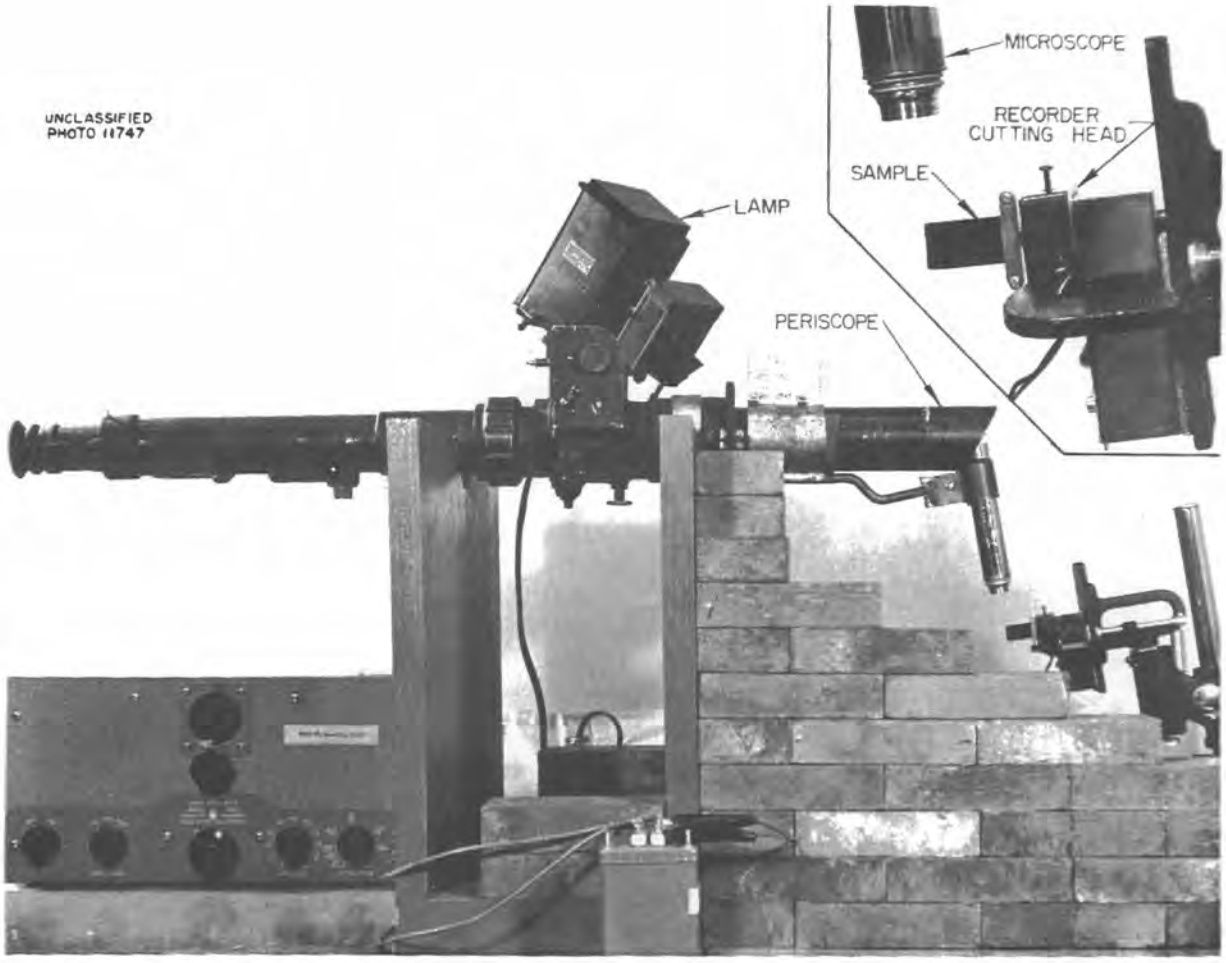

Fig. 85. Vibrating-Reed Apparatus.

TABLE 20. HEATING OF RUBBER CAUSED BY VISCOUS DAMPING

ELASTOMER	RADIATION EXPOSURE (10^{18} nvt)	RESONANT FREQUENCY (sec^{-1})	BAND WIDTH (sec^{-1})	DENSITY (g/cm^3)	THICKNESS (in.)	EFFECTIVE LENGTH FOR E_1 (in.)	E_1 (10^8 dynes/cm^2)	EFFECTIVE LENGTH FOR E_2 (in.)	E_2 (10^8 dynes/cm^2)	E_1/E_2	E_2/E_1^2
Natural rubber formulations											
P1S1C9	0	38	3.6	1.05	0.068	0.84	0.4	0.75	0.026	15	0.16
	0.25	57	2.4	1.05	0.068	0.82	0.8	0.75	0.026	31	0.04
	0.54	75	5.0	1.05	0.068	0.79	1.3	0.68	0.05	26	0.03
	1.3	133	28	1.05	0.068	0.74	3.0	0.59	0.20	15	0.02
32A43	0	87	12	1.19	0.074	0.77	1.4	0.64	0.12	12	0.06
	0.25	92	10	1.19	0.074	0.77	1.6	0.65	0.09	18	0.04
	2.4	220	55	1.21	0.074	0.69	6	0.49	0.4	15	0.01
Butadiene-styrene formulations											
Hycar OS-10 (P1S1C3)	0	140	148	1.12	0.082	0.55	0.9	0.35	0.12	8	0.15
	0.25	205	210	1.12	0.082	0.52	1.4	0.31	0.16	9	0.08
	0.54	308	107	1.13	0.082	0.49	2.3	0.33	0.16	14	0.03
	1.3	382	55	1.14	0.082	0.47	2.8	0.35	0.13	22	0.02
GR-S (32A47)	0	157	27	1.21	0.072	0.54	1.2	0.42	0.07	17	0.05
	0.25	204	28	1.21	0.072	0.52	1.8	0.40	0.08	22	0.02
	2.4	390	86	1.26	0.072	0.47	4	0.33	0.22	18	0.01

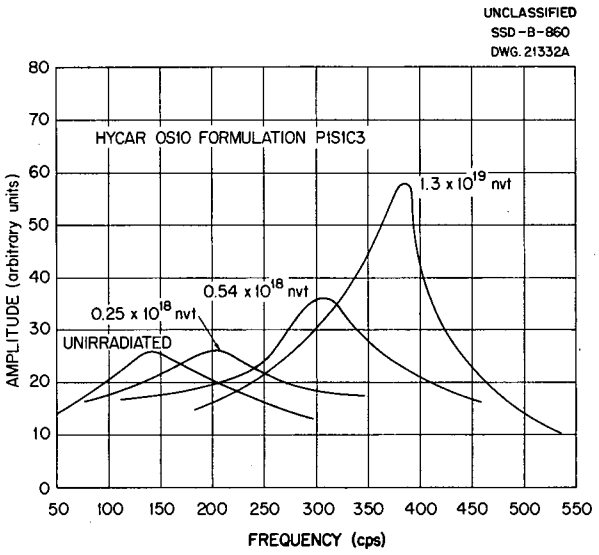

Fig. 86. Resonance of Vibrating Hycar OS-10 Reed.

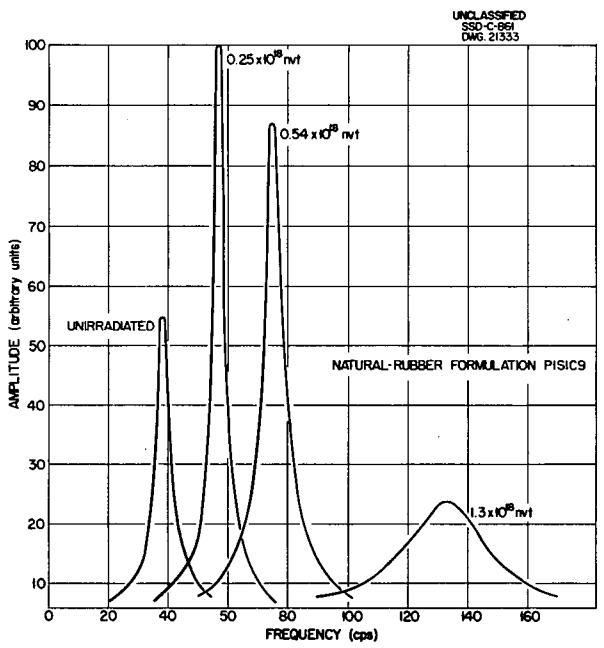

Fig. 87. Resonance of Vibrating Natural-Rubber Reed.

since the relation is complex[8] when E_1/E_2 is less than 5. There was some small amplitude dependence for Hycar OS-10 for the specimen size in Fig. 87. This size was chosen to allow the use of a constant specimen size for all the curves of Fig. 87, but no amplitude dependence was found when some of the specimens were made longer so as to decrease the resonant frequency. This suggests that amplitude dependence is due to heating effects.

It was shown previously that heating for constant cyclic straining is proportional to E_2 and that for constant cyclic stressing, the heating is proportional to E_2/E_1^2. These parameters are calculated in Table 20. The heating for constant straining shows initially a very small increase for natural rubber formulation P1S1C9 and a slight decrease for natural rubber formulation 32A43. For longer exposures when natural rubber has become hard and has lost most of its extensibility, the heating increases markedly. The GR-S formulation shows a somewhat greater initial increase than that given by the natural rubber formulations; the Hycar OS formulation (with less carbon black) shows the largest initial increase of all the formulations. The heating for constant stressing of all the formulations decreases with irradiation because of the increase in E_1 (i.e., because of the decrease in strain which is produced by a constant stress).

X-RAY DIFFRACTION PATTERNS OF PLASTICS

C. D. Bopp G. E. Klein

It was observed previously[11] that the patterns of polyethylene and of nylon show the same kind of radiation change in mechanical properties. Both are hardened by radiation, their elastic modulus is increased, breaking elongation is greatly decreased, and density is increased.

X-ray pattern changes are shown in Figs. 88 and 89. The two prominent peaks at 4.13 and 3.77 Å Bragg spacings in the pattern of unirradiated polyethylene correspond to peaks found in paraffin hydrocarbons; these peaks are due to the (110) and (200) planes.[12] Polyethylene is believed to have a crystal structure similar to that of the paraffins; however, in polyethylene, amorphous regions exist between the minute crystallites. The pattern of amorphous polyethylene gives a halo, with a maximum at about 4.6 Å. Figure 88 shows that irradiation destroys the crystalline peaks and increases the prominence of the halo; this result is

[11] C. D. Bopp, G. E. Klein, and F. A. Sherrill, *Solid State Quar. Prog. Rep. Aug. 10, 1952*, ORNL-1359, Table 8, p. 45.

[12] I. L. Hopkins, W. O. Baker, and J. B. Howard, *J. Appl. Phys.* 21, 206 (1950).

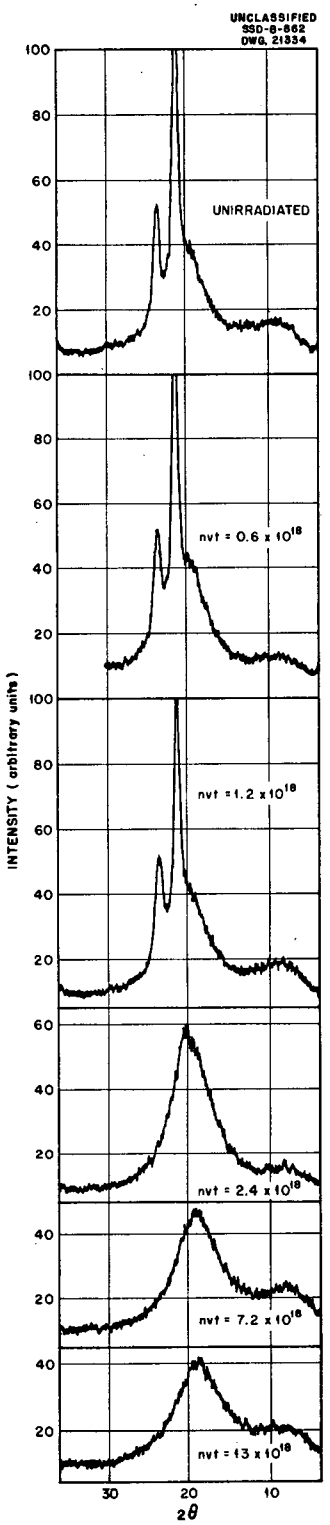

Fig. 88. X-Ray Diffraction Patterns of Irradiated Polyethylene.

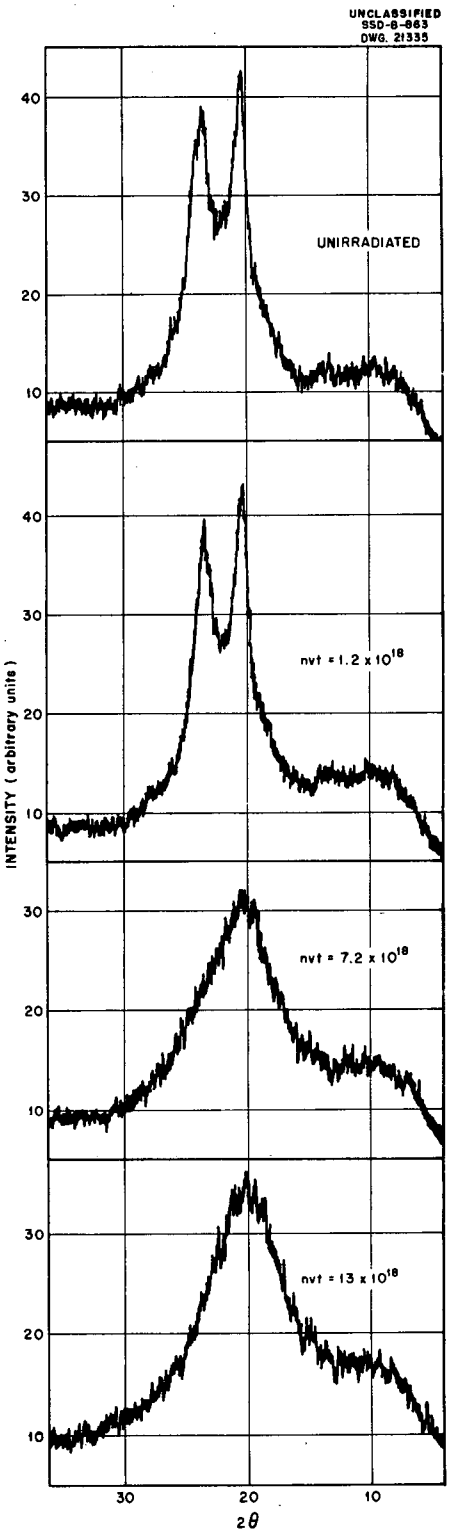

Fig. 89. X-Ray Diffraction Patterns of Irradiated Nylon FM-10001.

in agreement with another study of polyethylene.[13] In the present study, the 3.77-Å peak of unirradiated polyethylene appears with better resolution, although the shorter spacings have poorer resolution than that found in the previous study. In Fig. 89, analogous behavior is seen for nylon and for polyethylene.

Copper K_α radiation filtered with 5-mil nickel foil was used with a Norelco Geiger counter diffractometer. Specimens were cut from sheet material (polyethylene, 0.13 in. thick; nylon FM-10001, 0.042 in. thick). When the polyethylene sheet is elongated about 200% by stretching and the pattern is taken of the surface of the sheet parallel to the direction of stretching, the 3.77-Å peak has poorer resolution than that obtained for the unstretched material. For polyethylene crumbs prepared by filing or scraping of the sheet, this peak also has poorer resolution. A powder was prepared by dissolving the sheet material in hot oil and then precipitating out the polyethylene by diluting the solution with gasoline. The pattern of the powder prepared by this method is identical with the pattern of the original sheet. It would seem that no strain or orientation effects are present in the pattern of the original sheet.

Figure 88 shows very little change between the patterns with exposures of 2.4×10^{18} and 13×10^{18} nvt. This is taken to indicate that crystallinity is largely destroyed before the exposure at 2.4×10^{18} nvt. After an exposure of 2.4×10^{18} nvt, polyethylene and nylon are hard and glasslike. The rate of chemical cross-linking per unit of radiation exposure is about constant up to 13×10^{18} nvt, as is evidenced by the rate of increase in density and by the rate of gassing;[3] however, the rate of change in mechanical properties that are sensitive to crystal structure (hardness, elastic modulus, and breaking elongation) decreases greatly under the initial rate for exposure periods as great as 2.4×10^{18} nvt.

Irradiations were made in hole 19 of the ORNL graphite reactor.

[13] A. Charlesby, *J. Polymer Sci.* 10, 201 (1953).

SPECIAL PROJECTS

IRRADIATION OF QUARTZ

M. C. Wittels F. A. Sherrill

Studies of the lattice expansion[1,2,3] and the disordering of quartz crystals by fast-neutron irradiation have been continued with exposures up to 1.85×10^{20} nvt. Whereas it was previously found that the single-crystal lattice disrupts into a highly disordered polycrystalline material when irradiated by 1.35×10^{20} nvt, it has now been established that the single-crystal lattice remains coherent under bombardments up to 1.19×10^{20} nvt. The c-axis precession photographs (Fig. 90) indicate that the single-crystal lattice is still present, although highly disordered, after an irradiation of 1.19×10^{20} nvt. Figure 91 shows a natural singly terminated quartz crystal that has undergone this bombardment and has suffered a density loss of 12.6%; the density is 2.315 g/cc, and c/a is 1.068. It should be noted that the crystal reveals no macroscopic defects resulting from the irradiation.

The relation between density change and fast-neutron bombardment in quartz (Fig. 92) indicates that the initial rate of damage is probably small. One explanation for this is that the large c-direction holes must first be filled with dislocated atoms before the large expansion occurs. These holes are large enough to accept atoms or ions of 0.57-Å radius without a crowding effect. A consideration of bond rupture indicates that oxygen ions would be more easily displaced because only two Si-O bonds thus need to be broken. The large volume requirements of oxygen would result in a distorted lattice when atoms of this element are knocked into displaced positions.

It is probable that permanent damage is introduced into the quartz lattice at an early stage of bombardment. This was first noted by the absence of the

[1] M. C. Wittels and J. B. Trice, *Solid State Quar. Prog. Rep. Nov. 10, 1952*, ORNL-1429, p. 38.

[2] M. Wittels, *Phys. Rev.* 89, 656 (1953).

[3] M. C. Wittels, *Solid State Quar. Prog. Rep. Feb. 10, 1953*, ORNL-1506, p. 30.

well-known alpha ⇄ beta transformation,[3] and further evidence was indicated by the small initial rate of change of density. Since the c/a axial ratio of alpha quartz normally reaches a minimum of 1.092 at the transition temperature, 573°C, it might be expected that permanent damage would result if this ratio were lowered further. The plot of the axial ratio as a function of bombardment (Fig. 93) indicates that this minimum is reached with an irradiation of approximately 2×10^{19} nvt.

UNCLASSIFIED
PHOTO 11426

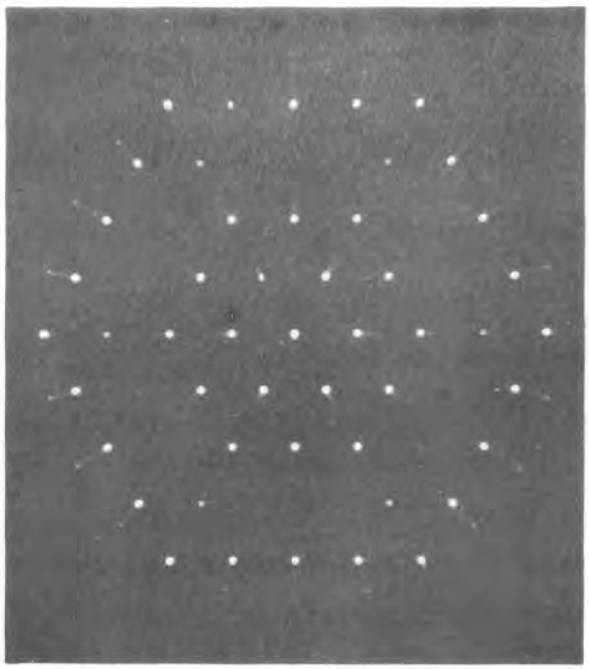

(a)

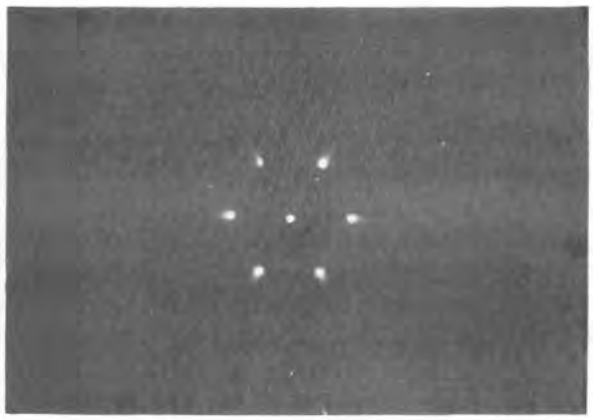

(b)

Fig. 90. c-Axis Precession Photographs of Quartz. (a) Before irradiation, density = 2.650, c/a = 1.100. (b) After 1.19×10^{20} nvt, density = 2.315, c/a = 1.068.

UNCLASSIFIED
PHOTO 11327

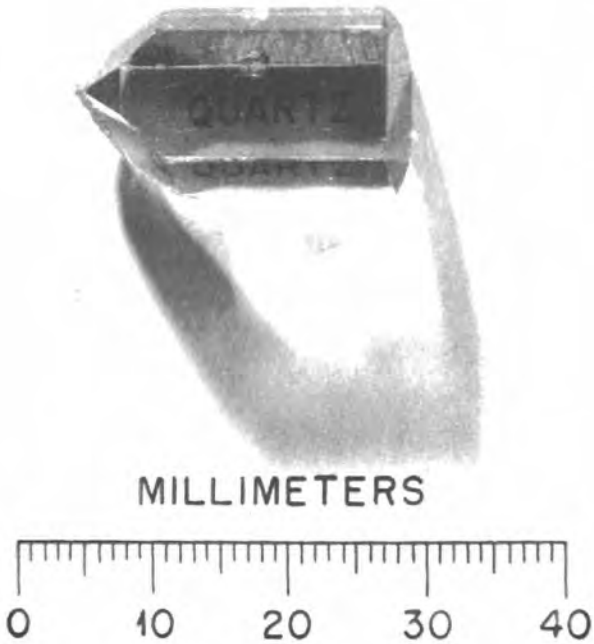

Fig. 91. Quartz After 1.19×10^{20} nvt Bombardment.

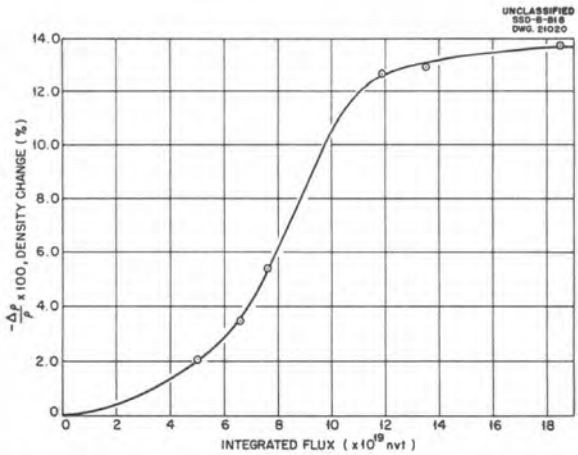

Fig. 92. Density Change of Quartz upon Fast-Neutron Bombardment.

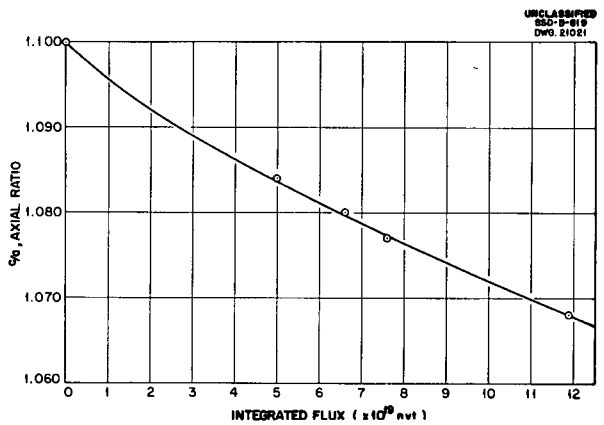

Fig. 93. Change in the Axial Ratio of Quartz with Fast-Neutron Bombardment.

This plot also indicates that the expansion is more strongly anisotropic in the initial stages of the expansion.

Debye-Scherrer patterns of quartz irradiated by 1.35×10^{20} and by 1.85×10^{20} nvt are similar to the pattern of vitreous silica. However, in both quartz patterns, a low degree of order still exists and is revealed by three very weak lines with spacings of 1.707, 2.00, and 3.27 Å. Annealing at 900°C of material irradiated by 1.35×10^{20} nvt produced a partially ordered quartz[4] with normal lattice parameters.

Samples of low tridymite, low cristobalite,[5] and samples of synthetic quartz containing 7% GeO_2 were secured from H. S. Yoder, Jr. of the Geophysical Laboratory. The samples were irradiated by 5.0×10^{19} nvt for testing the effects of neutron bombardment on polymorphs of SiO_2 and "impure" quartz. Debye-Scherrer patterns of the irradiated tridymite revealed no lattice-parameter changes, but the intensities of several reflections were reduced considerably. In the case of irradiated cristobalite, a general increase was observed in *d* spacings which indicates a lattice expansion. Again, many reflections were smeared out badly. Germania-bearing quartz was found to behave similarly to normal quartz upon neutron irradiation.

Since the density of quartz undergoes large changes under fast-neutron bombardment and since the frequencies of thin quartz plates have been altered 2 kc/sec in 10 megacycles/sec by x irradiation,[6] a simple survey experiment was devised for testing the effect of irradiation on the characteristic frequencies of quartz-crystal oscillators.

With the aid of a Stroboconn, an audio-signal generator, an oscilloscope, and a duel oscillator and mixer, the frequencies of some *y*-cut crystal bars were measured. These were crystals whose lengths were parallel to the *y* direction and whose cross sections were square. The faces in the *x* direction were plated with a thin film of aluminum and were notched in the middle, perpendicular to the *y* direction, with a shallow 0.003-in. groove. The dimensions and the driving frequencies of the crystals studied are as follows:

	Cross Section (mm)	Length (mm)	Driving Frequency (cps)
1A	4.8	21.2	130,900
B	4.8	20.8	134,400
2A	4.6	25.0	108,290
B	4.6	25.1	108,020
3A	5.7	35.0	78,000
B	5.7	16.0	168,000

Crystal 1B was irradiated with gamma rays from a Co^{60} source; the total exposure was 2.7×10^7 roentgens. No changes in oscillating frequency were observed within the limits of measurement, that is, ±20 cps in 100,000 cps. However, it was noted that the quartz had started to darken during the exposure period.

Crystals 3A and 3B were bombarded with a fast-neutron flux of 5×10^{19} nvt. These crystals would not drive the oscillators. The resonant frequencies were measured with an impedance bridge, but they were not sharply defined.

The activity rather than the frequency of neutron-bombarded quartz should be studied in the future.

IRRADIATION OF MISCELLANEOUS MATERIALS

M. C. Wittels F. A. Sherrill

The expansion[7] of diamond was observed after irradiations up to 2.2×10^{20} nvt. The x-ray density

(4) M. Wittels and F. A. Sherrill, "Some Effects of Fast Neutron Bombardment on Quartz," paper presented at American Physical Society Meeting, Washington, D.C., May 2, 1953.

(5) W. H. Sullivan and F. T. Howard, *ORNL Prog. Rep., June 1953*, ORNL-1576, p. 16.

(6) C. Frondel, *Am. Mineralogist* 30, 432 (1945).

(7) W. H. Zachariasen and H. A. Plettinger, *ANL Quar. Rep., Sept., Oct., and Nov. 1949*, ANL-4400, p. 12.

(Fig. 94) was lowered by 3.39% – a change approaching saturation. In connection with the lattice expansion of diamond, some single-crystal x-ray studies are now in progress. The use of diamond as a fast-neutron monitor[3] was previously discussed.

Cubic SiC bombarded by 1.35×10^{20} nvt reveals an x-ray density decrease of 2.51%. This change is slightly smaller than that found for diamond with the same irradiation. Cubic TiC, given the same irradiation, shows an x-ray density decrease of 1.15%.

No change in the lattice constants of silicon and germanium was found after an irradiation of 10^{20} nvt. Similar results were found for natural crystals of fluorite (CaF_2) and of calcite ($CaCO_3$) when they were bombarded by 5.0×10^{19} nvt.

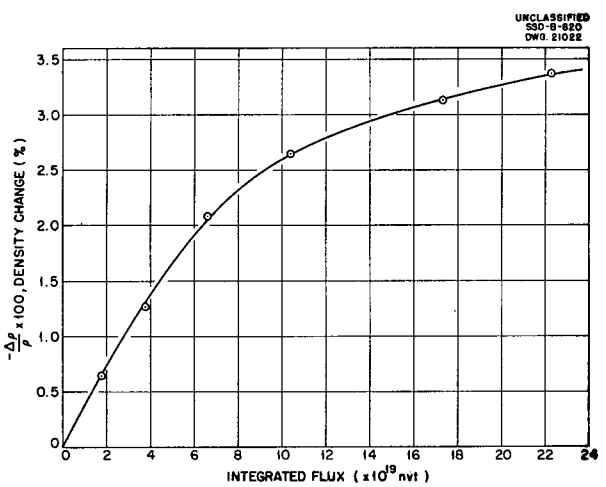

Fig. 94. X-Ray Density Change of Diamond Resulting from Fast-Neutron Bombardment.

USE OF K_β RADIATION FOR THE X-RAY ANALYSIS OF REFLECTIONS UNRESOLVED IN THE K_α REGION

G. E. Klein D. Binder
W. J. Sturm

In materials in which the $K_{\alpha_1\alpha_2}$ doublet cannot be clearly resolved in an x-ray pattern, it becomes difficult to observe line shapes and to accurately determine interplanar spacings. For such cases, the use of the K_β radiation permits a determination of both these features, providing that the material diffracts well enough to give lines of sufficient intensity.

The value of the method depends primarily on the relative intensity of K_{β_2} to K_{β_1} being approximately 1 to 80; so the K_{β_2} component rarely causes any interference worthy of consideration. Although the peaks resulting from the K_{β_1} and the K_{β_2} radiation are 20% broader than the corresponding peaks produced by the K_α radiation, they are separated appreciably, even for reflections in which an extreme amount of line-broadening renders the K_α reflections rather useless. The resulting peak produced by the K_{β_1} reflection clearly shows the line shape and the Bragg angle attributed to the particular plane of the crystal being considered.

With conventionally sealed-off x-ray tubes, the K_β reflections are easily obtained by merely omitting the filter which is normally employed for removing the K_β component, although experience has shown that enough of the K_β component is transmitted through a 0.0001-in. thickness of filter material so that, with strongly diffracting materials, a thin filter may be left in place.

Whereas the method described can be used with a conventional x-ray diffractometer, the alternative method would be to use either a monochromator for the x-ray beam or to use a double crystal diffractometer setup.

Application of the method has been made to the analysis of the reflections from single crystals of LiF (cf. "Neutron Irradiation of LiF Crystals," this report).

NEUTRON IRRADIATION OF LiF CRYSTALS

D. Binder W. J. Sturm

As discussed in the previous progress report,[8] the large cross section for the (n,α) reaction in Li^6 suggests that observable radiation damage effects may be produced in LiF at low neutron irradiations. The reaction converts slow reactor neutrons into energetic alphas and tritons that subsequently displace atoms in the lattice. This differs from the usual mechanism for displacement – the recoils from the less intense fast flux of the reactor.

The object of this investigation was to observe, by means of x-ray and density measurements, the lattice defects introduced into LiF single crystals by reactor irradiation. The possibility that these

[8] W. J. Sturm, D. Binder, and G. E. Klein, *Solid State Quar. Prog. Rep. Feb. 10, 1953*, ORNL-1506, p. 30.

two measurements may not be equivalent was suggested at one time by Miller and Russell[9] for a lattice containing vacancies and interstitials. They have since made recalculations and report that the two measurements should be equivalent.[10] In the original argument, the model proposed for a vacancy or interstitial was an expanded sphere placed in the interior of an elastic crystal block in which the atoms near the sphere were displaced further than those on the boundary of the block. It was assumed that the density was a measure of the lattice expansion on the boundary and that the x-ray lattice parameter was a measure of some average expansion. A calculation indicated that the lattice-parameter increase derived from x-ray measurements would be twice that derived from density measurements. The recalculation included the interaction of neighboring expansions more explicitly and indicated that there would be little, if any, difference between the measurements. The data from these experiments show that the two measurements of lattice parameter changes are in agreement within 20%.

X-ray parameter measurements of the LiF single crystals obtained from the Harshaw Chemical Company were made on a Norelco x-ray diffractometer. The instrument simultaneously rotates a Geiger counter detector at twice the angular velocity of the crystal holder. The alignment of the initial or zero position is accomplished by means of a steel bar. Since the cleaved crystal surface may not be absolutely flat on the holder, some method of zero correction is needed. Bragg angles of the 200 and 400 reflections of the resolved copper K_α doublet were zero-corrected by making them internally consistent. By assuming Bragg's law to hold, the ratio of the sines of the Bragg angles of the first- and second-order reflections of the α_1 and the α_2 lines should be one-half. Additions or subtractions of 1 min of arc or less from the angles were usually sufficient to obtain the best fit. The zero-corrected second-order Bragg angles of eight unirradiated crystals agreed to within ±0.3 minute. This error included a variation of about 1°C in the temperature or 0.15 min in the Bragg angle. The zero-corrected values of the 400 reflections were used throughout for the x-ray lattice-parameter changes. If the lines of irradiated crystals had been as sharp as those of the unirradiated crystals, the error in Bragg-angle change would have been ±0.42 minute. But since there was line-broadening, the error increased to ±0.6 min or 0.015% in lattice-parameter change.

Since the LiF single crystals used for this experiment were rather large, having a volume of 2 cc or more, it was possible to measure density by immersion-weighing techniques. The crystal to be measured was suspended by 1-mil wire in a volume of carbon tetrachloride. After thermal equilibrium of the system had been reached, the weight of the immersed and the unimmersed crystal was determined, various correction measurements were made, and the density was calculated.

For the density of CCl_4, the following relation[11] was used:

$$d_t = (d_s + 10^{-3}\,\alpha t + 10^{-6}\,\beta t^2)\ \pm 0.0002\ ,$$

where

d_s = 1.63255,
α = −1.9110,
β = −0.690,
t = temperature of the liquid.

On this basis, a curve of the density of unirradiated LiF as a function of temperature was made for use as a reference line for the measurement of density changes when the compound was irradiated and annealed. In the region between 20 and 26°C, the density of LiF was found to be

$$\rho_{(LiF)} = (2.64755 - 2.916 \times 10^{-4}\,t)\ \pm 0.00035\ ,$$

where t is the temperature of the crystal. Since all measurements of density were made relative to the unirradiated crystal, corrections for surface tension and air buoyancy were not needed, and the relation given above was used for these comparative determinations.

To compare the absolute accuracy of these measurements with the accuracy of other measurements of LiF density, the buoyancy and the surface-tension corrections were made, the uncertainty in CCl_4 density was introduced, and the relation became

$$\rho_{(LiF)} = (2.64663 - 2.916 \times 10^{-4}\,t)\ \pm 0.00048\ .$$

This agrees, within experimental error, with the

[9] P. H. Miller, Jr. and B. R. Russell, *J. Appl. Phys.* 23, 1163 (1952).

[10] B. R. Russell, *Technical Report No. 1*, Contract AF 18(600)-561, University of Pennsylvania Department of Physics.

[11] *International Critical Tables*, vol. III, p. 28, McGraw-Hill, New York, 1928.

values 2.63905 ± 0.0001 at 25°C[12] and 2.64030 ± 0.00014 at 20°C[13] given by independent measurements.

As a check on the x-ray and the density measurements, the absolute lattice parameters were calculated from both sets of data. At an average temperature of 26.0°C, the x-ray parameter is

$$a_x = 4.02730 \ (\pm 0.00037) \ \text{Å},$$

based on the copper K_{α_1} wavelength of 1.54050 (±0.00003) Å. The density parameter obeys the relation

$$a_\rho = \left(\frac{4M}{N}\right)^{1/3},$$

where

M = the molecular weight,
N = Avogadro's number,
ρ = the density.

The input data are:

M = 25.940 ± 0.001,
N = 6.02303 (±0.00036) × 10^{23} mole^{-1} (chemical scale),
ρ = 2.63905 ± 0.00048 at 26.0°C.

Then

$$a_\rho = 4.02645 \ (\pm 0.00036) \ \text{Å}.$$

This leaves an error of 0.00012 Å between the two parameters unaccounted for in the random errors of the measurement. Since no allowance was made for impurities in the LiF or the CCl_4 used in the density measurements, additional systematic errors are expected in computing a_ρ and could very well account for the discrepancy. These systematic errors would not affect the results for the relative changes in lattice parameters in the irradiation and the annealing studies.

For the reactor irradiations, an important correction arises which is exclusive of the measuring techniques. In comparing the change in the x-ray parameter, $(\Delta a/a)_x$, with the change in density, $(\Delta a/a)_\rho$, the neutron attenuation through the crystal must be considered. The thermal-neutron-absorption coefficient is 4.4 cm^{-1}, which indicates a need for the irradiation of thin crystals. The effects of successive irradiations of a thick crystal (2.5 × 1.3 × 0.53 cm) in hole 12 of the ORNL graphite reactor are shown in Fig. 95 to illustrate some general features of the experiment that are common to all crystals. Saturation of $(\Delta a/a)_x$ and $(\Delta a/a)_\rho$ is strong at 1×10^{17} nvt. The variation in $(\Delta a/a)_x$, the same for all thicknesses, is in general agreement with the data of Tucker and Senio[14] and shows that the damage is caused by displacements rather than by helium or tritium impurities. The impurities are produced in concentrations of (σ)(nvt), where σ is the Li(n,α) reaction cross section, or in concentrations up to 7×10^{-6}, and this would account, at most, for 0.005% of $(\Delta a/a)_x$.

The thick crystal was not ideal for calculating a neutron attenuation correction because its thickness is comparable to its other dimensions, and this would necessitate the consideration that neutrons were entering from all faces. To simplify the calculation, some Harshaw crystals, originally 0.8 cm thick and approximately 2.6 cm square, were cleaved to form four crystals from 0.16 to 0.21 cm thick and 2.6 cm square. These thin crystals were irradiated for various periods of time in hole 12 of the ORNL graphite reactor (used throughout the experiment), and the results were plotted as $(\Delta a/a)_x$ vs. $(\Delta a/a)_\rho$ in Fig. 96. The errors in this and in succeeding figures are the same for all points, but are indicated on only one point to simplify the figure. The straight-line plot indicates that saturation affects both parameters in the same way,

(12) C. A. Hutchison and H. L. Johnston, *J. Am. Chem. Soc.* 62, 3165 (1940).

(13) D. A. Hutchison, *J. Chem. Phys.* 13, 383 (1945).

(14) C. W. Tucker, Jr. and P. Senio, *Report of Metallurgy Section, March, April, May 1953*, KAPL-930, p. 88.

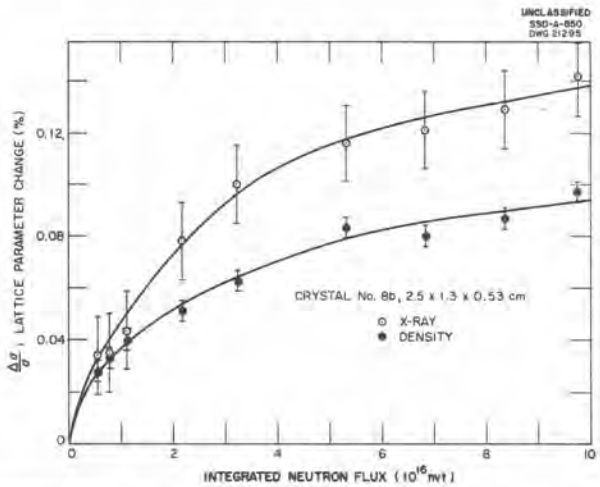

Fig. 95. Effect of Irradiation on Lattice Parameter of a Thick LiF Single Crystal.

Page 103 Column 1 Line 12 for $a_\rho = \left(\frac{4M}{N}\right)^{1/3}$,

read $a_\rho = \left(\frac{4M}{\rho N}\right)^{1/3}$,

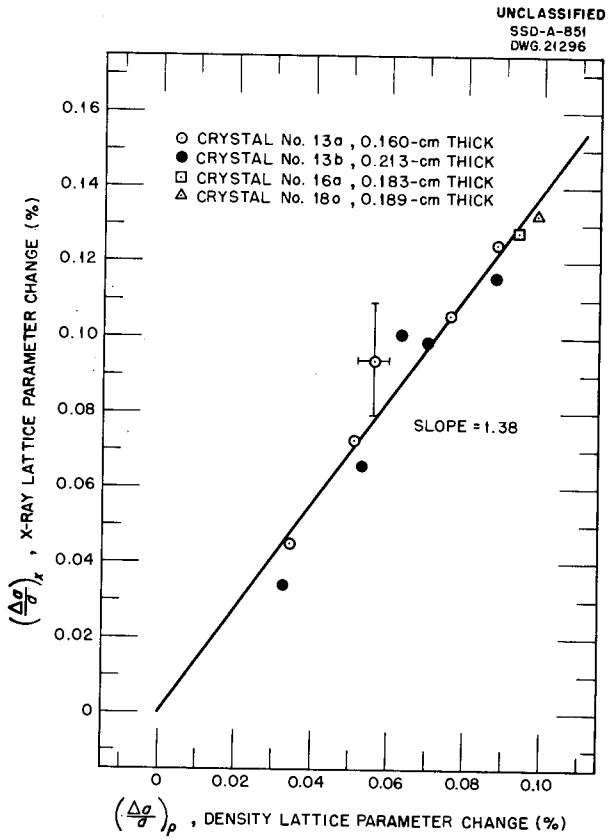

Fig. 96. X-Ray Lattice Parameter Change vs. Density Lattice Parameter Change for Irradiated Thin LiF Single Crystals.

within the errors of the measurement, and the slope indicates that $(\Delta a/a)_x$ is 1.38 times $(\Delta a/a)_\rho$, with an error of 4%.

If the variation of the slope from unity were caused by neutron attenuation, the slope would then equal the yield for the Li(n,α) reaction at the surface divided by the average yield for the whole crystal. To calculate this ratio, it is assumed that the incident neutron flux has two components – a thermal flux and a resonance flux. The thermal yield varies as $e^{-N\sigma_0 x}$, where N is the number of atoms per cubic centimeter, σ_0 is the thermal cross section, and x is the average distance the neutron travels. If the neutrons cross the surface in random directions, the average distance traveled is twice the distance from the surface. The ratio of the thermal to the resonance yield at the surface is given by the cadmium ratio for a "$1/v$" detector and is taken to be 33 (". . . for a graphite or deuterium pile . . .").[15] It is assumed that only the neutrons entering from two surfaces need to be considered (thin crystal). Then, if t is the thickness, the ratio R of the yield at the surface to the average yield is

$$R = \frac{1 + e^{-2N\sigma_0 t} + 0.03}{\overline{e^{-N\sigma_0 x}} + 0.03}$$

$$= \frac{1 + e^{-2N\sigma_0 t} + 0.03}{\frac{1}{N\sigma_0 t}\left(1 - e^{-2N\sigma_0 t}\right) + 0.03} .$$

The thin-crystal data in Fig. 96 contain points mostly from irradiations of crystals 13*a* and 13*b*; their values of t and R are tabulated below:

Crystal	t (cm)	R
13*a*	0.160	1.15
13*b*	0.213	1.27

The slope of the curve for $(\Delta a/a)_x$ vs. $(\Delta a/a)_\rho$ in Fig. 96 exceeds 1 by 0.38. Of this quantity, $\bar{R} - 1$ or 0.21 is accounted for by neutron attenuation; consequently, it is concluded that, for equivalent lattice distortions, x-ray parameter changes exceeded density parameter changes by 20% at most.

The results of thick-crystal irradiations are shown in Fig. 97. These crystals were all about 2.6 cm square by 0.8 cm, and the slope is, of course, larger (2.4).

Thick and thin crystals with about the maximum $\Delta a/a$ observed were chosen for annealing studies. The results of anneals at successively higher temperatures from 275 to 560°C are shown in Fig. 98 in which the original changes in the parameter are plotted with those remaining after the anneals.

The plot of the thin-crystal data closely approximates that of the corresponding irradiation data. The slope of the line is 1.42, and again, for the same defect concentration, $(\Delta a/a)_x$ exceeds $(\Delta a/a)_\rho$ by 20% at most. The thick-crystal curve converges toward the thin-crystal curve and then follows it to the origin. This is an indication that the order of the annealing process is higher

[15] D. J. Hughes, *Pile Neutron Research*, p. 63, Addison-Wesley, Cambridge, Mass., 1953.

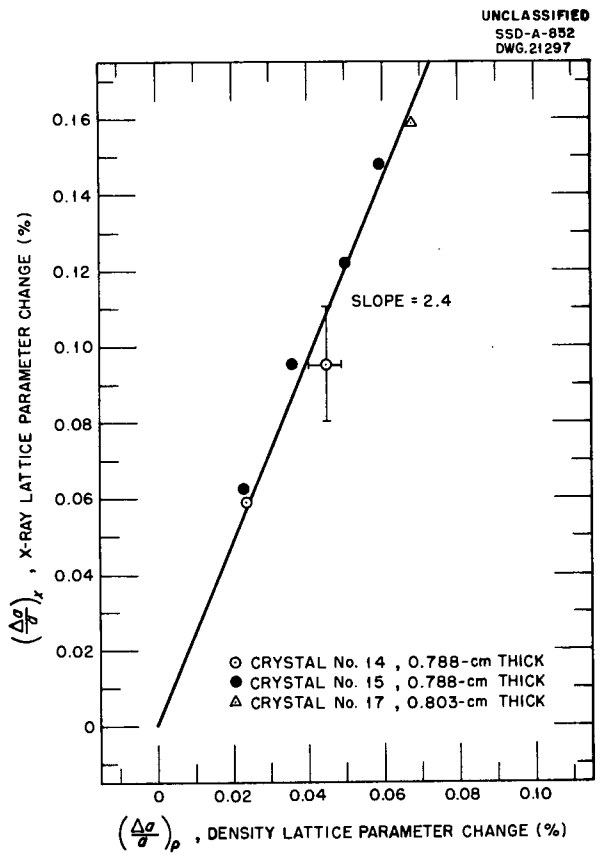

Fig. 97. X-Ray Lattice Parameter Change vs. Density Lattice Parameter Change for Irradiated Thick LiF Single Crystals.

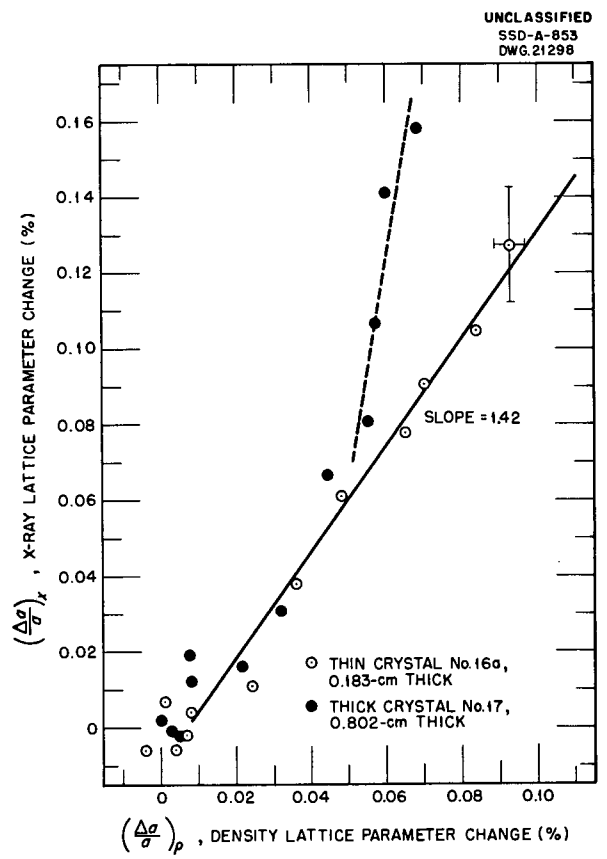

Fig. 98. X-Ray Lattice Parameter Change vs. Density Lattice Parameter Change for Irradiated LiF Single Crystals After Being Annealed at Various Temperatures.

than 1 and makes the defect concentration more uniform.

All x-ray measurements discussed thus far were made for the purpose of locating the position of the peak of the line diffracted from a single crystal of LiF. However, this was not the only property of the line which was found to vary with irradiation and annealing. With increasing irradiation and in the early stages of annealing, the width of the line at one-half maximum broadened markedly and returned to its original sharp condition as high annealing temperatures were reached.

In accord with the hypothesis of Dehlinger and Kochendörfer,[16] the variation of line width with Bragg angle might be expected to distinguish between effects caused by changes in particle size and those caused by lattice distortion. Changes resulting from strains in the lattice would be expected to broaden the line in such a manner that its width varies as tan θ, where θ is the Bragg angle. Changes resulting from particle-size changes in the diffracting medium would cause the line width to vary as λ sec θ, where λ is the wavelength of the x radiation used. By using the K_{α_1} and K_{α_2} radiation from copper and the $h00$ reflections available in two orders, 2θ maximums appeared in the region of $\pi/2$ and $\pi/4$ radians. The measurement of line width made at two-thirds maximum and plotted as a function of each of the parameters showed fair agreement with the tan θ variation expected if the broadening were caused by internal lattice strain.

(16) U. Dehlinger and A. Kochendörfer, *Z. Krist.* 101, 134 (1939).

A second striking property of the line diffracted by the irradiated LiF single crystal is its dissymmetry. Figure 99*a* shows the intensity distribution of the first-order Bragg maximums arising from the K_{α_1} and K_{α_2} lines in copper. The diffraction in this case is done by an unirradiated single crystal of LiF; the doublet is quite well separated, and the individual components are symmetrical. In Fig. 99*b*, the same lines diffracted from the same crystal after a reactor irradiation of 7×10^{16} nvt are shown. The lines show some symmetrical broadening (the tan θ variation discussed above) plus a strong dissymmetry, which increases the intensity on the side toward higher glancing angles. Because the K_α x-ray line is a strong doublet, it is not possible to determine much more about the nature of the dissymmetry from this curve.

By the use of the techniques described in a previous section (cf. "Use of K_β Radiation for the X-Ray Analysis of Reflections Unresolved in the K_α Region," this report), the copper K_β radiation was used, and this reduced the problem to the study of the broadening of a single line. Figure 100*a* shows the strong reflection of the K_{β_1} line from the unirradiated crystal, together with the relatively insignificant K_{β_2} reflection. The effect of irradiation upon the shape of the lines is shown in Fig. 100*b*. The observed shape of the line is shown as the solid trace; the resolution into components, based on the assumption that the intensity of the low-angle side of the main line arises entirely from the K_{β_1} component and that the main component of the resultant line is symmetrical, is shown by the dotted lines. On these assumptions,

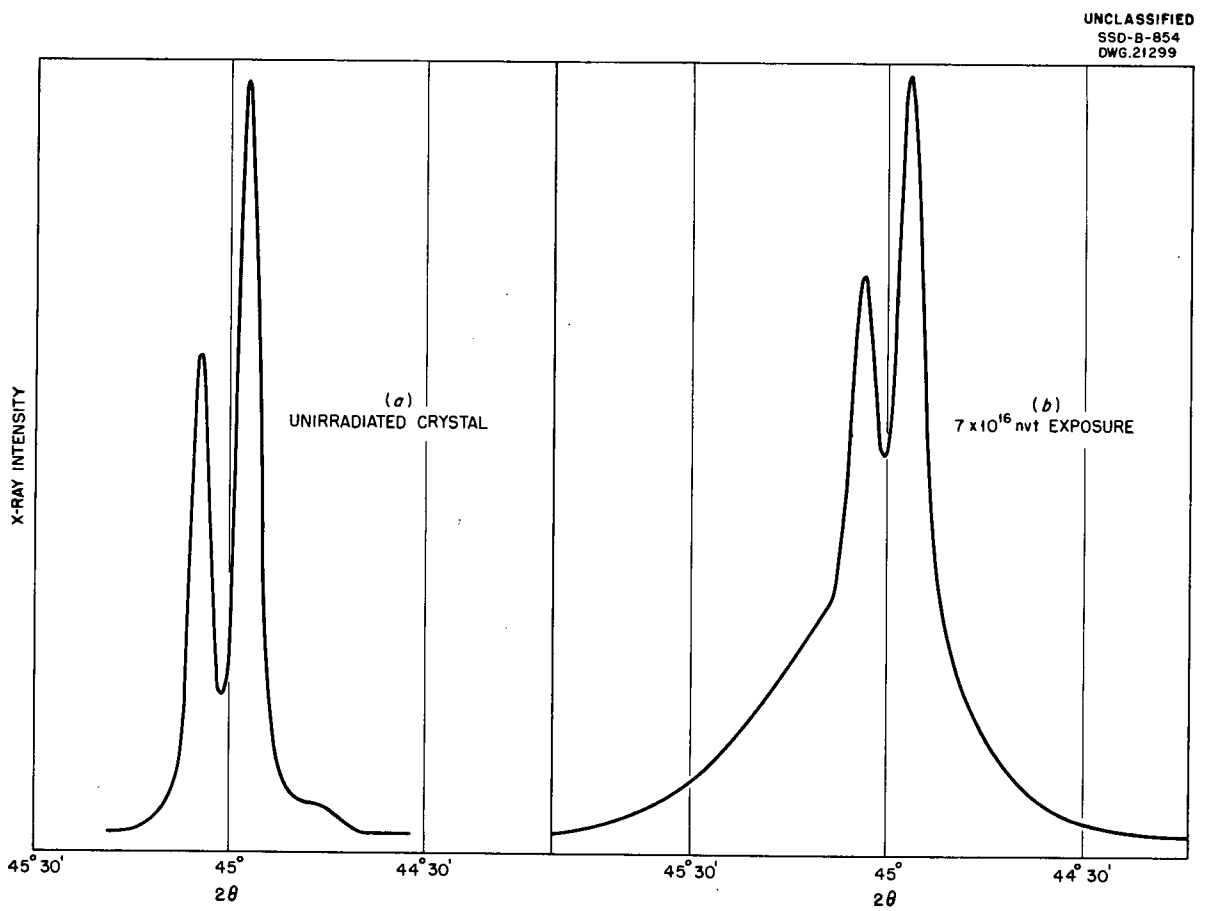

Fig. 99. Variation of X-Ray Intensity as a Function of the Bragg Angle for LiF Single Crystals Exposed to K_α Radiation.

the line is resolved into a strong, symmetrically broadened component plus a small amount of a second component which is peaked about 15 min from the main maximum and extends asymmetrically into the region of larger glancing angles.

The interpretation of the cause of the second, smaller component is not clear at this time.

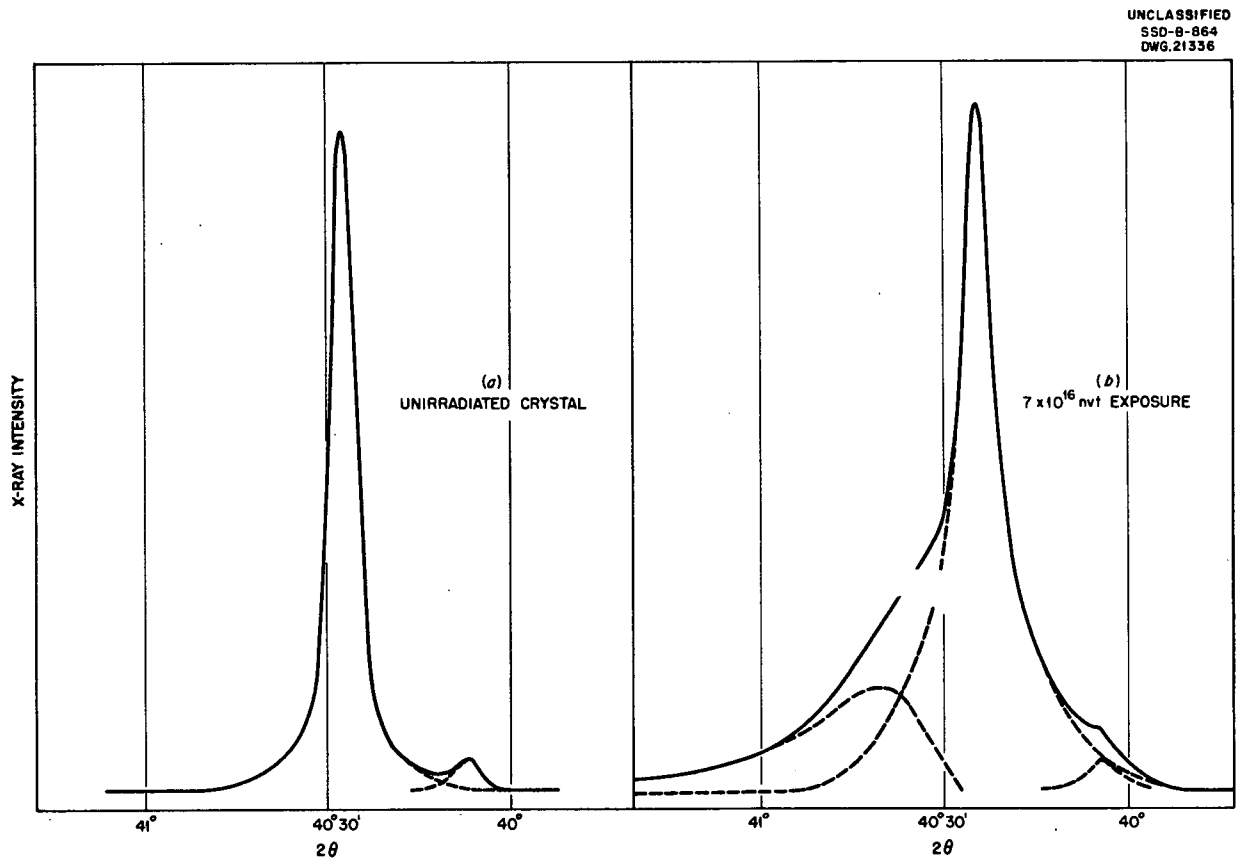

Fig. 100. Variation of X-Ray Intensity as a Function of the Bragg Angle for LiF Single Crystals Exposed to K_β Radiation.